Diplomarbeit

Dilepton Production in Elementary Nuclear Reactions within a BUU Transport Model

vorgelegt von

Janus Weil

<janus.weil@theo.physik.uni-giessen.de>

August 2008

Betreuer: Prof. Dr. Ulrich Mosel

JUSTUS-LIEBIG-UNIVERSITÄT GIESSEN

Institut für Theoretische Physik I
Fachbereich 07 - Mathematik und Informatik, Physik, Geographie

The key to getting the right answers
is asking the right questions.

Contents

1 Introduction

The main focus of this diploma thesis lies on "dilepton physics", meaning the observation of dileptons (i.e. lepton pairs) from nuclear reactions. Dileptons play a major role in modern hadron physics, since they can be used to gain information about processes happening inside nuclear matter, which would not be accessible otherwise. Their attractivity as a probe of nuclear reactions is mainly generated by the fact that leptons, unlike quarks and everything built from them (i.e. hadrons and nuclei), do not take part in the strong interaction. Thus they can traverse nuclear matter virtually undisturbed, being only slightly deflected by the electromagnetic field of the nucleus. These so-called Coulomb corrections are much smaller than the strong interactions that all hadronic probes are subject to, and can usually be neglected. The term "dilepton" in general is used to refer to a pair of leptons, i.e. e^+e^-, $\mu^+\mu^-$ or $\tau^+\tau^-$. In the context of this work however, it almost exclusively refers to an electron-positron pair.

Dileptons are particularly useful to study the properties of vector mesons inside nuclear matter. While the vacuum properties (like masses, decay widths etc) of most hadrons are known to reasonable accuracy today, it is a much-debated question how these properties change in nuclear matter and how they are influenced by the surrounding medium. In particular for vector mesons there have been various theoretical predictions regarding their in-medium masses and widths, which have triggered the interest of experimentalists, who have been trying to experimentally verify (or falsify) the predictions. And still after many years these questions have not been settled completely.
If we talk about vector mesons in this thesis, we usually refer to the light non-strange vector mesons ρ^0, ω and ϕ. All of these have a decay mode into e^+e^-, and if such a decay happens inside nuclear matter, the emanating lepton pair can carry the in-medium information outside to the detector, and through its invariant mass the in-medium mass of the meson can be reconstructed. In this way it is possible to measure the in-medium properties of the vector mesons.

Although a large amount of research is currently being done on dilepton production in heavy-ion collisions, we will concentrate on elementary nuclear reactions here, especially photon- and proton-induced reactions. These elementary collisions have a number of advantages, in particular they involve a more sharply defined density, and are simply cleaner in general.

For the numerical simulation of various nuclear processes we use the GiBUU model, which is a semi-classical BUU transport model, being developed at the University of Giessen. This model takes care of the correct transport-theoretical description of the hadronic degrees of freedom in nuclear reactions and all the subtleties this may involve, including the propagation, collisions and decays of particles in a nuclear environment.

We will start off in chapter 2 by describing the basics of the GiBUU model, before giving an overview over the properties of vector mesons in vacuum in chapter 3. Chapter 4 will provide some details on dilepton decays and the calculation of dilepton spectra, while chapter 5 will summarize the predicted in-medium effects on the vector meson properties. Chapters 6 and 7 come back to some more technical aspects, which one has to deal with when working with transport models, namely final state decisions and off-shell transport. After that chapter 8 will give an overview over the experimental status on dilepton production in elementary nuclear reactions. Then chapters 9 and 10 will describe some specific aspects of photon-induced as well as proton-induced reactions (including some discussion of possible backgrounds), before chapter 11 presents our results for both types of reactions, in the form of mass-differential dilepton spectra. Finally chapter 12 will close this thesis with a quick summary and an outlook.

2 The Transport Model

Today microscopic transport models are a common tool for the numerical simulation of nuclear reactions. A general overview over transport models can be found in [BG88] and [KB94]. One rather simple-minded class of transport models are the so-called "Cascade models", which basically treat the nucleus as a collection of point-like nucleons, so that nuclear collisions are reduced to the collisions of the nucleons. Usually a collision criterion is set up, assuming two nucleons which approach each other closer than some threshold to interact ("hard collisions").
Apart from that most Cascade models use a pretty simplified model of the nucleus. For instance they neglect any Fermi motion of the nucleons, assuming they are at rest inside the nucleus, and therefore they also cannot describe effects like Pauli blocking. Moreover, Cascade models usually do not include any mean field potentials.
Another, more complex, class of transport models are BUU models, which in contrast to the Cascade models include a mean field potential. This mean field is generated by the sum of all nucleons and binds them together in the nucleus. It also enables the model to give a Fermi momentum to the nucleons without the nucleus falling apart, which means that also Pauli blocking can be incorporated.
But the mean field also leads to the fact that the motion of the nucleons is much more complex than in a Cascade model, where the nucleons are not interacting in between their hard collisions. Now their dynamics is governed by the Boltzmann-Uehling-Uhlenbeck equation, which will be discussed in detail in this chapter.
Our approach to nuclear transport is a BUU model called "GiBUU" (i.e. "The Giessen BUU project") [GiB], which has been developed in Giessen for many years. It is a unified transport model which is intended for use with various types of nuclear reactions, including

- elementary eA, γA, νA, pA and πA reactions
- as well as heavy-ion collisions

in a broad energy range (MeV - GeV regime). In this work we will concentrate on elementary reactions (γA and pA) with energies of a few GeV.

2.1 The BUU equation

The general BUU equation, representing the basis of our transport model, is given by

$$\underbrace{[p_0 - H, g^<]}_{=I_V} + \underbrace{[Re(g), \Sigma^<]}_{=I_{off}} = \underbrace{\Sigma^< g^> - \Sigma^> g^<}_{=I_{coll}} \ . \tag{1}$$

Here $g^<$ denotes the Wigner transform of the real-time Green's function, g is the retarded Green's function and $g^>$ represents the density of hole states in phase space. H is the one-particle Hamiltonian, $\Sigma^<$ and $\Sigma^>$ are self energies (gain and loss term). For details see e.g. [Eff99] chapter 2.1 or [Leh03]. A full derivation can be found in [KB94]. The square brackets denote the Poisson brackets, which are defined as

$$[A, B] = \frac{\partial A}{\partial p_\mu}\frac{\partial B}{\partial x^\mu} - \frac{\partial A}{\partial x_\mu}\frac{\partial B}{\partial p^\mu} \ .$$

The BUU equation (1) consists of three parts: The right-hand side is usually called the "collision term", because it governs the decays and collisions of particles. It includes a gain term, which corresponds to the creation of particles, and a loss term, which corresponds to their destruction. The second Poisson bracket on the left-hand side is often referred to as the "off-shell term". It contains the off-shell dynamics of broad resonances. In this chapter we will neglect this term, and come back to it later in chapter 7. Finally, the first Poisson bracket, called the "Vlasov term", is the most basic part of the BUU equation. In the absence of the other terms, it describes the propagation of stable, non-interacting particles through a mean field.
Given $g^<$ and $g^>$, we can introduce the spectral function $\mathcal{A}$ and the width Γ by defining

$$\begin{aligned} \mathcal{A} &\equiv g^> \mp g^< = 2Im(g) \ , \\ \Gamma &\equiv \Sigma^> \mp \Sigma^< = 2Im(\Sigma) \ , \end{aligned}$$

where the upper sign applies to bosons, the lower one to fermions. In addition a phase space distribution function f is assumed to exist, which obeys

$$\begin{aligned} g^< &= f\mathcal{A} \ , \\ g^> &= (1 \pm f)\mathcal{A} \ . \end{aligned}$$

The spectral function can be shown to have a relativistic Breit-Wigner form if one uses a relativistic Hamiltonian:

$$\mathcal{A}(\mu) = \frac{2}{\pi} \frac{\mu^2 \Gamma}{(\mu^2 - M^2)^2 + \mu^2 \Gamma^2} \ .$$

Here the normalization is chosen such that

$$\int \mathcal{A}(\mu) d\mu = 1 \ .$$

The Hamiltonian H in eq. (1) is given in its most general relativistic form by

$$H = \sqrt{(\mu + U)^2 + (\vec{p} - \vec{A})^2} + A^0 \ , \tag{2}$$

with a scalar potential U and a vector potential $A^\mu = (A^0, \vec{A})$.

2.2 Test-Particle Ansatz

To solve the BUU equation numerically one usually makes a "test-particle" ansatz, which means replacing the continuous phase space distribution f by a large number of so-called test particles, whose distributions are given by sharp δ-functions:

$$f(\vec{r}, \vec{p}, t) \rightarrow \sum_i \delta(\vec{r} - \vec{r}_i(t)) \delta(\vec{p} - \vec{p}_i(t)) \ .$$

Also the spectral functions of the test particles are assumed to be δ-functions:

$$\mathcal{A}(\mu, t) \to \sum_i \delta(\mu - m_i(t)) \; .$$

Normally the masses m_i of the test particles should be constant. However, we will see in chapter 7 that in the off-shell propagation scheme the masses may vary for particles traveling through density gradients.
With the two replacements above, the total distribution of the particles, which was called $g^<$ before and which we will call F in the following, becomes

$$F(\vec{r}, \vec{p}, p^0, t) \equiv g^< = f\mathcal{A} \to \sum_i \delta(\vec{r} - \vec{r}_i(t))\delta(\vec{p} - \vec{p}_i(t))\delta(p^0 - p_i^0(t)) \; , \tag{3}$$

where we substituted the δ-function in mass with a δ-function in energy. This is equivalent (apart from normalization, which we left out here anyway), since mass and energy are related by (2).

2.3 Particle Propagation

Before trying to solve the full BUU equation (1), we will start by neglecting both the off-shell term as well as the collision term. This leaves us with the so-called Vlasov equation

$$[p_0 - H, F] = 0 \; , \tag{4}$$

which describes a situation where we have stable, non-interacting particles propagating through a mean field. To find the equations of motion for our test particles, we will have a closer look at this equation by expanding the Poisson bracket:

$$\begin{aligned}
[p_0 - H, F] &= \frac{\partial(p_0 - H)}{\partial p_\mu}\frac{\partial F}{x^\mu} - \frac{\partial(p_0 - H)}{\partial x_\mu}\frac{\partial F}{p^\mu} \\
&= \frac{\partial(p_0 - H)}{\partial p_0}\frac{\partial F}{\partial t} - \frac{\partial(p_0 - H)}{\partial \vec{p}}\frac{\partial F}{\partial \vec{x}} - \frac{\partial(p_0 - H)}{\partial t}\frac{\partial F}{\partial p_0} + \frac{\partial(p_0 - H)}{\partial \vec{x}}\frac{\partial F}{\partial \vec{p}} \\
&= \left(1 - \frac{\partial H}{\partial p_0}\right)\frac{\partial F}{\partial t} + \frac{\partial H}{\partial \vec{p}}\frac{\partial F}{\partial \vec{x}} - \frac{\partial H}{\partial \vec{x}}\frac{\partial F}{\partial \vec{p}} + \frac{\partial H}{\partial t}\frac{\partial F}{\partial p_0} \; .
\end{aligned}$$

From this we can write the time derivative of F as

$$\dot{F} = \frac{1}{1 - \frac{\partial H}{\partial p_0}}\left[\frac{\partial H}{\partial \vec{x}}\frac{\partial F}{\partial \vec{p}} - \frac{\partial H}{\partial \vec{p}}\frac{\partial F}{\partial \vec{x}} - \frac{\partial H}{\partial t}\frac{\partial F}{\partial p_0}\right] \; .$$

On the other hand we can get $\dot{F}$ from the test-particle ansatz (3):

$$\begin{aligned}
\dot{F} &= \frac{\partial F}{\partial \vec{p}_i}\dot{\vec{p}}_i + \frac{\partial F}{\partial \vec{x}_i}\dot{\vec{x}}_i + \frac{\partial F}{\partial p_i^0}\dot{p}_i^0 \\
&= -\frac{\partial F}{\partial \vec{p}}\dot{\vec{p}}_i - \frac{\partial F}{\partial \vec{x}}\dot{\vec{x}}_i - \frac{\partial F}{\partial p^0}\dot{p}_i^0 \; .
\end{aligned}$$

Combining both expressions yields the equations of motion for the test particles:

$$\begin{aligned}
\dot{\vec{x}}_i &= \frac{1}{1-\frac{\partial H}{\partial p_0}} \frac{\partial H}{\partial \vec{p}} , \\
\dot{\vec{p}}_i &= -\frac{1}{1-\frac{\partial H}{\partial p_0}} \frac{\partial H}{\partial \vec{r}} , \\
\dot{p}_i^0 &= \frac{1}{1-\frac{\partial H}{\partial p_0}} \frac{\partial H}{\partial t} .
\end{aligned} \tag{5}$$

The term $\partial H/\partial p_0$ will usually vanish. One of the rare cases where it does not, is when using an "off-shell potential" (see chapter 7). One can see that for $\partial H/\partial p_0 = 0$ the first two become the classical Hamiltonian equations. For $\partial H/\partial t = 0$ the last equation simply enforces energy conservation. In the numerical simulation one has to use discrete time steps, at which collisions can happen. In between the collisions the particles just propagate according to these equations.

2.4 On-Shell Approximation

One can simplify the BUU equation by making the approximation that the width Γ is small, so that all particles sit on their mass shell (i.e. $\mu = M$) and the spectral function becomes a δ-function:

$$\mathcal{A}(\mu) = \delta(\mu - M) .$$

Under this assumption one can show that the "off-shell term" vanishes, and the remainder of the BUU equation can be rewritten in terms of the phase space distribution function f, instead of $g^<$ and $g^>$:

$$\left(\frac{\partial}{\partial t} + \frac{\partial H}{\partial \vec{p}} \frac{\partial}{\partial \vec{r}} - \frac{\partial H}{\partial \vec{r}} \frac{\partial}{\partial \vec{p}} \right) f = \Sigma^<(1 \pm f) - \Sigma^> f . \tag{6}$$

This is the BUU equation in the on-shell approximation. For later use we introduce here a shorthand notation of this equation, labeling the left-hand-side Vlasov operator by D, so that the equation becomes:

$$Df = I_{coll} .$$

2.5 The Collision Term

Up to now we have not explicitly dealt with the fact that there are multiple species of particles involved in the nuclear reactions we want to simulate. There are some "stable" ones (N, Λ, π, K, etc), but also many unstable baryonic and mesonic resonances. In principle each particle species i has a corresponding phase space distribution function f_i, each of which obeys the BUU equation

$$D_i f_i = I_{coll} .$$

So there is actually not only one BUU equation, but many of them. Now without the collision term all particles propagate independently (under the influence of the mean field)

without interacting. But once we turn on the collision term we get interactions between the particles. In this respect the collision term is what couples all the BUU equations together. However, strictly speaking, the BUU equations are already coupled by the mean fields.
Now we can split up the collision term into several components, each characterized by the number of initial state particles which take part in the interaction:

$$I_{coll} = I_1 + I_2 + I_3 + \dots \; .$$

According to this scheme I_1 denotes the "one-body processes" (i.e. particle decays $A \to X$), I_2 stands for the two-body processes $A + B \to X$, and I_3 includes all three-body processes $A + B + C \to X$. In principle there would be also higher terms, but these only play a role at very high densities (see [Lar07]), and are not implemented in GiBUU.
But the collision term is also divided in a different respect, namely in terms of the energy regime: Since GiBUU is a unified transport model which has the ambition to be valid over a large range of energies, not all of the involved processes can be described via the same model. In particular there is a low energy part, where collisions are treated via a resonance model, and a high energy part, which is based on the Lund string model PYTHIA [Py]. The border between both parts is drawn at 2.2 GeV for baryon-meson collisions and at 2.6 GeV for baryon-baryon collision. In the region around this crossover, events from both models are mixed to get a smooth transition.

3 Vector Mesons in Vacuum

Before being able to study the in-medium behavior of vector mesons, one first has to know their vacuum properties. The following table shows some of the characteristics of the ρ, ω and ϕ meson:

	ρ^0	ω	ϕ
M [GeV]	775.5	782.65	1019.46
Γ [MeV]	149.4	8.49	4.26
$c\tau$ [fm]	1.3	23.4	44.4
hadr. BR	2π: 100%	3π: 89%	$2K$: 84%
		$\pi^0\gamma$: 9%	$\rho\pi^0$: 13%
		2π: 2%	3π: 3%
e^+e^- BR	$4.7 \cdot 10^{-5}$	$7.18 \cdot 10^{-5}$	$29.7 \cdot 10^{-5}$

Table 1: Vector meson properties.

Besides their pole mass and width, also the most important decay modes are listed (as implemented in the GiBUU model), which we will discuss now, starting with the hadronic decays, and after that treating the dilepton decays.

3.1 Hadronic Decays

For the parametrization of the hadronic decays of the vector mesons we follow the treatment of Manley [MS92], which assumes that the partial width of a particle V decaying into two particles a and b is given by:

$$\Gamma_{V\to ab}(m) = \Gamma^0_{V\to ab}\frac{\rho_{ab}(m)}{\rho_{ab}(M_0)}.$$

Here m is the actual mass of the particle V, M_0 is its pole mass, $\Gamma^0_{V\to ab} = \Gamma_{V\to ab}(M_0)$ is the partial width at the pole mass and the function ρ_{ab} is defined as:

$$\rho_{ab}(m) = \int dm_a^2 dm_b^2 \mathcal{A}_a(m_a^2)\mathcal{A}_b(m_b^2)\frac{p_f}{m}B_L^2(p_f R).$$

In this formula m_a and m_b denote the masses of the particles a and b (which are integrated over), $\mathcal{A}_a$ and $\mathcal{A}_b$ are their spectral functions and p_f is the final state momentum of a and b in the rest frame of V:

$$p_f^2(m, m_a, m_b) = \frac{1}{2m}\left(m^2 - (m_a + m_b)^2\right)\left(m^2 - (m_a - m_b)^2\right).$$

Finally, L is the orbital angular momentum of a and b in the final state and B_L are the so-called "Blatt-Weisskopf functions". The parameter R is usually called the "interaction radius", which is assumed to be 1 fm. In principle there could be multiple partial waves in the final state with different L, but we only use the lowest possible L which is allowed by angular momentum and parity conservation. The explicit expressions of the first few B_L are the following:

$$
\begin{aligned}
B_0(x) &= 1 \\
B_1(x) &= \frac{x}{\sqrt{1+x^2}} \\
B_2(x) &= \frac{x^2}{\sqrt{9+3x^2+x^4}}
\end{aligned}
$$

A summary plot of the vacuum widths of the vector mesons is shown in figure 1. Alternative parametrization can be found e.g. in [Müh07]/[KKW96]. We chose to use the Manley parametrization, since it has a flatter mass dependence, and therefore works better with our off-shell potential (see chapter 7). And since the mass dependence of this meson width has never really been measured, there is no way to tell which parametrization is the better one.

3.1.1 The ρ meson

The only significant hadronic decay mode of the ρ meson is $\rho \to \pi^+\pi^-$, which has a branching ratio of almost 100%. The general formula shown above can be simplified a lot when applied to the specific case of $\rho \to 2\pi$. This is due to the fact that here the decay products are 'stable' (i.e. with respect to the strong interaction), which means their spectral functions can be approximated by δ-functions and the integrals over m_a and m_b collapse. Furthermore, both decay products have equal masses, so that p_f simplifies to $p_f^2 = m^2/4 - m_\pi^2$. The angular momentum in the final state must be $L = 1$ (neglecting higher partial waves), since the ρ is a vector particle, while the pions are pseudo-scalars. This means that the function ρ_{ab} becomes

$$
\rho_{\pi\pi}(m) = \frac{R^2 p_f^3}{m(1+R^2 p_f^2)}.
$$

Since the 2π decay is the only decay mode of the ρ which is explicitly implemented in our model (the decay into e^+e^- is only implicitly implemented through our dilepton analysis, see chapter 4), we can only treat ρ mesons with masses larger than $2m_\pi$ in the vacuum. Lighter ones can not decay into 2π, and therefore would be practically stable. This means that we have to assume a minimal ρ mass of

$$
\mu_\rho^{min} = 2m_\pi
$$

in the vacuum. As we will see later, this limit will not be valid any more in medium.

3.1.2 The ω meson

The dominant decay channel of the ω meson is $\omega \to \pi^+\pi^-\pi^0$ with a BR of about 90%. Since the Manley analysis only treats two-body final states, we cannot apply it to this three-body decay. Instead we take the three-body decay width formula found in [PDG]:

$$
d\Gamma = \frac{1}{(2\pi)^5}\frac{1}{16M^2}|\mathcal{M}|^2|\vec{p}_1^*||\vec{p}_3|\,dm_{12}\,d\Omega_1^*\,d\Omega_3.
$$

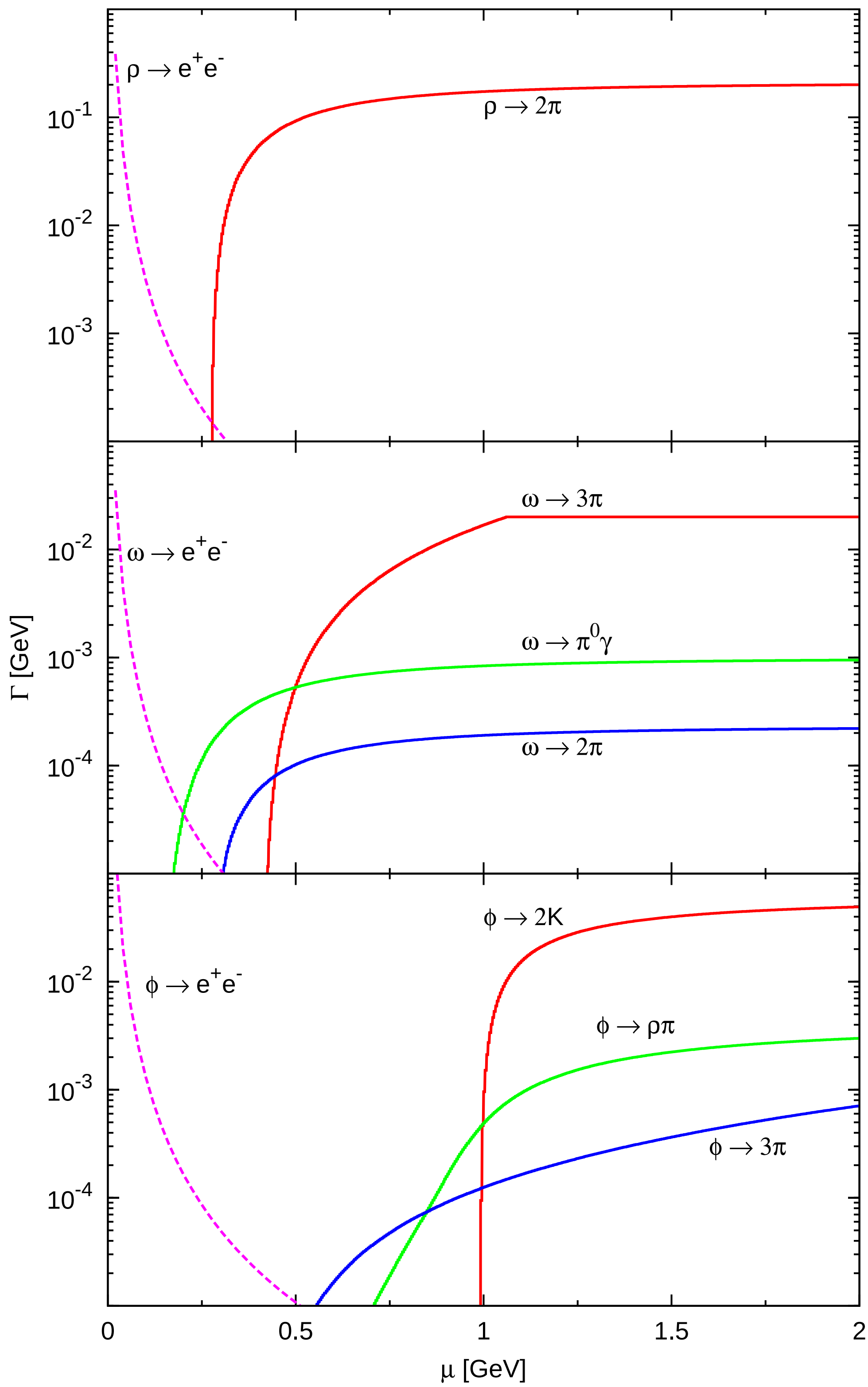

Figure 1: Vacuum decay widths of the ρ, ω and ϕ mesons.

For simplicity we assume the matrix element $\mathcal{M}$ to be constant, and the distribution of the angles Ω_1^* and Ω_3 to be isotropic. If we then forget about overall constant factors, we get the following dependency:

$$\Gamma \propto \frac{1}{M^2} \int |\vec{p}_1^*||\vec{p}_3| dm_{12}.$$

Here $m_{12} = (p_1 + p_2)^2$ is the invariant mass of particle 1 and 2, $|\vec{p}_1^*|$ is their absolute momentum in their CM frame and $|\vec{p}_3|$ is the absolute momentum of particle 3 in the rest frame of the decaying particle. After integrating out m_{12} numerically, this formula gives us the mass dependence of the width, which we normalize to the value at the pole mass. In addition we also limit the $\omega \to 3\pi$ width to values not larger than 20 MeV. This is done in order to avoid problems with the off-shell propagation (see chapter 7), which puts certain restrictions on the behavior of $\partial\Gamma/\partial m$ (i.e. it does not work if $\partial\Gamma/\partial m$ is too large).
The minor decay modes of the ω ($\omega \to \pi^0\gamma$ and $\omega \to \pi^+\pi^-$, both below 10%), are treated via the Manley parametrization (analogous to $\rho \to \pi^+\pi^-$), with $L = 1$ for both.
The lightest decay mode which is implemented for the ω is $\pi^0\gamma$. Therefore ω mesons in the vacuum cannot be lighter than

$$\mu_\omega^{min} = m_\pi \ ,$$

since the vacuum spectral function vanishes below this value.

3.1.3 The ϕ meson

For the ϕ meson, the two-body decays ($\phi \to K\bar{K}$ and $\phi \to \rho\pi$) are again treated via the Manley analysis, while $\phi \to \pi^+\pi^-\pi^0$ is treated analogously to $\omega \to \pi^+\pi^-\pi^0$. The lower limit for vacuum masses here is

$$\mu_\phi^{min} = 3m_\pi.$$

3.2 Leptonic Decays

The leptonic decay widths of the vector mesons can be calculated using the theory of vector meson dominance (VMD), which assumes that the photon couples to hadrons dominantly via an intermediate vector meson. We will discuss here shortly two different flavors of VMD.

3.2.1 Strict VMD

The most radical form of VMD is the so-called strict vector meson dominance, which is sometimes also referred to as the second representation of VMD. It assumes that the photon couples to hadrons exclusively via vector mesons, and is described by the following Lagrangian [OC97]:

$$\mathcal{L}_{sVMD} = -\frac{1}{4}F_{\mu\nu}F^{\mu\nu} - \frac{1}{4}V_{\mu\nu}V^{\mu\nu} + \frac{1}{2}m_V^2 V_\mu V^\mu - gV_\mu J^\mu - \frac{em_V^2}{g_V}V_\mu A^\mu + \frac{1}{2}\left(\frac{e}{g_V}\right)^2 m_V^2 A_\mu A^\mu.$$

Here A_μ is the photon field, $F_{\mu\nu} = \partial_\mu A_\nu - \partial_\nu A_\mu$ its field tensor, V_μ is the vector meson field and J^μ is the hadronic current, describing all hadron fields except the vector mesons. The first two terms in the Lagrangian are simply the kinetic terms of the photon and vector meson fields, the third is the vector meson mass term and the fourth couples the vector mesons to other hadrons (e.g. $\rho \to 2\pi$). The last term is a photon mass term, which is an artifact of this strict VMD model. What is actually most interesting to us is the second-to-last term, which couples the vector meson field to the photon:

$$\mathcal{L}_{\gamma V} = -\frac{e m_V^2}{g_V} A_\mu V^\mu.$$

So the vector mesons can only decay to e^+e^- via an intermediate photon. For a vector meson of mass μ the decay width then is proportional to the squared photon propagator (i.e. $\propto \mu^{-4}$) and a phase space factor, i.e. the final state momentum of the leptons

$$p_f = \sqrt{\mu^2/4 - m_\pi^2} \approx \frac{\mu}{2},$$

which is just linearly proportional to μ if one neglects the pion mass. This means that overall the dilepton decay width is proportional to μ^{-3}, and can be parametrized in the following way:

$$\Gamma_{V\to e^+e^-}(\mu) = C_V \frac{m_V^4}{\mu^3}.$$

Here m_V is the vector meson pole mass, and C_V is a constant which can be determined by the mass and width at the pole (values taken from [PDG]):

V	m_V [MeV]	Γ_{tot} [MeV]	Γ_{ee}/Γ_{tot}	Γ_{ee} [keV]	$C_V = \Gamma_{ee}/m_V$
ρ	775.5	149.4	$4.70 \cdot 10^{-5}$	7.022	$9.055 \cdot 10^{-6}$
ω	782.65	8.49	$7.18 \cdot 10^{-5}$	0.610	$7.789 \cdot 10^{-7}$
ϕ	1019.46	4.26	$29.7 \cdot 10^{-5}$	1.265	$1.241 \cdot 10^{-6}$

Table 2: Dilepton decay constants for $V \to e^+e^-$.

3.2.2 Extended VMD

In addition to strict VMD, there is also an alternative formulation of VMD, commonly referred to as extended VMD or the first representation of VMD. In contrast to strict VMD it does not demand the photon-hadron-coupling to go exclusively via vector mesons. Its Lagrangian has the following form [OC97]:

$$\mathcal{L}_{eVMD} = -\frac{1}{4}F_{\mu\nu}F^{\mu\nu} - \frac{1}{4}V_{\mu\nu}V^{\mu\nu} + \frac{1}{2}m_V^2 V_\mu V^\mu - gV_\mu J^\mu - eA_\mu J^\mu - \frac{e}{2g_V}F_{\mu\nu}G^{\mu\nu}.$$

The first four terms here have already appeared in the sVMD Lagrangian, and it is the last two that make the difference. The second-to-last term is the direct photon-hadron-coupling, which was absent in sVMD, while the last term is the photon-VM-coupling, which here takes a tensor form (with the vector meson field tensor $G_{\mu\nu} = \partial_\mu V_\nu - \partial_\nu V_\mu$).

One virtue of this model is that it does not require a photon mass term (in contrast to sVMD), and in principle it should be considered superior. Using eVMD one can determine the dilepton decay width of the vector mesons to be:

$$\Gamma_{V\to e^+e^-}(\mu) = C_V \frac{\mu}{M_V}.$$

Now the problem is that we actually cannot use the eVMD model in our transport calculation. The reason for this is that here the photon has two ways for interacting with hadrons: the direct coupling and the coupling through vector mesons. To calculate dilepton production rates one would have to add both contributions coherently. But since we use a transport model where the vector mesons are propagated explicitly, this coherent summation is not possible. Therefore we have to use the sVMD width for the dilepton decays of the vector mesons.

4 Dilepton Decays

This chapter will provide some more detail about the physics of dileptons and the most important dileptonic decay modes. As said before, one main aim of studying dileptons is to analyze the properties of vector mesons in nuclear matter. Since the neutral vector mesons ρ^0, ω and ϕ all have a direct decay mode into an electron-positron pair, the invariant mass of the vector meson in nuclear matter can be reconstructed if the dilepton pair is measured. In addition to the direct decay modes some particles also have Dalitz decays involving dileptons, e.g. into $e^+e^-\gamma$ or $e^+e^-\pi^0$. These are not quite as useful as the direct modes, since the invariant mass cannot be reconstructed from the dilepton only, but they are still relevant (at least as a background) and will also be included in the analysis. Apart from the vector mesons, we also include some dileptonic decay channels of the π^0, the η and the $\Delta^{(+,0)}$. Unfortunately, the branching ratios of most dileptonic decays are only in the sub-permille range, which means these events are relatively rare and therefore hard to detect. Nevertheless, there are a number of experiments which have done successful dilepton measurements (see chapter 8). The following table gives a summary of all dileptonic decay modes included in the analysis:

particle	mass [MeV]	width [MeV]	decays	BR
ρ^0	775.5	149.4	$\rightarrow e^+e^-$	$4.7 \cdot 10^{-5}$
ω	782.65	8.49	$\rightarrow e^+e^-$	$7.2 \cdot 10^{-5}$
			$\rightarrow \pi^0 e^+e^-$	$7.7 \cdot 10^{-4}$
ϕ	1019.46	4.26	$\rightarrow e^+e^-$	$2.97 \cdot 10^{-4}$
π^0	134.98	$7.8 \cdot 10^{-6}$	$\rightarrow e^+e^-\gamma$	1.2%
η	547.51	$1.3 \cdot 10^{-3}$	$\rightarrow e^+e^-$	$7.7 \cdot 10^{-5}$
			$\rightarrow e^+e^-\gamma$	0.6%
$\Delta^{(+,0)}$	1232	118	$\rightarrow N^{(+,0)}e^+e^-$	$7.7 \cdot 10^{-4}$

Table 3: Dilepton decays.

4.1 Elementary Cross Sections

In the following elementary cross section formulae will be derived from first principles.

4.1.1 Direct Dilepton Decays

The most important production process of dileptons is the direct decay of a vector meson: $V \rightarrow e^+e^-$. Here the cross section for this process will be calculated, assuming that the vector meson was created by photo-production on a nucleon. This can easily be generalized to other VM-production mechanisms (e.g. proton-induced processes). More details can be found in [Eff99] and [Müh07].
So we want to derive the cross section of a two-stage process: $\gamma N \rightarrow XV \rightarrow Xe^+e^-$. We start by writing the cross section in terms of a matrix element, the phase space and some boosting and normalization factors:

$$d\sigma_{N\gamma\to Xe^+e^-} = \frac{(2\pi)^4}{4|\vec{p}_{N\gamma}|\sqrt{s}}|\mathcal{M}_{N\gamma\to Xe^+e^-}|^2 d\Phi_3(N\gamma\to Xe^+e^-).$$

Now we can (approximately) factorize both the matrix element and the phase space:

$$|\mathcal{M}_{N\gamma\to XV\to Xe^+e^-}|^2 = |\mathcal{M}_{N\gamma\to XV}|^2\cdot|\mathcal{P}_V|^2\cdot|\mathcal{M}_{V\to e^+e^-}|^2$$
$$d\Phi_3(N\gamma\to XV\to Xe^+e^-) = d\Phi_2(N\gamma\to XV)d\Phi_2(V\to e^+e^-)(2\pi)^3 dp_V^2$$

Further we have $dp_V^2 = d\mu^2 = 2\mu d\mu$, where μ is the mass of the vector meson, and the two-particle phase space factor can be evaluated in its CM frame:

$$d\Phi_2(V\to e^+e^-) = \frac{1}{4(2\pi)^6}\frac{|\vec{p}_{e^+e^-}|}{\mu}d\Omega_{e^+e^-}.$$

Also, the matrix element for the leptonic decay of the vector meson can be written in terms of the corresponding width by using:

$$\Gamma_{V\to e^+e^-} = \frac{|\vec{p}_{e^+e^-}|}{8\pi\mu^2}|\mathcal{M}_{V\to e^+e^-}|^2.$$

Moreover, the vector meson propagator

$$\mathcal{P}_V = \frac{1}{M^2 - s - i\sqrt{s}\Gamma_V^{tot}}$$

is related to the spectral function by

$$\mathcal{A}_V = \frac{2\mu}{\pi}Im\mathcal{P}_V = \frac{2\mu^2}{\pi}\Gamma_V^{tot}|\mathcal{P}_V|^2.$$

(Remark: The spectral function is normalized so that $\int\mathcal{A}(\mu)d\mu = 1$.)
So the matrix element becomes

$$|\mathcal{M}_{N\gamma\to XV\to Xe^+e^-}|^2 = |\mathcal{M}_{N\gamma\to XV}|^2\frac{4\pi^2}{|\vec{p}_{e^+e^-}|}\mathcal{A}_V\frac{\Gamma_{V\to e^+e^-}}{\Gamma_V^{tot}}.$$

Now, if we put all this together, the cross section is:

$$\frac{d\sigma_{N\gamma\to XV\to Xe^+e^-}}{d\mu} = \sigma_{N\gamma\to XV}\cdot\mathcal{A}_V(\mu)\cdot\frac{\Gamma_{V\to e^+e^-}(\mu)}{\Gamma_V^{tot}(\mu)}.$$

Here, the cross section $\sigma_{N\gamma\to XV}$ has absorbed the corresponding matrix element and phase space factor, and the angular integration $d\Omega_{e^+e^-} = 4\pi$ has been carried out.

4.1.2 Dalitz Decays

In analogy to the last section, one can compute the cross section for the process $\gamma N\to XQ\to Xe^+e^-Y$, where a particle Q is produced, which has a Dalitz decay mode $Q\to e^+e^-Y$:

$$\frac{d\sigma_{N\gamma\to XQ\to Xe^+e^-Y}}{d\mu} = \int d\mu_Q\mathcal{A}_Q(\mu_Q)\frac{1}{\Gamma_Q^{tot}}\frac{d\Gamma_{Q\to e^+e^-Y}}{d\mu}\sigma_{\gamma N\to XQ}(s)$$

This looks similar to the cross section for the direct dilepton decay, but includes an additional integration over the mass μ_Q of the intermediate particle. For $d\Gamma_{Q\to e^+e^-X}/d\mu$ certain form factors and parametrizations are used, which can be found in [Eff99, chapter 2.7].

4.2 Dilepton Spectra on the Nucleus

Now that we know the cross section for the elementary processes, we have to deal with dilepton production on a nucleus. We calculate this using the GiBUU model, which has been introduced in chapter 2. However, the model includes only hadronic decays explicitly. The dilepton decays are not implemented, since they are so rare. And even if they were implemented, it would take a long time to produce a dilepton spectrum by explicitly letting particles decay into dileptons.
Therefore we use a time integration technique (sometimes called the "shining method"), to compute dilepton spectra. This means that we do not wait for a vector meson to actually decay into a dilepton pair, but continuously integrate up its probability to do such a decay over its whole lifetime. To get the dilepton rate from a vector meson V, one basically has to calculate the following space-time integral:

$$\frac{dN_{V\to e^+e^-}}{d^3p d\mu} = \int_0^\infty dt d^3r \frac{1}{(2\pi)^3} F_V(\vec{r},t,\vec{p},\mu) \frac{\Gamma_{V\to e^+e^-}(\mu)}{\gamma}.$$

Here $F_V(\vec{r},t,\vec{p},\mu)$ is the phase space distribution function of a vector meson V. In principle the time integral has to be done up to infinity, but of course at some point all vector mesons have decayed (implying $F_V = 0$). Actually one can already stop the simulation at some time t_f, where all the mesons have propagated out of the nucleus, since in vacuum the time dependence of the phase space function is simply given by an decaying exponential:

$$F_V(t) = F_V(t_f) \cdot e^{-\Gamma_V(t-t_f)/\gamma}.$$

This means the time integral can be carried out analytically, and one is left with

$$\begin{aligned}\frac{dN_{V\to e^+e^-}}{d^3p d\mu} &= \int_0^{t_f} dt d^3r \frac{1}{(2\pi)^3} F_V(\vec{r},t,\vec{p},\mu) \frac{\Gamma_{V\to e^+e^-}(\mu)}{\gamma} \\ &+ \int d^3r \frac{1}{(2\pi)^3} F_V(\vec{r},t_f,\vec{p},\mu) \frac{\Gamma_{V\to e^+e^-}(\mu)}{\Gamma_V(\mu)}.\end{aligned}$$

For the Dalitz decay of a particle $Q \to e^+e^-X$ one can calculate the dilepton rate analogously to the direct decay, but in addition an integration over the 4-momentum of X has to be performed, which can be rewritten as an integral over the 4-momentum of Q:

$$\frac{dN_{Q\to e^+e^-X}}{d^3p d\mu} = \int_0^\infty dt d^3r \frac{d^3p_Q}{(2\pi)^3} d\mu_Q F_Q(\vec{r},t,\vec{p}_Q,\mu_Q) \frac{1}{\gamma} \frac{d\Gamma_{Q\to e^+e^-X}(\mu)}{d^3p d\mu}.$$

To sum up, the fig. 2 gives an overview over all hadronic contributions to the dilepton spectrum for the example of a γC reaction with a photon energy of 1.5 GeV.
However, this is not the full story yet. This plot has been obtained by using the vacuum spectral functions for the production of vector mesons inside the nucleus. Consequently,

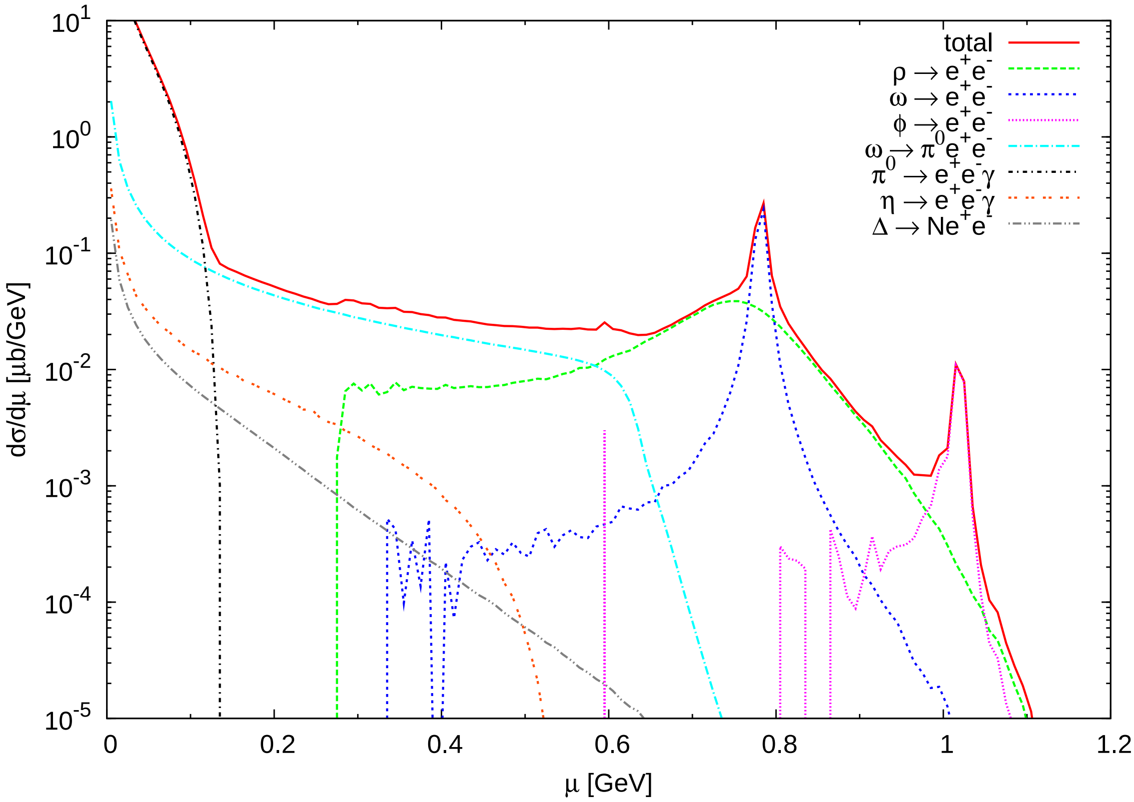

Figure 2: Dilepton spectrum for $\gamma + C$@1.5 GeV (vacuum spectral functions).

one can see that e.g. for the ρ channel, there is a sharp cutoff at $\mu = 2m_\pi$, since the ρ decays almost exclusively into $\pi^+\pi^-$, so below the 2π threshold the vacuum spectral function of the ρ is assumed to be zero. Analogously the threshold for the ω lies at $\mu = m_\pi$, and for the ϕ at $\mu = 3m_\pi$ (those can not be observed in the plot due to low statistics). Also one can see that the spectra of the direct decays are proportional to the VM spectral function, but weighted with a factor μ^{-3}, so that the lower end of the spectrum gets boosted significantly.

In a full-featured analysis one would have to include additional medium effects like a broadening of the vector meson width inside the nucleus, due to collisions with the nucleons (see chapter 5). This would mean that in the medium the spectral function would not vanish any more below their vacuum thresholds, and we could produce e.g. ρ mesons with $\mu < 2\pi$ inside the nucleus. If such a particle would propagate out into the vacuum, it would be stable with respect to strong decays (and, therefore, very long-lived). To solve this problem, one has to take care of a correct description of the propagation of "off-shell" particles (i.e. particles with masses far from the pole mass), and in particular their mass evolution when traversing density gradients. This will be done in chapter 7. After these issues have been dealt with, we will present some full in-medium spectra for various reactions in chapter 11.

4.3 Coulomb Corrections

In principle the leptons are deflected by the Coulomb interaction while leaving the nucleus. However this only gives very small deviations in the dilepton spectra, even for heavy nuclei, and can be neglected in most cases.
In [Müh07, chapter 6.4] it has been estimated that the invariant mass deviation which is caused by Coulomb corrections is usually less than 1 MeV, which is smaller than the experimental resolution of most detectors. Therefore we safely neglect Coulomb corrections throughout this work.

5 In-Medium Effects

Since we want to learn about in-medium properties of vector mesons, we have to study how these properties change when going from vacuum into the nuclear medium. The first thing one can think of are standard nuclear many-body effects, which imply a broadening of the meson width due to collisions with nucleons, as well as a possible appearance of additional peaks in the mass spectrum through coupling to baryonic resonances. On top of these rather well-known effects a possible shift of the pole mass in the medium has been predicted (see [BM88, BR91, HL92, LPM98]), which could be connected to the (partial) restoration of chiral symmetry in the medium.

5.1 Collisional Broadening

The width of mesons traveling through the medium is modified, because the mesons interact with the nucleons and their collisions generate an additional contribution to their full width, which is then given by the sum of the vacuum decay width and the collisional width:

$$\Gamma_{tot}(\mu, |\vec{p}|, \rho) = \Gamma_{vac}(\mu) + \Gamma_{coll}(\mu, |\vec{p}|, \rho) \ .$$

Since this additional contribution is generated by the interaction between the mesons and the nucleons of the surrounding medium, we first examine the cross sections for this interaction.

5.1.1 VN Cross Sections

In our transport model, several processes are implemented which contribute to the cross section of collisions between nucleons and vector mesons. For the ρ meson, these are

$$\begin{aligned} \rho N &\rightarrow \pi N \\ &\rightarrow \rho N \\ &\rightarrow R \ . \end{aligned}$$

The last one denotes the excitation of the nucleon into any baryonic resonance R. This actually represents the dominant contribution to the ρN cross section, and has several components, most notably the $D_{13}(1520)$, $S_{31}(1620)$ and $D_{33}(1700)$. Also the elastic process $\rho N \rightarrow \rho N$ is assumed to go via an intermediate resonance: $\rho N \rightarrow R \rightarrow \rho N$.
All resonance cross sections $\sigma_{ab \rightarrow R}$ in our model are computed from the corresponding partial widths $\Gamma_{R \rightarrow ab}$ (see [Eff99, ch. 2.4.1]), which in turn are taken from the Manley analysis [MS92].
Figure 3 shows the total VN cross sections with respect to mass and momentum of the vector meson, assuming a nucleon at rest. For the ρ meson one can recognize three ridges, which are the contributions of the aforementioned resonances, running along lines of constant $\sqrt{s}$. For large energies the Donnachie-Landshoff parametrization is used [DL95]

$$\sigma_{VN} = X s^{\epsilon} + Y s^{-\eta} \ ,$$

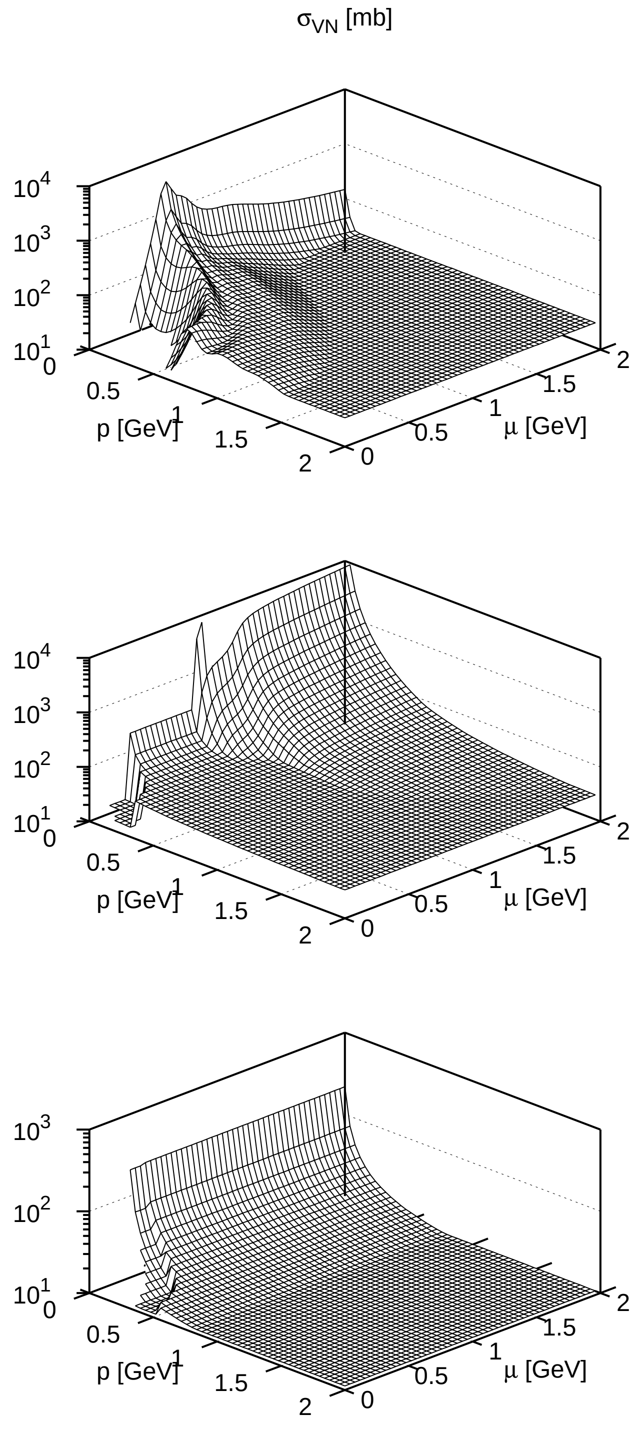

Figure 3: ρN, ωN and ϕN cross sections.

which is motivated by Regge theory. The first term represents Pomeron exchange and the second one ρ, ω, f, a exchange. The two constants $\epsilon = 0.0808$ and $\eta = 0.4525$ are the same for all processes, while the parameters X and Y are being fit separately for ρN, ωN and ϕN. In the plotted region the parametrization is almost constant and produces the flat plane above the resonance region.
For the ω meson, the following processes are included:

$$\begin{aligned} \omega N &\rightarrow \pi N \\ &\rightarrow \pi\pi N \\ &\rightarrow \omega N \\ &\rightarrow R\,. \end{aligned}$$

The cross section for the πN channel is obtained via detailed balance from the inverse reaction

$$\sigma_{\omega N \rightarrow \pi N} = \frac{1}{3}\frac{p_f^2}{p_i^2}\sigma_{\pi N \rightarrow \omega N},$$

where the parametrizations by Golubeva are used for $\sigma_{\pi N \rightarrow \omega N}$ [Gol97]. For the elastic ωN channel the parametrization by Lykasov are used [Lyk99]:

$$\begin{aligned} \sigma_{\omega N}^{el} &= [5.4 + 10 \cdot \exp(-0.6p)] \text{ mb}\,, \\ \sigma_{\omega N}^{inel} &= \left[20 + \frac{4}{p}\right] \text{ mb}\,. \end{aligned}$$

They only depend on the laboratory momentum p of the ω meson. The inelastic parametrization is used for the $\pi\pi N$ channel, whose cross section we assume to be

$$\sigma_{\omega N \rightarrow \pi\pi N} = \sigma_{\omega N}^{inel} - \sigma_{\omega N \rightarrow \pi N}.$$

Recently there are indications that the parametrization of the inelastic ωN cross section by Lykasov may be too small by a factor of ≈ 3 [Kot08], but this has not yet been incorporated in our analysis. The resonance contributions for the ω interfere strongly among each other, and it is hard to make out individual contributions.
The ϕN cross section has the following components in our model:

$$\begin{aligned} \phi N &\rightarrow \pi N \\ &\rightarrow \pi\pi N \\ &\rightarrow \phi N\,. \end{aligned}$$

For all of these the Golubeva parametrizations have been used. For the ϕ no resonance contributions are implemented.

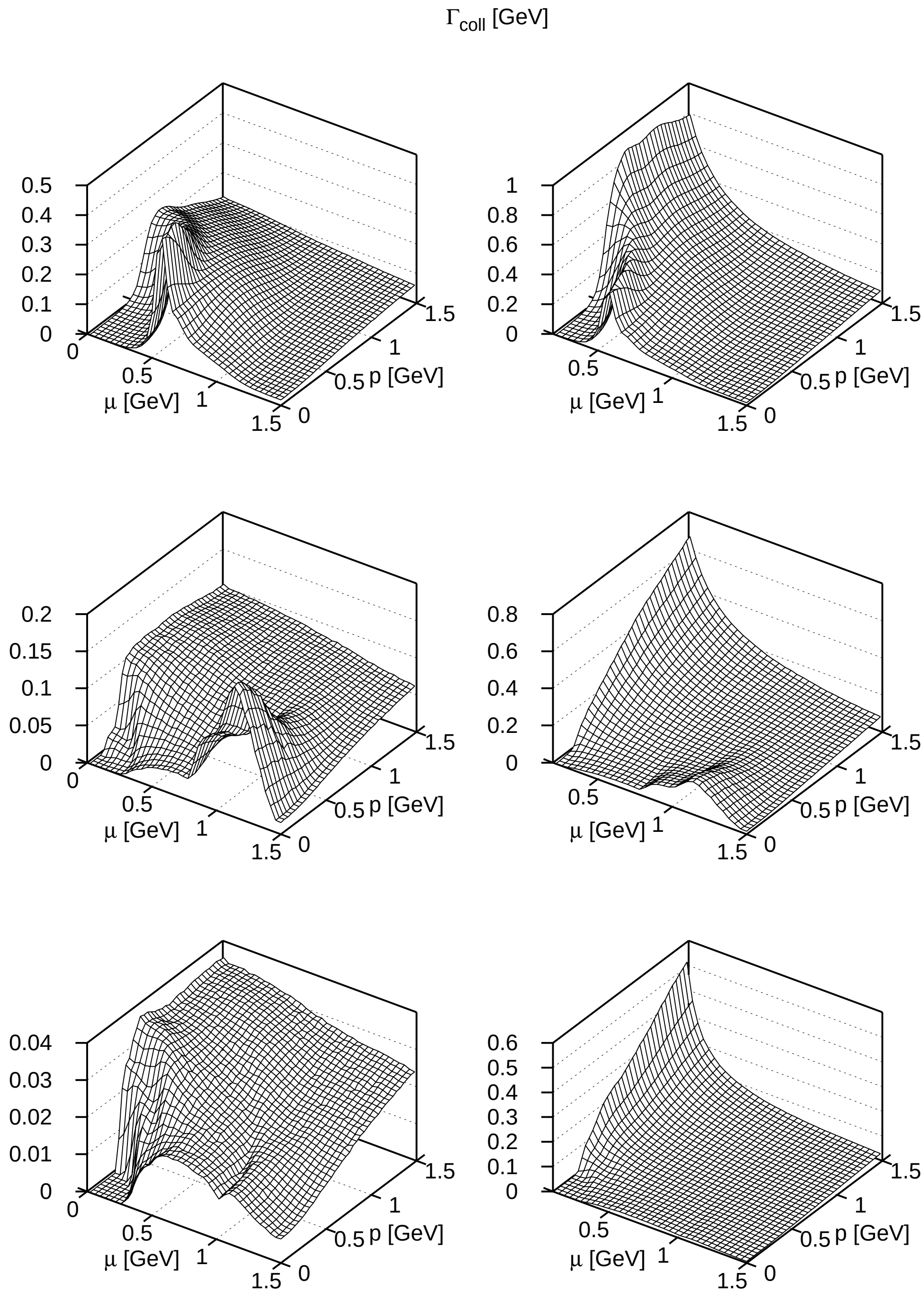

Figure 4: Collisional width of the ρ, ω and ϕ meson (from top to bottom) at density ρ_0 in the lab frame (left) and in the meson rest frame (right).

5.1.2 Collisional Width

Assuming infinite nuclear matter, low density and zero temperature, the collisional width in the rest frame of the nucleus (which is usually identical to the "laboratory frame") can be calculated as follows:

$$\Gamma_{coll} = \rho < v_{rel}\sigma_{VN} > . \tag{7}$$

Here the brackets indicate a momentum integral over the Fermi sphere, ρ denotes the density, v_{rel} is the relative velocity of the scattering partners, σ_{VN} is the inclusive cross section for the collision of a nucleon N and a vector meson V. A full derivation of this formula can be found in [Eff99, chapter 2.4.2].
The in-medium width plays an important role for two different effects: The first one is off-shell propagation (see chapter 7), where the in-medium width is needed in the lab frame, as displayed in eq. (7). In addition to this we also need the in-medium width for in-medium spectral functions, according to which we assign the masses of particles which are produced inside the nucleus (see chapter 6). For this purpose the in-medium width is needed in the meson rest frame, which is related to eq. (7) by a simple Lorentz factor:

$$\Gamma^{(RF)} = \gamma \cdot \Gamma^{(lab)} .$$

In principle the collisional width depends on the mass and absolute momentum of the meson as well as the proton and neutron density in the medium: $\Gamma_{coll}(m, |\vec{p}|, \rho_p, \rho_n)$. Figure 4 shows the mass and momentum dependence of the collisional width for the ρ, ω and ϕ meson at normal nuclear density $\rho_0 = 0.17\,\mathrm{fm}^{-3}$ (in isospin symmetric nuclear matter, where $\rho_p = \rho_n = \rho_0/2$), both in the meson's rest frame and the laboratory frame. The density dependence is not shown here, but can be assumed to be linear according to eq. (7), apart from some Pauli blocking effects.
For the ρ meson the large bump is the contribution of the $D_{13}(1520)$ resonance. The other resonance contributions (mentioned above) are too small to be recognized in a linear plot.

5.2 Pole Mass Shift

In addition to the effects discussed in the last section, also a shift of the pole mass has been predicted for vector mesons in the medium. This has first been claimed by Bernard and Meissner [BM88], and was later investigated by Brown and Rho [BR91], who used an effective Lagrangian approach to predict that the pole mass of the vector mesons should drop by about 20% at normal nuclear density, based on the assumption of chiral symmetry restoration:

$$\frac{m_V^*(\rho_0)}{m_V} \approx 0.8 .$$

Just shortly after them Hatsuda and Lee came to a similar result using QCD sum rules [HL92]. They derived a linear scaling law of the pole mass with respect to density:

$$\frac{m_V^*(\rho)}{m_V} \approx 1 - \alpha \frac{\rho}{\rho_0} . \tag{8}$$

In their theory the parameter α was estimated to be $\alpha = 0.16 \pm 0.06$, which is consistent with the $\alpha = 0.20$ of Brown and Rho. However, Hatsuda and Lee assumed the ρ spectral function to be a simple δ-function in their analysis.

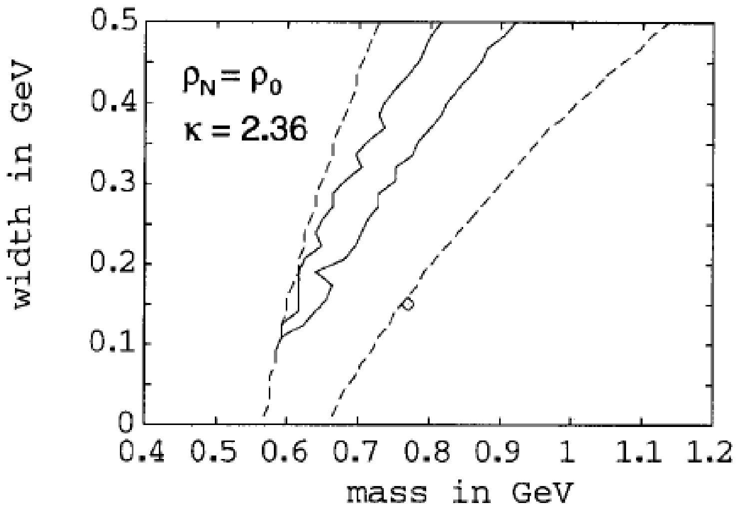

Figure 5: Constraints on in-medium properties of the ρ meson via QCD sum rules [LPM98].

Later it was found by Leupold and Mosel [LPM98] that QCD sum rules can not only be satisfied by a simple mass shift as proposed by Hatsuda/Lee, but also by a combination of mass shift and a simultaneous broadening of the width. They assumed a Breit-Wigner spectral function, and could constrain the allowed values of in-medium pole mass and width to a certain band, as shown in figure 5 for the ρ meson at nuclear saturation density ρ_0 (where the vacuum values are marked by a dot). For the dashed band the sum rule is fulfilled with a deviation of $d \leq 1\%$, for the full band the deviation is $d \leq 0.2\%$. Both use a Borel window of $\Delta M^2 \geq 0.6\,\text{GeV}^2$. The parameter κ parametrizes the deviation of the the four-quark condensate from a product of two-quark condensates, and characterizes one of the three parameter sets examined in [LPM98].
This band of allowed values leaves room for various scenarios: One possibility to fulfill the sum rule would be the pure dropping mass scenario as predicted by Brown/Rho and Hatsuda/Lee, another one would be an increase of the width while the pole mass is left unchanged. And in principle also an increasing pole mass is possible if the increase in width is large enough.
Such a rising ρ mass has been proposed e.g. in [Pis95], motivated by the idea that the ρ might become degenerate with the heavier a_1 if chiral symmetry is restored. However, such an upward shift seems rather unlikely in the sum rule analysis of [LPM98], since it would require a very large width. If we assume a typical value of $\Gamma_{coll} \approx 100$ MeV for the ρ meson (as predicted by our model), we arrive at a total in-medium width of $\Gamma_{tot} \approx 250$ MeV, which would be consistent with a downward mass shift on the order of roughly 10-15%.
In our simulations we include the possibility of an in-medium mass shift of the vector mesons through a density dependent scalar potential

$$V_S = -\alpha M_V \frac{\rho(\vec{r})}{\rho_0} ,$$

where α denotes the mass shift parameter in the notation of Hatsuda/Lee, M_V is the vacuum pole mass of the vector meson V, and $\rho_0 = 0.168\,\mathrm{fm}^{-3}$ is the nuclear saturation density. This scalar potential results in a Hamiltonian

$$H = \sqrt{(\mu + V_S)^2 + \vec{p}^{\,2}} ,$$

and has the effect that the vector mesons acquire an effective in-medium mass of

$$\mu^* = \mu + V_S .$$

In particular the in-medium pole mass becomes

$$\mu_0^* = \left(1 - \alpha \frac{\rho(\vec{r})}{\rho_0}\right) M_V .$$

This exactly corresponds to the prediction (8) of Hatsuda/Lee. We also use their value of $\alpha = 0.16$ in our simulations, which may or may not be the true value. Most experiments measure a smaller value of α, if any.
We use the same value of α for all three vector mesons, while in principle there is no reason that it should be equal for all of them. So instead of one parameter α, one may have three distinct parameters α_ρ, α_ω and α_ϕ.

6 Final State Decisions

One non-trivial part of the collision term is choosing masses and momenta for final state particles. This is easy if only stable particles are produced, since their masses are fixed. But if there are unstable particles in the final state, which have a finite width, we have to choose the final state by Monte Carlo decision according to the differential cross section of the process. To accomplish this, we use standard statistical techniques, precisely speaking a combination of the inversion method and the rejection method, see e.g. [Dev86]. Since this is a very basic and important part of the numerical simulation, which is being performed very frequently, one has to make sure that it is done in a very efficient way. For these reasons it is worth to investigate this problem in detail.

6.1 Two-body Final States

As shown in [Leh03, chapter 4.7], the differential cross section for two-body final states can be expressed as

$$\frac{d\sigma_{X\to ab}}{d\mu_a d\mu_b d\Omega} = \frac{1}{64\pi^2 s}\frac{p_{ab}}{p_i}\mathcal{A}_a(\mu_a)\mathcal{A}_b(\mu_b)|\mathcal{M}_{X\to ab}(s)|^2. \tag{9}$$

Here, $\sqrt{s}$ is the total energy in the center-of-mass (CM) frame, p_{ab} is the CM momentum in the final state, while p_i is the CM momentum in the initial state. The spectral functions here should be normalized to $\int \mathcal{A}(\mu)d\mu = 1$.

Now the probability for selecting any final state is proportional to the differential cross section, and we can simply forget about any factors which are constant or already fixed by the initial state (e.g. s, p_i and $\mathcal{M}_{X\to ab}(s)$):

$$\frac{d\sigma_{X\to ab}}{d\mu_a d\mu_b d\Omega} \;\propto\; p_{ab}\mathcal{A}_a(\mu_a)\mathcal{A}_b(\mu_b) = p_{ab}\prod_i \mathcal{A}_i(\mu_i).$$

Of course the product runs over $i = a, b$. Since we do not care about constant factors, the spectral functions can be conveniently normalized to $\mathcal{A}_i(M_i) = 1$, where M_i is the pole mass and $\Gamma_i^0 = \Gamma_i(M_i)$ is the pole width:

$$\mathcal{A}_i(\mu) = \frac{\mu^2\Gamma_i^0\Gamma_i(\mu)}{(\mu^2 - M_i^2)^2 + \mu^2\Gamma_i^2(\mu)}.$$

Here we will start with the assumption that the spectral functions only depend on the mass μ. This is not true any more if one takes into account collisional widths in the medium (where they can also depend on the absolute momentum $p = |\vec{p}|$), which will be discussed later.

According to eq. (9), the final state is fixed by choosing the masses μ_a and μ_b and the solid angle Ω in the CM frame, and in principle one has to choose the masses μ_a and μ_b according to the spectral functions. However, this is not directly possible, since one can not write down an analytic integral of the relativistic Breit-Wigner function (not even if the width is constant). This can only be done for the non-relativistic Breit-Wigner function, which we start with as an approximation. By a change of variable

$$y_i = 2\arctan\left[2\frac{\mu_i - M_i}{\Gamma_i^0}\right], \tag{10}$$

it follows that

$$\frac{dy_i}{d\mu_i} = \frac{\Gamma_i^0}{(\mu_i - M_i)^2 + (\Gamma_i^0/2)^2},$$

which we normalize to

$$\mathcal{B}_i \equiv \frac{\Gamma_i^0}{4}\frac{dy_i}{d\mu_i} = \frac{(\Gamma_i^0/2)^2}{(\mu_i - M_i)^2 + (\Gamma_i^0/2)^2}.$$

This is just the non-relativistic Breit-Wigner function, with $\mathcal{B}_i(M_i) = 1$. If we now choose y_i from a flat distribution, we get μ_i by inverting (10), which is then distributed according to the non-relativistic Breit-Wigner function. Rewriting the cross section in terms of the y_i yields

$$\frac{d\sigma_{X\to ab}}{dy_a dy_b d\Omega} \propto p_{ab}\prod_i \mathcal{A}_i(\mu_i)\frac{d\mu_i}{dy_i} = p_{ab}\prod_i \frac{\mathcal{A}_i(\mu_i)}{\mathcal{B}_i(\mu_i)}.$$

This is as far as we get analytically (via the inversion method). The rest has to be done with the numerical rejection method, for which we need to guess the maximum of the above expression as precisely as possible. This is easy for the pre-factor p_{ab}, whose maximum can simply be obtained by kinematics, but for $\mathcal{A}_i/\mathcal{B}_i$ it may be quite hard in general (at least it can be done for each particle separately). To make an educated guess for this maximum, we take a look at the ratio $\mathcal{Q}_i(\mu_i) \equiv \mathcal{A}_i(\mu_i)/\mathcal{B}_i(\mu_i)$ for the special case of a constant width Γ_i.

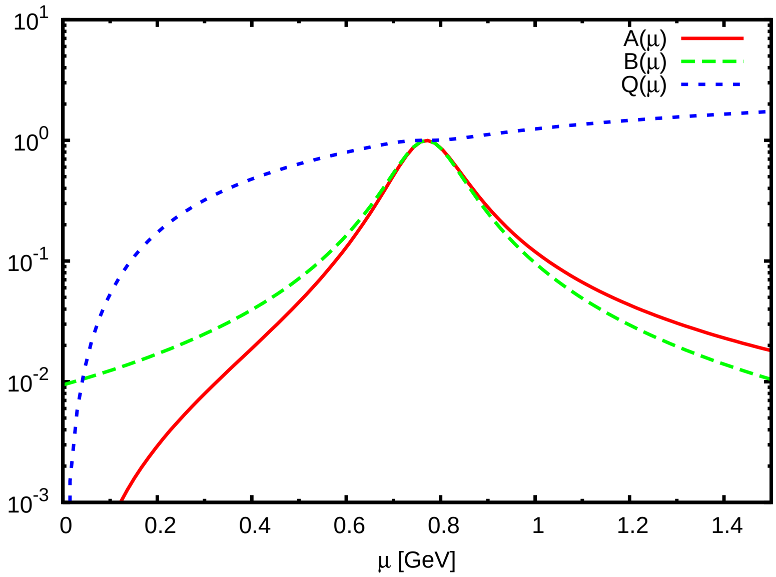

Figure 6: Relativistic and non-relativistic Breit-Wigner spectral functions and their ratio for the ρ meson with a constant width of $\Gamma = 150\,\mathrm{MeV}$.

One can show that under these conditions $\mathcal{Q}$ obtains its maximal value for $\mu \to \infty$:

$$\mathcal{Q}_{max} = \lim_{\mu \to \infty} \mathcal{Q}(\mu) = 4.$$

Knowing this maximum, the probability for accepting any μ in the final state is given by

$$\mathcal{P} = \mathcal{Q}(\mu)/\mathcal{Q}_{max}.$$

However, in general masses can not be infinitely large, but are constrained by kinematical conditions ($\mu < \mu_{max}$), so that the actual maximum may be smaller than 4. As one can see from fig. 6, $\mathcal{Q}$ is rising monotonously in μ, which means that the actual maximum is given by

$$\mathcal{Q}_{max} = \mathcal{Q}(\mu_{max}).$$

However, this approach is based on the assumption that $\Gamma = const$, and may not be true in the general case. But still it is a good first approximation, and much more efficient than just boldly assuming $\mathcal{Q}_{max} = 4$ (which also holds only for $\Gamma = const$). To account for the effects of mass-dependent width $\Gamma_i(\mu)$, one can just introduce a scaling factor c_i, which depends on the particle species and its width:

$$\mathcal{Q}_{max} = c_i \mathcal{Q}(\mu_{max}).$$

The constant c_i can be determined for each particle species by trial and error.
To sum up, we can choose a final state in the following way:

1. Generate a random y_i from a flat distribution.

2. Calculate μ_i, which then is distributed according to a non-relativistic Breit-Wigner distribution (as a first approximation).

3. The rejection method tells us that the probability for accepting this μ_i as the correct final state mass is given by $\mathcal{P}_i = \mathcal{Q}_i(\mu_i)/\mathcal{Q}_{max}$, which gets us from the non-relativistic to the relativistic Breit-Wigner distribution.

4. All this has to be done for both particles simultaneously, and the total probability for accepting the generated final state is given by $\mathcal{P}_{tot} = \mathcal{P}_a \mathcal{P}_b \cdot p_{ab}/p_{ab}^{max}$.

In the common case that particles are produced inside the nucleus, one of course has to use the full in-medium width (i.e. the sum of vacuum width and collisional width). This introduces the additional subtlety that the spectral function depends not only on mass, but also on momentum. However, this can be handled in the exact same way as before, with adjusted scaling factors c_i.
Another thing one has to take care of for in-medium production is that the usual minimal mass limits are not valid any more, since particles acquire an in-medium width which is non-vanishing down to $\mu = 0$, even if their vacuum width is negligible below a certain threshold (cf. chapter 3). Therefore we can not use the vacuum thresholds for in-medium production, and instead have to assume a threshold of $\mu_{min} = 0$.

6.2 Three-body Final States

The differential cross section for three-body final states can be written as:

$$\frac{d\sigma_{X\to abc}}{d\mu_a d\mu_b d\mu_c d|\vec{p}_a| d\Omega_a d|\vec{p}_b| d\phi_b} = \frac{1}{8(2\pi)^5 s}\frac{1}{p_i\sqrt{s}}\frac{|\vec{p}_a||\vec{p}_b|}{E_a E_b}\mathcal{A}_a(\mu_a, p_a)\mathcal{A}_b(\mu_b, p_b)\mathcal{A}_c(\mu_c, p_c) \times|\mathcal{M}_{X\to abc}(s)|^2$$

Analogously to the two-body final states, we can again drop out constant factors, and make a change of variables $\mu_i \to y_i$:

$$\frac{d\sigma_{X\to abc}}{dy_a dy_b dy_c d|\vec{p}_a| d\Omega_a d|\vec{p}_b| d\phi_b} \propto \frac{|\vec{p}_a||\vec{p}_b|}{E_a E_b}\prod_i \frac{\mathcal{A}_i(\mu_i, p_i)}{\mathcal{B}_i(\mu_i)}.$$

In this case we need to choose eight values to fix the final state: the three masses, $|\vec{p}_a|$, Ω_a, $|\vec{p}_b|$ and ϕ_b. In principle this is done in the same way as for the two-body case: First make the transformation $\mu_i \to y_i$ and then use the rejection method. Also the same considerations for finding the maximum can be applied here, one just has a different pre-factor.

7 Off-Shell Transport

Our discussion of the transport model in chapter 2 was based on the on-shell approximation, and did not include any off-shell dynamics, i.e. particles were assumed to sit on their mass-shell, and their width was neglected. In this chapter we want to go beyond this approximation and try to treat off-shell particles in the right way, which is particularly important for our treatment of the vector mesons, since especially the ρ meson has a very large width. This is not a trivial task, and different solutions have been proposed.

7.1 Off-Shell Equations of Motion

7.1.1 Non-Relativistic Kinematics

To include the full off-shell dynamics of particles with large widths, one would like to solve the general BUU equation (1) with a test-particle ansatz (3). This has been done in [Leu00] using non-relativistic kinematics, which yields the following equations of motion for the test-particles:

$$\begin{aligned}
\dot{\vec{r}}_i &= \frac{\vec{p}_i}{m} + \frac{1}{2m}\frac{\partial}{\partial \vec{p}_i} Re(\Sigma_i) + \frac{\Delta E_i}{\Gamma_i}\frac{\partial \Gamma_i}{\partial \vec{p}_i} \,, \\
\dot{\vec{p}}_i &= -\frac{1}{2m}\frac{\partial}{\partial \vec{r}_i} Re(\Sigma_i) - \frac{\Delta E_i}{\Gamma_i}\frac{\partial \Gamma_i}{\partial \vec{r}_i} \,, \\
\frac{d}{dt}(\Delta E_i) &= \frac{\Delta E_i}{\Gamma_i}\dot{\Gamma}_i \,.
\end{aligned} \tag{11}$$

One can see that assuming $\Gamma_i = const.$ turns this into the classical Hamiltonian EOM [cf. eq. (5)], with a non-relativistic Hamiltonian $H_i = (\vec{p}_i^{\,2} + Re(\Sigma_i))/2m$. In addition each equation now includes a term which depends on the width via its space and momentum gradients or its time derivative. Here $\Delta E_i = E_i - H_i$ denotes the deviation from the "on-shell" energy (called the "off-shellness"). From the last equation we see that in contrast to the classical equations, the energy and mass of the test particles now changes with time when the width Γ changes (e.g. when the particle travels through a medium with density gradients). The last equation also implies that

$$\frac{d}{dt}\left(\frac{\Delta E_i}{\Gamma_i}\right) = 0, \tag{12}$$

so that $\Delta E_i/\Gamma_i = const.$ This is an important fact, which we will come back to later.

7.1.2 Relativistic Kinematics

In addition to this non-relativistic treatment, a solution for the general BUU equation via the test-particle ansatz has also been found using relativistic kinematics (see [CJ00a],[CJ00b]):

$$\begin{aligned}
\dot{\vec{r}}_i &= \frac{\vec{p}_i}{E_i} + \frac{1}{2E_i}\left[\frac{\partial}{\partial \vec{p}_i} Re(\Sigma_i) + \frac{m_i^2 - M^2}{\Gamma_i}\frac{\partial \Gamma_i}{\partial \vec{p}_i}\right] , \\
\dot{\vec{p}}_i &= -\frac{1}{2E_i}\left[\frac{\partial}{\partial \vec{r}_i} Re(\Sigma_i) + \frac{m_i^2 - M^2}{\Gamma_i}\frac{\partial \Gamma_i}{\partial \vec{r}_i}\right] , \\
\frac{d}{dt}(m_i^2) &= \frac{m_i^2 - M^2}{\Gamma_i}\dot{\Gamma}_i .
\end{aligned} \tag{13}$$

These relativistic equations of motion are similar in structure to the non-relativistic ones and contain them as a limiting case. Here a relativistic Hamiltonian $H_i = E_i = \sqrt{m_i^2 + \vec{p}_i^{\,2} + Re(\Sigma_i)}$ is used.

7.2 Off-Shell Potential

Instead of directly using the equations of motion, one can emulate them by introducing a so-called "off-shell potential". This method has been developed in [Eff99] and assumes the mass of a test-particle to be $\mu = m_0 + \Delta\mu$, where m_0 denotes the pole mass and $\Delta\mu$ is the so-called "off-shellness". Due to the way that this off-shellness enters the Hamiltonian, it can be viewed as a scalar potential, hence the name "off-shell potential":

$$H = \sqrt{\mu^2 + \vec{p}^{\,2}} = \sqrt{(m_0 + \Delta\mu)^2 + \vec{p}^{\,2}} . \tag{14}$$

Since the off-shellness is treated like a normal scalar potential, this method is inherently energy conserving. Now one demands that

$$\frac{\Delta\mu}{\Gamma_{tot}}(t) = const. \tag{15}$$

In the non-relativistic limit this is equivalent to eq. (12), since $\Delta\mu = \Delta E$. Then the time development of the off-shellness is given by

$$\Delta\mu(t) = \frac{\Delta\mu(t_0)}{\Gamma_{tot}(t_0)}\Gamma_{tot}(t) . \tag{16}$$

This method by construction obeys the last equation of (11), and can be shown to fulfill also the first two, see [Leh03, chapter 5.2]. In this sense the off-shell potential is "non-relativistic" (although we use a relativistic Hamiltonian), since it obeys the non-relativistic EOM (and not the relativistic ones). Moreover it has been mentioned in [Leh03] that it is not possible to find a potential which obeys the relativistic EOM.
It is important to note here that the width Γ_{tot} has to be evaluated in the same reference frame at all times t and t_0, otherwise $\Delta\mu$ is no Lorentz scalar. Consequently, one may not choose this frame to be the rest frame of the particle, since the momentum of the particle may change, causing its rest frame at time t to differ from its rest frame at time t_0. Therefore the most obvious choice of reference frame is the "laboratory" frame, i.e. the rest frame of the nucleus, in which we will always evaluate the total width Γ_{tot} in eq. (16).

Often the additional assumption is made that the width Γ_{tot} is proportional to the density ρ (i.e. neglecting the vacuum width and using a low-density approximation), which implies that the time development of the off-shellness can be simplified to

$$\Delta\mu(t) = \Delta\mu(t_0)\frac{\rho(t)}{\rho(t_0)} \ .$$

Both [Eff99] and [Leh03] work under this assumption. It is easier to implement numerically, since the density $\rho = \rho(\vec{r})$ only depends on the spatial coordinate, and not on momentum. This assumption has the following limitations: If a particle (which has been produced in the medium) propagates out into the vacuum, the density gradually goes to zero, and therefore the off-shellness goes to zero and the mass simply becomes the pole mass (since the vacuum width was neglected). This is fine for stable particles with vanishing vacuum width, but for particles with finite lifetime and large width (like the ρ) it is problematic, since their vacuum spectral function does not restrict all particles to be on-shell.

In this thesis we follow the treatment of [Bu08], working with the more general off-shell potential (16), without assuming $\Gamma_{tot} \propto \rho$. For the sake of a clear notation, we introduce an abbreviation for the constant factors in (16):

$$X_{off} \equiv \frac{\Delta\mu(t_0)}{\Gamma_{tot}(t_0)} = const.$$

This so-called "off-shell parameter" is constant for each test-particle, and can be determined from the initial conditions at the creation of the particle. It enables us to re-write the mass as

$$\mu = m_0 + \Delta\mu = m_0 + X_{off}\Gamma_{tot}(t) \ .$$

Here the mass evolution also depends on the momentum of the particle, since the collisional width depends on momentum (see chapter 5): $\Gamma_{tot} = \Gamma_{tot}(\rho_n, \rho_p, \mu, |\vec{p}|)$. This introduces additional subtleties in the numerical implementation, since we have to deal with a momentum-dependent potential.

In [Leh03] the off-shell potential method has been compared numerically to the predictions of the fully relativistic equations of motion (13), and (at least for the nucleon) only slight discrepancies have been found.

However, for vector mesons like the ρ the non-relativistic treatment via the off-shell potential is not expected to work as nicely, since the ρ is rather light and has a large width. Hence the assumptions of small velocity and small width are questionable.

7.3 Problem: Tachyonic Particles

In section 2.3 we showed that in the framework of the BUU model the velocity of the particles is given by

$$\vec{v} = \frac{1}{1 - \frac{\partial H}{\partial p_0}}\frac{\partial H}{\partial \vec{p}} \ .$$

Now we will investigate the impact of the off-shell potential on the test-particle velocity, with the Hamiltonian given in (14), where the term $\partial H/\partial p_0$ actually is of importance. The p_0-dependence of H basically comes from the fact that Γ_{tot} enters the Hamiltonian through the off-shellness $\Delta\mu$, while Γ_{tot} itself depends on μ, which can be translated into a dependence on p_0 (this will be explicitly carried out in the calculations below).
In the following we use $p = |\vec{p}|$ as a shorthand for the absolute 3-momentum. We start by explicitly calculating the momentum gradient of H:

$$\begin{aligned}
\frac{dH}{d\vec{p}} &= \frac{\partial H}{\partial \vec{p}} + \frac{\partial H}{\partial \mu}\frac{\partial \mu}{\partial \vec{p}} \\
&= \frac{\vec{p}}{H} + \frac{\mu}{H}\frac{\partial \mu}{\partial p}\frac{\partial p}{\partial \vec{p}} \\
&= \frac{\vec{p}}{H} + \frac{\mu}{H}\frac{\vec{p}}{p}\frac{\partial \mu}{\partial \Gamma}\frac{\partial \Gamma}{\partial p} \\
&= \frac{\vec{p}}{H}\left[1 + \frac{\mu}{p}X_{off}\frac{\partial \Gamma}{\partial p}\right] .
\end{aligned}$$

Analogously the derivative dH/dp_0 can be shown to be

$$\begin{aligned}
\frac{dH}{dp_0} &= \frac{\partial H}{\partial \mu}\frac{\partial \mu}{\partial p_0} \\
&= \frac{\mu}{H}\frac{\partial \mu}{\partial \Gamma}\frac{\partial \Gamma}{\partial p_0} \\
&= \frac{\mu}{H}X_{off}\frac{\partial \Gamma}{\partial \mu}\frac{\partial \mu}{\partial p_0} \\
&= \frac{p_0}{H}X_{off}\frac{\partial \Gamma}{\partial \mu} .
\end{aligned}$$

Combining these expressions, we can write the velocity as

$$\begin{aligned}
\vec{v} &= \frac{1}{1-\frac{\partial H}{\partial p_0}}\frac{\partial H}{\partial \vec{p}} \\
&= \frac{\vec{p}}{H}\left[\frac{1+\frac{\mu}{p}X_{off}\frac{\partial \Gamma}{\partial p}}{1-\frac{p_0}{H}X_{off}\frac{\partial \Gamma}{\partial \mu}}\right] \\
&= \frac{\vec{p}}{p}\left[\frac{p+\mu X_{off}\frac{\partial \Gamma}{\partial p}}{H-p_0X_{off}\frac{\partial \Gamma}{\partial \mu}}\right] .
\end{aligned} \tag{17}$$

In the simplest case, without off-shell potential or any other potentials, the velocity is just $\vec{v} = \vec{p}/H$, which is of course guaranteed to obey the relativistic speed-of-light limit $|\vec{v}| < 1$ (using c=1).
However, from eq. (17) we see that this is not necessarily true any more if we use the off-shell potential, because we get an additional factor which depends on the off-shell parameter X_{off} and on the behavior of the width ($d\Gamma/d\mu$ and $d\Gamma/dp$). All three of these

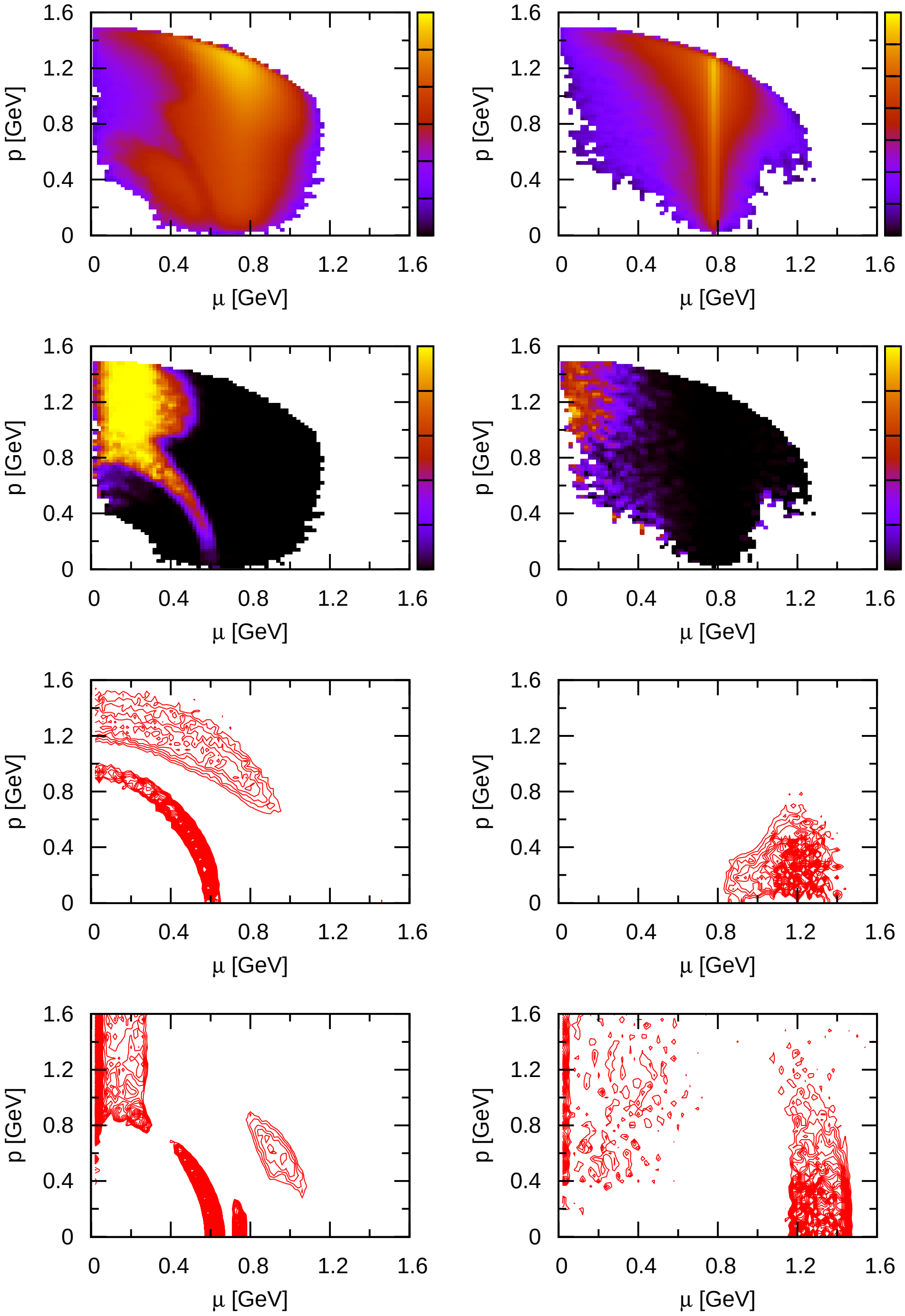

Figure 7: From top to bottom: Total mass-momentum distribution, percentage of tachyons, negative regions of $d\Gamma/dp$ and $d\Gamma/d\mu$, for ρ (left) and ω (right) mesons.

parameters in principle do not have any size constraints and can be either positive or negative. [As a side-remark we note that even the fully relativistic equations of motion do not guarantee to obey the limit $|\vec{v}| < 1$, if the self energies or widths behave badly, as one can see from eq. (13).]

There are two scenarios in which we can get unphysical "tachyons" (i.e. particles with a velocity larger than the speed of light):

1. the numerator gets large if X_{off} and $d\Gamma/dp$ have the same sign (and large absolute values):
   (a) $X_{off} < 0$ and $d\Gamma/dp < 0$
   (b) $X_{off} > 0$ and $d\Gamma/dp > 0$
2. the denominator gets small (possibly even negative) if X_{off} and $d\Gamma/d\mu$ have the same sign (and large absolute values):
   (a) $X_{off} < 0$ and $d\Gamma/d\mu < 0$
   (b) $X_{off} > 0$ and $d\Gamma/d\mu > 0$

Tachyonic problems are of course more likely to appear for particles which are already close to the speed of light, which is the case when they have a large momentum and a small mass. Small masses (below the peak mass) correspond to $X_{off} < 0$, while large masses (above the peak) have $X_{off} > 0$. From this one can conclude that the cases 1a and 2a are much more problematic than 1b and 2b.
Figure 7 shows the time-integrated distribution of rho and omega mesons for a $\gamma + {}^{40}Ca$ reaction with $E_\gamma = 1.5\,\mathrm{GeV}$. The first row represents the total distribution of particles, while the second row shows the fraction of particles which are tachyonic.
One can see that for the ρ as well as for the ω meson, tachyons appear (almost) exclusively below the peak mass (where $X_{off} < 0$), confirming our prejudice. For the ρ they appear in two bands, which coincide with those areas where $d\Gamma/dp$ is negative (i.e. case 1a). Those two bands merge for masses below 300 MeV, where $d\Gamma/d\mu$ is negative (i.e. case 2a). The derivatives of Γ are also shown in fig. 7. One can even recognize the tachyonic distribution as an "inverted" image in the total distribution, because we simply throw away all the tachyons we find (since they are unphysical).
For the ω the tachyonic region below 400 MeV actually seems to be connected to a slightly negative $d\Gamma/d\mu$ (i.e. case 2a). The distribution of the ϕ meson is not plotted, because it is almost free of tachyons. This has several reasons: The ϕ is heavier than the ρ and ω mesons, it has a rather small width and also there are no resonances contributing to the ϕN cross section (which means its derivatives are more well-behaved).

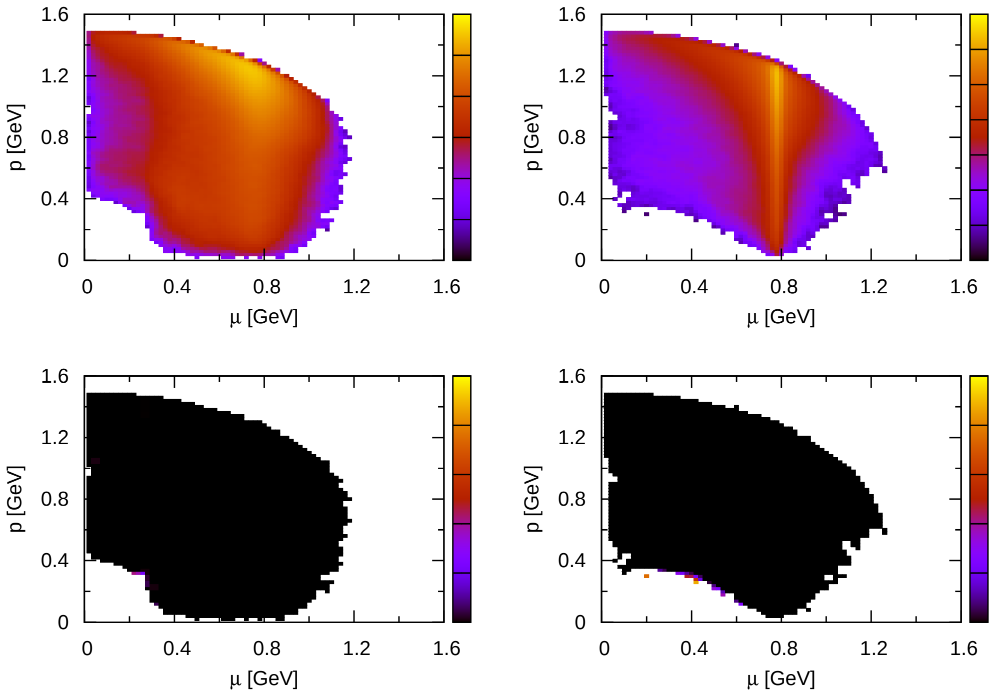

Figure 8: Mass-momentum distribution of ρ (left) and ω (right) mesons: Total distribution (top) and tachyonic particles (bottom), for $\sigma_{VN} = const.$

7.4 Solution

Overall this problem of tachyonic particles is rather dramatic, because a large part of the vector meson spectrum is simply "cut away". What makes it even more dramatic is the fact that the tachyons are not distributed homogeneously over the whole spectrum, but tend to appear in certain areas. There are even areas (indicated in yellow) where basically 100% of the particles become tachyonic and only a tiny fraction of the spectrum actually "survives". Moreover, this happens mostly in the area below the peak mass, which is really the most interesting one if one looks at dilepton spectra.

This means that for our purpose these tachyonic effects simply cannot be tolerated, and we have to find a way to overcome them. Recalling that the effects are connected to the derivatives $d\Gamma/dp$ and $d\Gamma/d\mu$, i.e. the structure of the total in-medium width, the simplest way to accomplish this task is to avoid any structure in the width. Hence the VN cross section is assumed to be constant, taking the following average values:

$$\begin{aligned} \sigma_{\rho N} &= 30\,\text{mb}\ , \\ \sigma_{\omega N} &= 30\,\text{mb}\ , \\ \sigma_{\phi N} &= 10\,\text{mb}\ . \end{aligned}$$

With $\Gamma_{coll} = \sigma\rho v$ and assuming $v \approx 1$ this translates into the following collisional widths at normal nuclear density ($\rho = \rho_0 = 0.168\,\mathrm{fm}^{-3}$):

$$\begin{aligned} \Gamma_\rho^{(coll)} &\approx 100\,\mathrm{MeV}\,, \\ \Gamma_\omega^{(coll)} &\approx 100\,\mathrm{MeV}\,, \\ \Gamma_\phi^{(coll)} &\approx 33\,\mathrm{MeV}\,. \end{aligned}$$

We will work with this assumption from now on, and all the results in the remaining part of this thesis will be based on it. Nevertheless, we use this simplification only for the off-shell potential, i.e. the propagation of the particles. In the collision term, where the particle widths are needed for the determination of particle masses in the final state, we still use the full in-medium widths from chapter 5.
To show that this really cures the tachyonic problems, fig. 8 shows the same distributions as fig. 7, but now using a constant σ_{VN} instead of the full cross sections. One can clearly see that almost all the tachyons are gone, and only very few of them remain at the edges of the distribution (their origin might be numerical issues).

7.5 Spectral Evolution

To check whether our off-shell propagation scheme (using the constant cross sections from the previous section) really works, tests of the spectral evolution of vector mesons traveling through a medium have been performed, by setting up a "Gedankenexperiment", in which we shoot a beam of vector mesons on a ^{40}Ca nucleus, and turn off the collision term in our model. This means that there are neither explicit collisions nor decays, so that the vector mesons are stable and (almost) non-interacting. They simply propagate through the nuclear medium, the only medium effect being that their masses change with density, according to the off-shell potential. This is a nice way of benchmarking the off-shell propagation in a clean environment, without other effects interfering.

7.5.1 Propagation through the nucleus

In the first setup we investigate, the vector mesons are initialized in the vacuum and propagate through the nucleus. We have done this with ρ, ω and ϕ mesons having a momentum of $p = 1.2\,\mathrm{GeV}$, and the results are shown in fig. 9. For each particle species we show the initial spectral distribution in the vacuum, an "in-medium" distribution after a time of $t = 10\,\mathrm{fm}/c$ where most of the mesons should be inside the nucleus, and a final distribution at a later time when all the mesons should have propagated through the nucleus and should be in vacuum again.
One can see that for the most part this works quite well. The distribution broadens when the test-particles enter the nucleus, and comes back to the starting value when they propagate out. But there are also some discrepancies: For the ρ meson the starting distribution is reconstructed very nicely in the region between 0.5 and 1.5 GeV. Around $m = 0.5\,\mathrm{GeV}$ there is a sharp cutoff, and the spectrum below is missing. This is due to the fact that the lower part of the spectrum is shifted so far down in the medium that the masses of the test-particles become negative. Since negative masses are unphysical, those test-particles are taken out of the simulation and are missing in the spectrum afterwards.

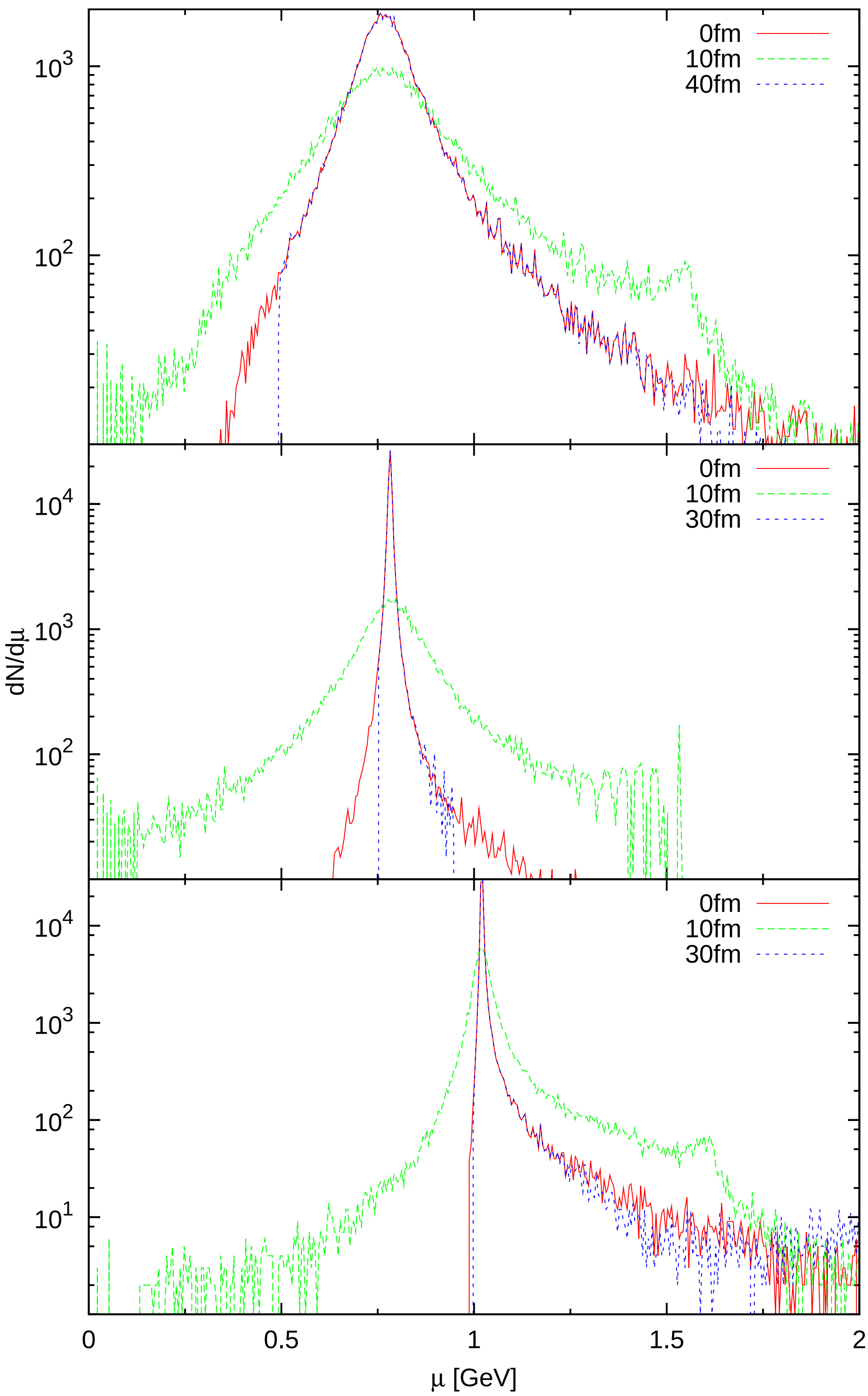

Figure 9: Spectral evolution of ρ, ω and ϕ mesons propagating through a Ca nucleus.

Above 1.5 GeV one can also see a slight difference, which may be connected to the fact that the heavier particles are slower (since all have the same momentum of 1.2 GeV) and may not have completely propagated out of the nucleus yet. In the in-medium distribution one can see a smaller peak appearing, which probably also is an effect of differing velocities (the lighter particles are already in the medium, while the heavier ones are still in vacuum, the small peak marking the transition).

For the ω one observes the same cutoff at low masses as for the ρ, but in addition there is also a cutoff at higher masses. This upper cutoff has a similar reason as the lower one: Particles above the pole mass increase their mass when they propagate into the medium, according to the off-shell potential. We assume that the energy of the each single particle is conserved during propagation, so that this increase in mass causes a decrease in momentum. Therefore, the mass cannot increase to arbitrary values, but is limited by the total energy of the particle. If the mass is shifted up so far that it exceeds the energy, energy conservation can not be achieved any more (since the momentum would have to become imaginary). In this unphysical case we have to take the particle out of the simulation, and this causes the upper cutoff in the ω spectral function.

In principle there would also be a back-coupling to the nucleus in the off-shell propagation, which we neglect. When including this back-coupling, the conservation of the single-particle energies would not be valid any more, being replaced by energy conservation of the whole system.

For the ϕ one can see that the in-medium distribution does not quite reach down to zero, which means there is no significant cutoff effect on the lower end of the vacuum distribution. Also the upper part of the spectrum is reconstructed quite nicely.

Summing up, the cutoff effects seen in this setup are due to the fact that the mass evolution of particles traveling through density gradients is limited to the interval $\mu \in [0, E]$. The off-shell potential however does not inherently respect these physical boundaries, which results in the described cutoff effects. This problem presumably would not be solved by using the fully relativistic equations of motion instead of an off-shell potential.

7.5.2 Propagation out of the nucleus

Now we investigate a second setup, in which the vector mesons are initialized inside the nucleus, i.e. with their in-medium spectral function, and then propagate outwards into the vacuum. Figure 10 shows for each particle the in-medium distribution which we start with, the resulting vacuum distribution after the particles have propagated out of the nucleus and an intermediate distribution while they are in transition.

One has to be aware that the in-medium distribution, which we start with, is not necessarily the same as the in-medium distribution we got in the previous setup, since we now have a different physical situation. Before, we produced particles in the vacuum and let them propagate into the medium. Now it is the other way around: We produce particles in the medium and let them propagate into the vacuum. There is absolutely no reason for the in-medium distributions in both cases to be equal. In the same way there is no reason why in this second setup we should end up with a normal vacuum distribution after particles have propagated out of the nucleus.

And indeed we see some slight differences. Most prominently, in the vacuum distribution of the ρ there is now a small second peak appearing on the lower end of the spectrum. This is probably connected to the differing in-medium distribution, and the fact that

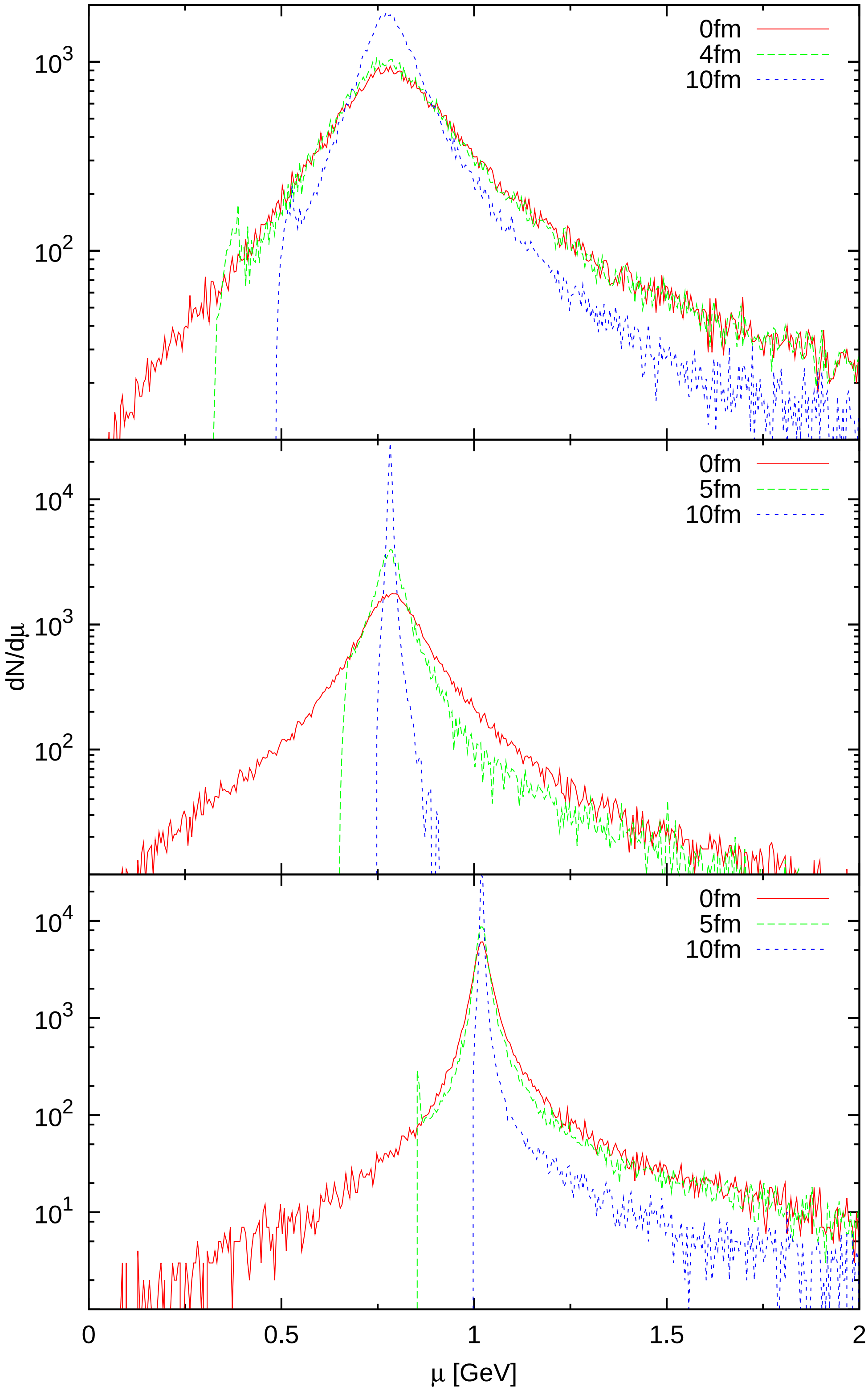

Figure 10: Spectral evolution of ρ, ω and ϕ mesons propagating out of a Ca nucleus.

while the particles propagate out, the distribution is being compressed to a smaller range of masses. This shrinking of the distribution means that the many sub-threshold particles we produce in the medium are being squeezed into a much smaller mass-interval in the vacuum and in this way produce this artificial peak. The vacuum distributions of the ω and ϕ carry no additional bumps, but still their intermediate distributions show similar effects.

One thing which is actually the same here and in the previous setup is the position of the lower cutoffs in the final vacuum distribution of ρ and ω, reinforcing our assumption that they are simply caused by the $m = 0$ cutoff in the in-medium distribution.

All in all one can say that, despite a few problems, the off-shell propagation of vector mesons seems to work pretty well, in that it correctly broadens the spectral functions in the medium and it reproduces the initial vacuum distribution after propagating through a nucleus. The issues with tachyonic particles have been dealt with in a sensible manner, but there is basically no way to get rid of the cutoff effects seen in the previous figures, because they are connected to the fact that some test-particles acquire negative masses in the medium, which cannot be avoided.

Of course, one way to improve our off-shell propagation scheme would be to use the the relativistic equations of motion (13) instead of an off-shell potential. This would hopefully resolve most of the tachyonic issues we had to deal with when propagating highly relativistic mesons, and allow us to use the full VN cross section, including resonance contributions, without putting too many restrictions on the actual shape of σ_{VN}. Unfortunately it was not feasible to implement the relativistic equations of motions in the scope of this diploma thesis, and so this remains as a possible future improvement of the model.

8 Experimental Status

The first experimental hints of changes of the vector meson properties in the nuclear medium have been observed in heavy-ion collisions. In 1995 the CERES collaboration reported an enhancement of the dilepton yield in the mass region $0.3\,\mathrm{GeV} < \mu < 0.7\,\mathrm{GeV}$ in S-Au collisions at 200 AGeV at the CERN SPS [Ag95]. While their original setup could not spot the reason for this enhancement because of low statistics and resolution, data from an upgraded experiment using 158 AGeV Pb-Au collisions seems to favor a broadening of the ρ meson over a mass shift [Ada06]. The NA60 collaboration has measured dimuon pairs from 158 AGeV In-In collisions and finds a strong broadening but essentially no mass shift of the ρ spectral function [Ar05]. In contrast, the STAR experiment at RHIC has observed a decrease of the ρ mass by measuring the $\rho \to \pi^+\pi^-$ decay in 200 AGeV Au-Au collisions [Ads04].
In this work we focus on elementary collisions instead of heavy-ion collisions, since the former have several advantages: At first they are much "cleaner" in a certain sense, i.e. the nucleus stays very close to its ground state and is only slightly excited, which means that the density stays approximately constant ($\rho \lesssim \rho_0$). This is nice since one wants to observe effects which depend strongly on density. In heavy-ion collisions however, the measured results are integrated over intervals in density and temperature, and therefore are harder to interpret quantitatively. Moreover the predicted effects are large enough already at nuclear saturation density ρ_0, so that they could be measured in elementary reactions.
Regarding the final state, vector mesons can be observed either via their hadronic or their leptonic decays. The advantage of the hadronic decays is of course that they have much larger branching ratios than the leptonic ones. However the produced hadrons will interact with the nuclear medium, hindering the exact reconstruction of the vector meson. Apart from the heavy-ion experiments, there have also been a few attempts to exploit hadronic decay modes in elementary (especially photon-induced) nuclear reactions. For example $\omega \to \pi^0\gamma$ has been measured by the CBELSA/TAPS collaboration in γNb reactions at the ELSA facility [Tr05]. They claim to find an in-medium mass of $m_\omega^{med} = 722\,\mathrm{MeV}$ at an average $\rho = 0.6\rho_0$, and a width of $\Gamma_\omega^{med} = 55\,\mathrm{MeV}$. For the ρ, the TAGX collaboration has measured in-medium modifications in $^{12}C(\gamma, \pi^+\pi^-)X$ reactions [Hu03]. Also the $\phi \to K^+K^-$ decay has been measured in photon-induced reactions at SPring-8 [Ish05]. We will not go into details on these experiments here, since our focus lies on leptonic final states.
Although the branching ratios of the leptonic decays are rather small (on the order of 10^{-5}), dileptons are actually better suited to investigate mesonic in-medium properties than the hadronic decay modes, due to their weak interaction with the nuclear medium. There are three important experiments which have set out to measure dileptons from elementary nuclear collisions:

- g7@JLAB
- E325@KEK
- HADES@GSI

In the following we will shortly describe their experimental setups and give an overview over the results they have obtained so far.

8.1 g7@JLAB

The g7 experiment at Jefferson Lab (Virginia, USA) was the first to measure the reaction $\gamma A \rightarrow e^+e^-X$. This reaction has the unique advantage that it utilizes electromagnetic probes in both the production and decay channel, thereby minimizing initial-state as well as final-state interactions. The g7 collaboration uses a tagged bremsstrahlung photon beam with energies in the range of roughly 0.8 to 3.5 GeV, which is produced from a primary 3-4 GeV electron beam from the CEBAF accelerator. The photon beam is being shot at various nuclear targets (like ^2H, ^{12}C, ^{48}Ti, ^{56}Fe, ^{208}Pb), and the outcoming dileptons are measured with the CLAS detector ("CEBAF Large Acceptance Spectrometer"). It is very important to distinguish e^+e^- pairs from $\pi^+\pi^-$ pairs, which is done with a misidentification factor on the order of 10^{-7}. Data was taken in 2002 and has been compared to simulations of the GiBUU transport model [Nas07]. The result of the analysis is that there is no significant mass shift, while the width is consistent with the collisional broadening predicted by the GiBUU model. Their estimate of the mass shift parameter $\alpha = 0.02 \pm 0.02$ cannot exclude a shift of zero, and they give an upper limit of $\alpha < 0.053$ with a 95% confidence level. This is not necessarily inconsistent with the CBELSA/TAPS result of a 14% mass drop of the ω meson, since ρ and ω may have different medium modification mechanisms, and also the meson momenta in both experiments differ. Figure 11 shows the background subtracted g7 data for the Fe-Ti target, together with a BUU fit of the ρ, ω and ϕ channels.

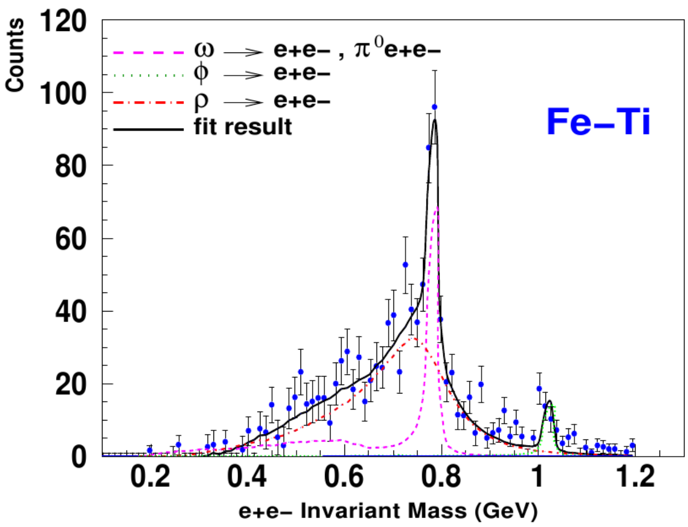

Figure 11: Experimental results from JLAB [Nas07].

Data from this experiment is also used to investigate the absorption of ω and ϕ mesons in nuclei by measuring their nuclear transparencies, and a strong depletion of the ω and ϕ peaks has been found for increasing target masses. This alternative approach may give additional insight on the in-medium widths of ω and ϕ mesons, since it is hard to observe them decaying inside the nucleus due to their long lifetimes. Lately a follow-up experiment has been proposed ("g7b") to increase statistics and make momentum-dependent measurements.

8.2 E325@KEK

The E325 experiment at KEK (Kamiokande, Japan) has measured dileptons from proton-induced reactions. They use 12 GeV protons from the KEK-PS and shoot them on a number of different targets (e.g. C, Cu), measuring dilepton pairs with the E325 detector. Data has been taken in several runs since 1998. Their analysis of the ω meson [Nrk06] does indeed find a significant mass drop, with a parameter $\alpha = 0.092 \pm 0.002$ (which is consistent with the theoretical prediction of Hatsuda/Lee), but curiously they do not see any broadening at all, which is in contradiction to the CBELSA/TAPS result. Their data for the Cu target is shown in fig. 12. The fits have been obtained with the nuclear cascade code JAM [Nar99].

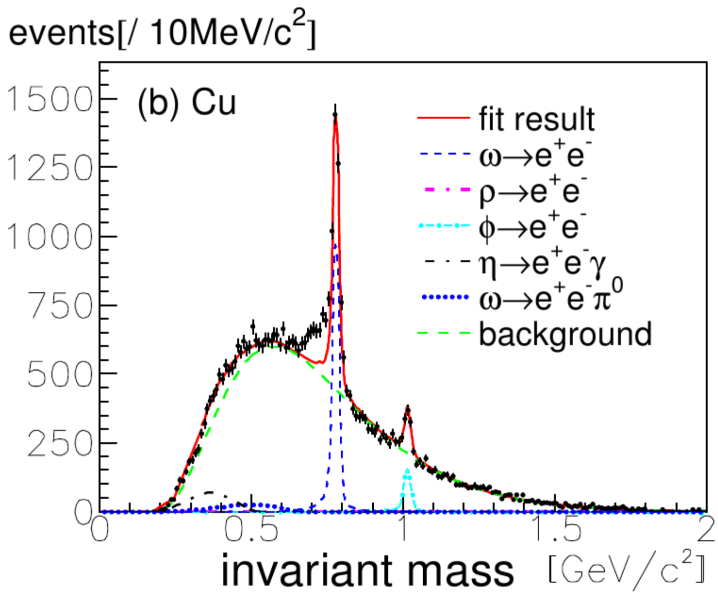

Figure 12: Experimental results from KEK [Nrk06].

In addition to the given geometrical acceptance of the detector, they put further acceptance cuts on the data, e.g. cuts on rapidity ($0.6 < \eta < 2.2$), transverse momentum ($p_T < 1.5$ GeV) and opening angle ($50° < \theta < 150°$) of the dilepton pair. They have no results for the ρ meson, since the ρ signal is buried in the large combinatorial background, which is due to the high proton energy resulting in large final state multiplicities. However, they collected enough data to do an analysis of the ϕ meson, which suggests a mass drop of about 3%, but only very little broadening [Mut07]. Since the experiment is operated at fairly high proton energies, vector mesons with large momenta can be produced, but only low-momentum ϕ mesons have a significant probability to decay inside the nucleus. Therefore they split their data for the ϕ in several regions of $\beta\gamma = p/m$, and find a medium modification only in the lowest region ($\beta\gamma < 1.25$) and for heavy target nuclei.

8.3 HADES@GSI

The third important experiment is HADES, the High Acceptance Di-Electron Spectrometer, at GSI (Darmstadt, Germany). The HADES collaboration has already measured pp and AA reactions at different energies, and have published results for C+C collisions at 2 AGeV [Ag07]. Besides their heavy-ion program, they also have a dedicated program for vector meson production in pA collisions (see proposal S333 at [HAD]). Although no pA data has been produced so far, this will happen quite soon: A p+Nb run with 3.5 GeV protons is scheduled for Sept./Oct. 2008.

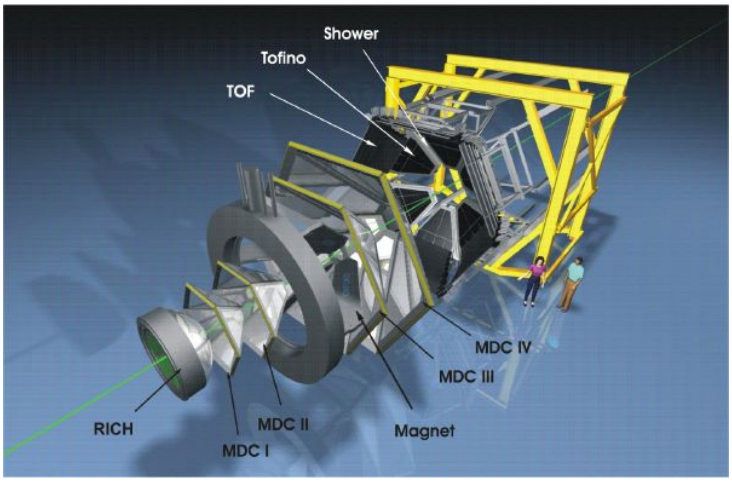

Figure 13: The HADES detector [HAD].

9 Photon-Induced Reactions

This chapter deals with any aspects which are specific to photon-nucleus reactions. First of all, if we want to calculate dilepton spectra from vector meson decays, we have to know how these vector mesons themselves are produced. This will be discussed in the first section of this chapter. Then we have to take into account possible background processes: The hadronic Dalitz backgrounds, which have already been mentioned in chapter 4, as well as non-hadronic contributions, the most important of which is the Bethe-Heitler process.

9.1 Photo-production of light Vector Mesons

To get the correct dilepton yields, one of course has to describe correctly how the vector mesons are produced in the first place, before they decay and eventually produce dilepton pairs. In our model the exclusive cross sections for the photo-production of vector mesons on a nucleon, i.e. $\gamma + N \to V + N$ (with $V = \rho^0, \omega, \phi$), are adjusted to experimental data with the following ansatz [Eff99]:

$$\sigma_{\gamma N \to VN} = \frac{1}{p_i s} \int_0^{\mu_{max}} d\mu |\mathcal{M}_V|^2 p_f \mathcal{A}_V(\mu) \ .$$

In this formula we integrate over the mass μ of the vector meson V, up to a maximum of $\mu_{max} = \sqrt{s} - m_N$. The center-of-mass momentum of the initial and final state is denoted by p_i and p_f, respectively, and $\sqrt{s}$ is the total energy available for the reaction. The spectral function of the vector meson is given by

$$\mathcal{A}_V(\mu) = \frac{2}{\pi} \frac{\mu^2 \Gamma_{tot}(\mu)}{(\mu^2 - M_V^2)^2 + (\mu \Gamma_{tot}(\mu))^2} \ .$$

Here, M_V is the pole mass of the vector meson, and Γ_{tot} its total width, which for simplicity is assumed to be the vacuum width. The initial and final momenta can be expressed as

$$\begin{aligned} p_i &= \frac{1}{2\sqrt{s}} \left(s - m_N^2 \right) \ , \\ p_f &= \frac{1}{2\sqrt{s}} \sqrt{\left(s - (m_N + \mu)^2 \right) \left(s - (m_N - \mu)^2 \right)} \ . \end{aligned}$$

We choose the following parametrization of the matrix elements $\mathcal{M}_V$ to fit the data:

$$\begin{aligned} |\mathcal{M}_\rho|^2 &= 160 \mu b \cdot \ \mathrm{GeV}^2 \ , \\ |\mathcal{M}_\omega|^2 &= \frac{p_f^2}{2(\sqrt{s} - 1.73\,\mathrm{GeV})^2 + p_f^2} \cdot 80 \mu b \cdot \ \mathrm{GeV}^2 \ , \\ |\mathcal{M}_\phi|^2 &= 4 \mu b \cdot \ \mathrm{GeV}^2 \ . \end{aligned}$$

The matrix elements for ρ and ϕ are constant, while $|\mathcal{M}_\omega|^2$ in principle depends on $\sqrt{s}$ and on μ (through p_f). However, we assume $\mu = M_\omega$ in the matrix element, so that $|\mathcal{M}|^2$ can be pulled out of the integration in all three cases.

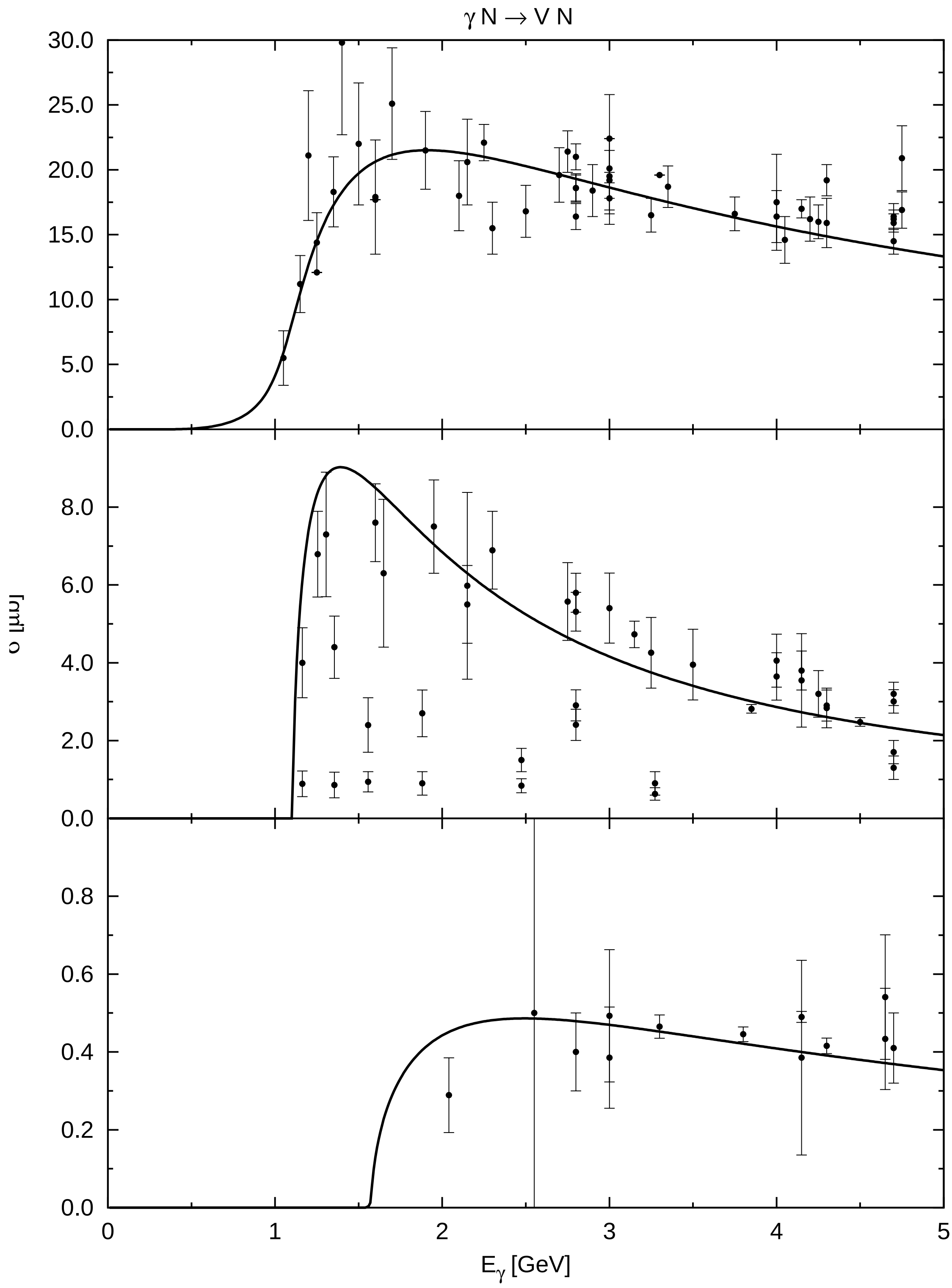

Figure 14: $\gamma N \to VN$ cross sections ($V = \rho, \omega, \phi$).

The cross sections we obtain after plugging in these matrix elements and numerically performing the integration are shown in fig. 14 as a function of the photon energy E_γ, in comparison to experimental data (taken from [PDG]).
For photon-induced reactions, we will work in the JLAB energy regime of up to 4 GeV. One can see from the plot that in this region our parametrization seems to fit the data rather well. At higher energies however, this parametrization is not as good, and other fits are used, which are not of interest here, since we only work at low energies.
Later on we will show some results for a typical energy of $E_\gamma = 1.5\,\text{GeV}$. In this case the CM energy of the γN interaction is given by (assuming the nucleon is at rest):

$$\sqrt{s} = \sqrt{2m_N E_\gamma + m_N^2} \approx 1.92\,\text{GeV} \tag{18}$$

This is the mean value of the CM energy. If we now include Fermi momentum ($p_F \approx 0.26\,\text{GeV}$), we can also get larger or smaller values, depending on the orientation of the nucleon momentum relative to the photon beam:

$$\sqrt{s}_{max} = \sqrt{2E_\gamma(m_N + p_N) + m_N^2 - p_N^2} \approx 2.10\,\text{GeV}$$

$$\sqrt{s}_{min} = \sqrt{2E_\gamma(m_N - p_N) + m_N^2 - p_N^2} \approx 1.69\,\text{GeV}$$

So this is the approximate range of CM energies in the primary γN reaction (neglecting nucleon potentials), for a photon energy of 1.5 GeV. For coherent photo-production the CM energy would be even larger, since m_N would be replaced by the nuclear mass in eq. (18).
Since even the maximum energy for the primary γN collisions is below the high energy threshold of 2.2 GeV, and the secondary collisions can not have energies higher than this, most of the secondary collisions will be treated via the low-energy resonance model, while only very few are expected to go via PYTHIA (through event mixing around the threshold).

9.2 Hadronic Backgrounds

To get a correct description of all Dalitz backgrounds in the dilepton spectrum, one would have to include more channels in the primary γN interaction, besides $\gamma N \to VN$, as for example:

$$\begin{aligned}
\gamma N &\to R \\
&\to N\pi \\
&\to N\pi\pi \\
&\to NV\pi \\
&\to \cdots
\end{aligned}$$

This has not been done so far, but is an important extension to be done in the future. Despite these missing channels in the primary interaction, our dilepton spectra from photon-induced reactions still include some Dalitz backgrounds, which come from the secondary interactions and just miss the contributions from the primary interaction. However, in experimental spectra, most of the Dalitz contributions are anyway removed by geometrical and kinematical cuts, since only the direct channels $V \to e^+e^-$ are of interest.

9.3 The Bethe-Heitler Process

For photon-induced reactions there is one other "non-hadronic" process that contributes significantly to dilepton spectra: the so-called Bethe-Heitler Process, i.e. the direct photo-production of a lepton pair on a nucleon, as shown in the following Feynman diagram:

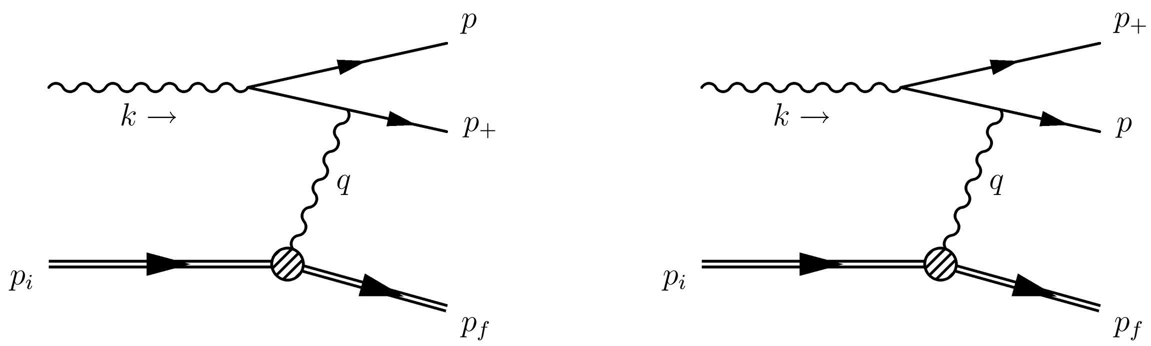

Figure 15: Feynman diagrams for the Bethe-Heitler process.

The kinematics of the process can be described as follows: An incoming photon with four-momentum k produces a lepton pair. The negative lepton has four-momentum p, the positive one p_+. The lepton mass is denoted by m. p_i is the initial four-momentum of the nucleon, m_n its mass. p_f is the final four-momentum of the nucleon. We are only looking at elastic processes, where the nucleon survives in the final state and only its momentum changes. The four-momentum which is exchanged between the nucleon and one of the leptons is denoted by $q = k - p - p_+ = p_f - p_i$. In the following we will calculate the (mass differential) cross section for this process.

9.3.1 The Leptonic Tensor

The upper part of the diagrams in fig. 15 is pure QED and can be computed by applying the standard Feynman rules:

$$\begin{aligned} i\mathcal{M} &= \bar{u}_s(p)(-ie\gamma^\nu)\epsilon_\nu(k)\frac{i}{-(\not{k}-\not{p})-m}(-ie\gamma^\mu)v_r(p_+) \\ &\quad +\bar{u}_s(p)(-ie\gamma^\mu)\frac{i}{\not{k}-\not{p}_+-m}(-ie\gamma^\nu)\epsilon_\nu(k)v_r(p_+) \\ &= -ie^2\bar{u}_s(p)\left[\not{\epsilon}(k)\frac{1}{\not{p}-\not{k}-m}\gamma^\mu+\gamma^\mu\frac{1}{\not{k}-\not{p}_+-m}\not{\epsilon}(k)\right]v_r(p_+) \\ &= -ie^2\bar{u}_s(p)\left[\not{\epsilon}(k)\frac{\not{p}-\not{k}+m}{(p-k)^2-m^2}\gamma^\mu+\gamma^\mu\frac{\not{k}-\not{p}_++m}{(k-p_+)^2-m^2}\not{\epsilon}(k)\right]v_r(p_+) \end{aligned}$$

With $p^2 = p_+^2 = m^2$ and $k^2 = 0$ the denominators can be further simplified:

$$i\mathcal{M} = \frac{i}{2}e^2\epsilon_\rho(k)\bar{u}_s(p)\left[\gamma^\rho\frac{\not{p}-\not{k}+m}{p\cdot k}\gamma^\mu + \gamma^\mu\frac{\not{k}-\not{p}_+ + m}{p_+\cdot k}\gamma^\rho\right]v_r(p_+)$$

The numerators can be simplified using the Dirac equation:

$$\begin{aligned}
\bar{u}(p)\gamma^\rho(\not{p}+m) &= \bar{u}(p)(2p^\rho - \not{p}\gamma^\rho + m\gamma^\rho) = \bar{u}(p)2p^\rho - \underbrace{\bar{u}(p)(\not{p}-m)}_{=0}\gamma^\rho = \bar{u}(p)2p^\rho \\
(-\not{p}_+ + m)\gamma^\rho v(p_+) &= -2p_+^\rho v(p_+) + \gamma^\rho\underbrace{(\not{p}_+ + m)v(p_+)}_{=0} = -2p_+^\rho v(p_+)
\end{aligned}$$

So we obtain:

$$i\mathcal{M} = \frac{i}{2}e^2\epsilon_\rho(k)\bar{u}_s(p)\left[\frac{2p^\rho - \gamma^\rho\not{k}}{p\cdot k}\gamma^\mu + \gamma^\mu\frac{\not{k}\gamma^\rho - 2p_+^\rho}{p_+\cdot k}\right]v_r(p_+)$$

To calculate a cross section we need to square this matrix element and sum over the spins of the electron and positron. Then we can use the spin sum relations $\sum_s u_s(p)\bar{u}_s(p) = \not{p}+m$ and $\sum_s v_s(p)\bar{v}_s(p) = \not{p}-m$. To get an unpolarized cross section, we also average over all possible photon polarizations and make the replacement $\sum_\epsilon \epsilon_\rho\epsilon_\sigma^* \to -g_{\rho\sigma}$:

$$\begin{aligned}
\frac{1}{4}\sum_\epsilon\sum_{s,r}|\mathcal{M}|^2 &= \frac{e^4}{16}\sum_\epsilon \epsilon_\rho(k)\epsilon_\sigma^*(k)\sum_{s,r}\bar{u}_s(p)\left[\frac{2p^\rho - \gamma^\rho\not{k}}{pk}\gamma^\mu + \gamma^\mu\frac{\not{k}\gamma^\rho - 2p_+^\rho}{p_+k}\right] \\
&\quad \cdot v_r(p_+)\bar{v}_r(p_+)\left[\frac{\gamma^\sigma\not{k} - 2p_+^\sigma}{p_+k}\gamma^\nu + \gamma^\nu\frac{2p^\sigma - \not{k}\gamma^\sigma}{pk}\right]u_s(p) \\
&= \frac{e^4}{16}\sum_\epsilon \epsilon_\rho(k)\epsilon_\sigma^*(k)Tr\left[\frac{2p^\rho - \gamma^\rho\not{k}}{pk}\gamma^\mu + \gamma^\mu\frac{\not{k}\gamma^\rho - 2p_+^\rho}{p_+k}\right](\not{p}_+ - m) \\
&\quad \cdot\left[\frac{\gamma^\sigma\not{k} - 2p_+^\sigma}{p_+k}\gamma^\nu + \gamma^\nu\frac{2p^\sigma - \not{k}\gamma^\sigma}{pk}\right](\not{p}+m) \\
&= \frac{e^4}{16}Tr\left[\frac{2p^\rho - \gamma^\rho\not{k}}{pk}\gamma^\mu + \gamma^\mu\frac{\not{k}\gamma^\rho - 2p_+^\rho}{p_+k}\right](m - \not{p}_+) \\
&\quad \cdot\left[\frac{\gamma_\rho\not{k} - 2p_{+\rho}}{p_+k}\gamma^\nu + \gamma^\nu\frac{2p_\rho - \not{k}\gamma_\rho}{pk}\right](m+\not{p})
\end{aligned}$$

Now the leptonic tensor is defined as $\frac{1}{4}\sum_\epsilon\sum_{s,r}|\mathcal{M}|^2 \equiv e^4L^{\mu\nu}$ and can be written as

$$L^{\mu\nu} = \frac{Tr}{16}\left[\frac{2p^\rho - \gamma^\rho\not{k}}{pk}\gamma^\mu + \gamma^\mu\frac{\not{k}\gamma^\rho - 2p_+^\rho}{p_+k}\right](m - \not{p}_+)\left[\frac{\gamma_\rho\not{k} - 2p_{+\rho}}{p_+k}\gamma^\nu + \gamma^\nu\frac{2p_\rho - \not{k}\gamma_\rho}{pk}\right](m+\not{p})$$

At this point we have to take the trace of various combinations of γ matrices. For this we need the following basic relations:

- $\{\gamma^\mu, \gamma^\nu\} = 2g^{\mu\nu}, \qquad \not{p}\not{p} = p^2$

- $tr(\gamma^\mu) = 0 = tr(\gamma^\mu ... \gamma^\nu)$ for any odd number of γ matrices
- $tr(\gamma^\mu \gamma^\nu) = 4g^{\mu\nu}, \qquad tr(\gamma^\mu \gamma^\nu \gamma^\rho \gamma^\sigma) = 4(g^{\mu\nu} g^{\rho\sigma} - g^{\mu\rho} g^{\nu\sigma} + g^{\mu\sigma} g^{\nu\rho})$
- $\gamma^\rho \gamma_\rho = 4, \qquad \gamma^\rho \gamma^\mu \gamma_\rho = -2\gamma^\mu, \qquad \gamma^\rho \gamma^\mu \gamma^\nu \gamma_\rho = 4g^{\mu\nu}$

Further, the hadronic tensor has the property that $q^\mu W_{\mu\nu} = 0$ and $W_{\mu\nu} = W_{\nu\mu}$.
In addition we can derive the following relations for this process:

- $p_+ q = -pk - q^2/2$
- $pq = -p_+ k - q^2/2$
- $m^2 + pp_+ = q^2/2 + pk + p_+ k$

By using the above relations the hadronic tensor can be transformed into:

$$\begin{aligned} L^{\mu\nu} \;&=\; \frac{m^2\left(\frac{1}{2}q^2 g^{\mu\nu} - 2p_+^\mu p_+^\nu\right)}{(pk)^2} + \frac{m^2\left(\frac{1}{2}q^2 g^{\mu\nu} - 2p^\mu p^\nu\right)}{(p_+k)^2} - \left(\frac{p_+k}{pk} + \frac{pk}{p_+k}\right) g^{\mu\nu} \\ &\quad + \frac{2(q^2 - 2m^2) p_+^\mu p^\nu - q^2 (p_+ p) g^{\mu\nu} - q^2 k^\mu k^\nu}{(pk)(p_+k)} \end{aligned}$$

9.3.2 The Hadronic Tensor

The Hadronic Tensor is defined to be

$$\begin{aligned} W_{\mu\nu} \;&\equiv\; \sum_f \langle p_i | j_\mu(0) | f \rangle \langle f | j_\nu(0) | p_i \rangle (2\pi)^3 \delta^4(q + p_i - p_f) e^{-2} \\ &\equiv\; \left(p_{i\mu} - \frac{q_\mu (p_i q)}{q^2}\right)\left(p_{i\nu} - \frac{q_\nu (p_i q)}{q^2}\right) \frac{W_2}{m_n^2} - \left(g_{\mu\nu} - \frac{q_\mu q_\nu}{q^2}\right) W_1 \; . \end{aligned}$$

We only need the elastic part of the nucleon form factors, which is in dipole approximation

$$\left\{ \begin{array}{c} W_{2,p} \\ W_{1,p} \\ W_{2,n} \\ W_{1,n} \end{array} \right\} = \frac{2m_n \delta(p_f^2 - p_i^2)}{(1 + \frac{t}{0.71\,\mathrm{GeV}})^4} \left\{ \begin{array}{c} (1 + 2.79^2\tau)/(1+\tau) \\ 2.79^2\tau \\ 1.91^2\tau/(1+\tau) \\ 1.91^2\tau \end{array} \right\} ,$$

where $t \equiv -q^2$ and $\tau \equiv t/(4m_n^2)$. Here, as is the remaining derivation of the Bethe-Heitler cross section, we assume momentum-independent potentials. For momentum-dependent potentials the phase space factors would have to be modified.

9.3.3 Contracting the Tensors

After contracting both tensors, we end up with two parts, one of which is proportional to W_1, the other one to W_2:

$$-L^{\mu\nu}W_{\mu\nu} = \lambda_1 W_1 + \lambda_2 W_2$$

They have the following form:

$$\begin{aligned}
\lambda_1 &= \frac{m^2\left(q^2+2m^2\right)}{(pk)^2} + \frac{m^2\left(q^2+2m^2\right)}{(p_+k)^2} + \frac{4m^4-q^4}{(pk)(p_+k)} \\
&\quad - \frac{2(q^2+2m^2+p_+k)}{pk} - \frac{2(q^2+2m^2+pk)}{p_+k}
\end{aligned}$$

$$\begin{aligned}
\lambda_2 &= -\frac{m^2\{q^2(1/2-E/m_n)+2E^2\}}{(p_+k)^2} - \frac{m^2\{2(E_k-E+q^2/(2m_n))(E_k-E)+q^2/2\}}{(pk)^2} \\
&\quad - \frac{(2m^2-q^2)[2E(E-E_k)+q^2/2((E_k-2E)/m_n+1)]-q^2E_k^2}{(p_+k)(pk)} \\
&\quad + \frac{q^2/m_n(m_n+E-E_k-q^2/(2m_n))+pk}{p_+k} + \frac{q^2/m_n(m_n-E)+p_+k}{pk}
\end{aligned}$$

λ_1 is completely Lorentz invariant, and can be evaluated in any reference frame. λ_2 is expressed in the nucleon rest frame, where E is the electron energy and E_k the energy of the incident photon.

9.3.4 Cross Section

To get the cross section for the Bethe-Heitler process, we need three ingredients:

- the squared matrix element $|\mathcal{M}|^2$ for the process
- the Lorentz invariant n-body phase space factor $d\Phi_n$
- a pre-factor which is not Lorentz invariant and determines the transformation properties of the cross section

We have calculated the matrix element in the previous parts of this chapter. It is given by the contraction of the hadronic and leptonic tensors times a factor of e^6 for the three electromagnetic vertices and $1/q^4$ which is the (squared) propagator of the exchanged photon:

$$|\mathcal{M}|^2 = \frac{e^6}{q^4} L^{\mu\nu}\tilde{W}_{\mu\nu}$$

However, we have to be careful here, since a part of phase space is already included in the hadronic tensor. Therefore we define

$$W_{\mu\nu} \equiv \tilde{W}_{\mu\nu}\delta\left(p_f^2 - p_i^2\right)$$

so that $\tilde{W}_{\mu\nu}$ is the hadronic tensor without these phase space parts.
Also, the following relation holds:

$$\delta\left(p_f^2 - p_i^2\right) = \delta^{(4)}(p + p_+ + p_f - p_i - k)\frac{d^3 p_f}{2E_f}$$

This can be shown in the following way:

$$\begin{aligned}
\delta\left(p_f^2 - p_i^2\right) &= \delta\left((p_f^0)^2 - \vec{p}_f^{\,2} - p_i^2\right) = \frac{1}{2p_f^0}\delta\left(p_f^0 - \sqrt{p_i^2 + \vec{p}_f^{\,2}}\right) \\
&= \frac{1}{2p_f^0}\delta\left(p_f^0 - \sqrt{p_i^2 + \vec{p}_f^{\,2}}\right)\delta\left(p_f^0 + E + E_+ - E_i - E_k\right) dp_f^0 \\
&= \frac{1}{2E_f}\delta(E_f + E + E_+ - E_i - E_k) \\
&= \frac{1}{2E_f}\delta(E_f + E + E_+ - E_i - E_k)\delta^{(3)}\left(\vec{p}_f + \vec{p} + \vec{p}_+ - \vec{p}_i - \vec{k}\right) d^3 p_f \\
&= \delta^{(4)}(p_f + p + p_+ - p_i - k)\frac{d^3 p_f}{2E_f}
\end{aligned}$$

The phase space factor for a process with n particles in the final state in general is given by:

$$d\Phi_n = \left[\prod_f \frac{d^3 p_f}{(2\pi)^3}\frac{1}{2E_f}\right](2\pi)^4 \delta^{(4)}(P - \sum p_f)$$

In our case ($n = 3$) this is:

$$d\Phi_3 = \frac{1}{(2\pi)^5}\frac{d^3 p}{2E}\frac{d^3 p_+}{2E_+}\frac{d^3 p_f}{2E_f}\delta^4(p + p_+ + p_f - p_i - k)$$

The last component of the cross section is the Lorentz boost factor, which in our case is just

$$\frac{m_i}{(k \cdot p_i)}$$

So, if we combine all the three parts described above, the cross section for the Bethe-Heitler process on the nucleon is:

$$\begin{aligned}
d\sigma &= \frac{m_i}{(k \cdot p_i)} \cdot d\Phi_3 \cdot |\mathcal{M}|^2 \\
&= \frac{m_i}{(k \cdot p_i)} \cdot \frac{1}{(2\pi)^5}\frac{d^3 p}{2E}\frac{d^3 p_+}{2E_+}\frac{d^3 p_f}{2E_f}\delta^4(p + p_+ + p_f - p_i - k) \cdot \frac{e^6}{q^4}L^{\mu\nu}\tilde{W}_{\mu\nu} \\
&= \frac{e^6}{(2\pi)^5}\frac{m_i}{4(k \cdot p_i)}\frac{d^3 p}{E}\frac{d^3 p_+}{E_+}\frac{1}{q^4}(L^{\mu\nu}W_{\mu\nu})
\end{aligned}$$

9.3.5 Mass-Differential Cross Section

To get from the cross section calculated in the previous section to the mass-differential cross section, we first introduce the Mandelstam variables $s = (p_i+k)^2$ and $t = (p_f - p_i)^2 = q^2$. We also define $p_d \equiv p + p_+$, which is the four momentum of the dilepton, and $M \equiv \sqrt{p_d^2}$, which is its invariant mass.
Then we will differentiate the cross section by M. For this purpose we use eq. (38.12) from [PDG] to split up phase space:

$$d\Phi_3(p_i + k; p, p_+, p_f) = d\Phi_2(p_i + k; p_f, p_d) d\Phi_2(p_d; p, p_+) \frac{dM^2}{2\pi}$$

Now we express the two-body phase space factors each in their CM frame, see [PS95, ch. 4.5]:

$$d\Phi_2(P; p_1, p_2) = \frac{1}{(2\pi)^2} \frac{|\vec{p}_1|}{4E_{com}} d\Omega$$

So that we get:

$$\begin{aligned} d\Phi_3 &= \frac{1}{(2\pi)^5} \frac{|\vec{p}^*| d\Omega^*_{ee}}{4M} \frac{|\vec{p}_f| d\Omega_f}{4\sqrt{s}} dM^2 \\ &= \frac{1}{(2\pi)^5} \frac{|\vec{p}^*| d\Omega^*_{ee}}{2} \frac{|\vec{p}_f| d\Omega_f}{4\sqrt{s}} dM \end{aligned}$$

where we used $dM^2 = 2MdM$. Here $|\vec{p}^*|$ is the absolute value of electron (and positron) in the dilepton rest frame, and Ω^*_{ee} the corresponding solid angle. $|\vec{p}_f|$ is the absolute value of the final nucleon momentum in the center of mass frame, and Ω_f its angle.
Putting everything together and using $\alpha = e^2/(4\pi)$, we finally end up with

$$\begin{aligned} \frac{d\sigma}{dM} &= \frac{m_i}{(k \cdot p_i)} \cdot \frac{d\Phi_3}{dM} \cdot |\mathcal{M}|^2 \\ &= \frac{m_i}{(k \cdot p_i)} \cdot \frac{1}{(2\pi)^5} \frac{|\vec{p}^*| d\Omega^*_{ee}}{2} \frac{|\vec{p}_f| d\Omega_f}{4\sqrt{s}} \cdot \frac{e^6}{q^4} L^{\mu\nu} \tilde{W}_{\mu\nu} \\ &= \frac{\alpha^3}{\pi^2} \frac{m_i}{4(kp_i)} \frac{1}{t^2\sqrt{s}} |\vec{p}^*| d\Omega^*_{ee} |\vec{p}_f| d\Omega_f L^{\mu\nu} \tilde{W}_{\mu\nu} \,. \end{aligned}$$

9.3.6 Bethe-Heitler on the Nucleus

If one is interested not only in the Bethe-Heitler process on a single nucleon, but on a whole atomic nucleus, one has to take into account the momentum distribution of the nucleons.
In the Fermi gas model the density of states in a volume L^3 is given by

$$dn = g \left(\frac{L}{2\pi} \right)^3 d^3p \,,$$

where g is the degeneracy factor, which is here $g = 4$, for there can be two protons (spin up/down) plus two neutrons with the same momentum allowed by the Pauli principle.

From the density of states we get the total number of states by integrating up to the Fermi momentum p_F:

$$N = g\left(\frac{L}{2\pi}\right)^3 \int_0^{p_F} d^3p = g\left(\frac{L}{2\pi}\right)^3 4\pi p_F^3/3 \; .$$

Then the particle density is

$$\rho = \frac{N}{L^3} = \frac{g}{6\pi^2} p_F^3 \; ,$$

which in turn means that the Fermi momentum is proportional to the cubic root of the density:

$$p_F = \left(\frac{6\pi^2}{g}\rho\right)^{1/3} \; .$$

Now the Local Thomas-Fermi Approximation (LTFA) assumes that the above result holds not only for constant density, but also for the case of a varying, location dependent density $\rho(r)$, with the consequence that the Fermi momentum is location-dependent too:

$$p_F(r) = \left(\frac{6\pi^2}{g}\rho(r)\right)^{1/3} \; .$$

Then the phase space function is given by

$$f(\vec{r}, \vec{p}) = g \cdot \Theta(p_F(\vec{r}) - |\vec{p}|) \; .$$

For our calculation of the Bethe-Heitler process we will assume a Woods-Saxon density

$$\rho(r) = \frac{\rho_0}{1 + e^{(r-r_0)/a}} \; ,$$

where ρ_0 is (approximately) the density at the center of the nucleus, being determined by the normalization condition $A = \int \rho(r) d^3r$. Further $r_0 = 1.2\ \mathrm{fm} \cdot A^{1/3}$ is the nuclear radius and a is the so-called “diffuseness”, which is usually around 0.5 fm.
Moreover, we have to take into account the effect of Pauli blocking, which implies that a nucleon, having interacted with the incoming photon through the Bethe-Heitler process, cannot have an arbitrary final momentum p_f, because this momentum may already be occupied by other nucleons, so that it is forbidden by the Pauli principle. This introduces an additional Pauli factor $(1 - f)$ which affects the final momentum of the nucleon. Now we can write down the cross section for the Bethe-Heitler process on the nucleus as a phase space integral over the elementary cross section, multiplied by the phase space density f and the Pauli factor:

$$\langle\sigma\rangle = \int \frac{d^3p_i}{(2\pi)^3} d^3r\, f(\vec{r}, \vec{p_i}) \sigma(\vec{p_i}) \left[1 - f(\vec{r}, \vec{p_f})\right] \; .$$

The angular integration over Ω_f which is implicit inside $\sigma(\vec{p_i})$ cannot be carried out on its own, but has to incorporate the additional Pauli factor.
Now we will compare the Bethe-Heitler cross section to the hadronic contributions of the dilepton spectrum for a γPb reaction at a photon energy of $1.5 GeV$ (with vacuum spectral functions), which is shown in fig. 16.

The hadronic contribution is the sum of all the hadronic channels, which have been shown already in fig. 2. One can see that the Bethe-Heitler contribution clearly exceeds the hadronic contribution over most parts of the spectrum, and only the ω and ϕ peaks are large enough to reach out of this background.

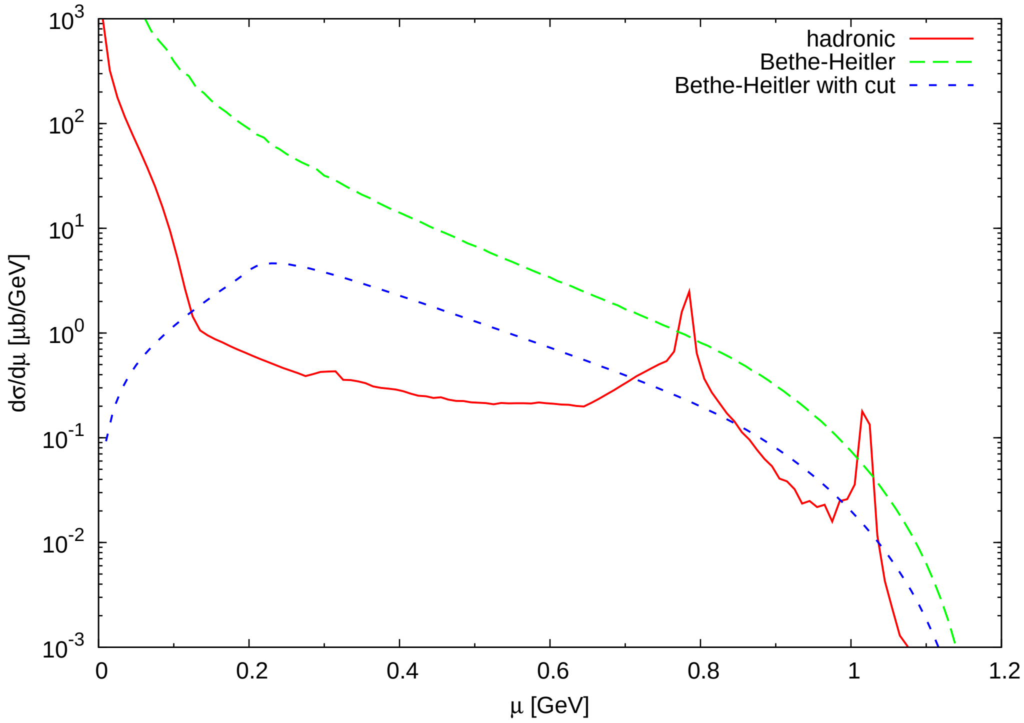

Figure 16: Dilepton spectrum for $\gamma + Pb$@1.5 GeV with Bethe-Heitler contributions.

However, the Bethe-Heitler contribution can be greatly suppressed by applying cuts on the lepton momenta. In fig. 16, cuts of $pk > 0.01GeV^2$ and $p_+k > 0.01GeV^2$ have been used (where p, p_+ and k are the four-momenta of the electron, positron and incident photon). A cut on pk practically translates into a cut on the azimuthal angle of the lepton, since pk is small at forward angles and large at backward angles, so that the cuts mentioned above exclude leptons in the very forward region (which usually can not be measured experimentally). One can see that these cuts suppress the Bethe-Heitler spectrum mostly at low masses, in particular they remove the pole at $\mu = 0$. Note that the cuts have not been applied to the hadronic spectrum. For experimental data, often cuts on the opening angle between the two leptons are used, which have a similar effect, suppressing the low-mass part of the spectrum.

10 Proton-Induced Reactions

This chapter will discuss some specifics of proton-induced reactions. First of all, at the proton energies which we will investigate (SIS & KEK-PS), most of the particle collisions are performed via the string model PYTHIA. We had to build some enhancements into PYTHIA (concerning spectral functions), which will be discussed in the first section. As in the photon case, there are also some specific background processes, of which we will mainly discuss the Bremsstrahlung contribution. Actually, there are many more processes, but most of these (like e.g. Drell-Yann, Open Charm etc) mainly contribute to the dilepton spectrum above the mass region of the light vector mesons. This region is not of interest to us, and so these processes will not be considered here.

10.1 Spectral Functions in PYTHIA

We want to study proton-induced reactions at two different proton energies: Protons with $E_{kin} = 3.5$ GeV from the SIS accelerator at GSI and protons with $E_{kin} = 12$ GeV from the KEK proton synchrotron. The center-of-mass energy for the collision with a nucleon in a fixed target is given by $\sqrt{s} = \sqrt{2m_N(E_{kin} + 2m_N)}$, which means that we have to deal with primary nucleon-nucleon collisions of about $\sqrt{s} = 3.18$ GeV for SIS and $\sqrt{s} = 5.10$ GeV for KEK.
As mentioned in chapter 2, the Lund string model PYTHIA represents the high-energy part of our transport model, and is used for any baryon-baryon collision with a CM energy of $\sqrt{s} > 2.6$ GeV.
Clearly the primary collisions for both SIS and KEK are above this threshold, and therefore the major part of all collisions (primary, but also secondary) is treated through PYTHIA. For most of the high-energy processes which PYTHIA is usually used for, the exact shape of the spectral functions is not of great importance, and so (for simplicity and efficiency) PYTHIA does not use the full relativistic spectral functions, but only the non-relativistic Breit-Wigner functions (with a constant width), which in addition are cut off symmetrically around the pole mass.
For our purpose these approximations are much too crude, and so we had to modify PYTHIA to include the full relativistic Breit-Wigner spectral functions without any cut-offs. This is important since the dilepton spectrum is directly proportional to the spectral functions of the vector mesons, multiplied with an additional factor of μ^{-3}, which boosts the spectral functions at small μ and makes it even more important to use the right spectral shape.
Moreover, PYTHIA normally does not include any in-medium effects in the spectral functions, and so we had to make additional modifications to use the in-medium spectral functions. However, due to the way in which particle production works in PYTHIA, it was not possible to use the full momentum-dependent in-medium width here (which is being used for in-medium spectral functions in the low-energy part of GiBUU). So we use the approximations from section 7.4 for the PYTHIA spectral functions.

10.2 Nucleon-Nucleon Bremsstrahlung

A new class of effects which contribute to the dilepton spectrum of proton-induced reactions are nucleon-nucleon bremsstrahlung and similar radiative corrections. These can be described by effective Lagrangian models of the nucleon-nucleon interaction based on meson exchange, see [SM03] and [KK05]. The Feynman diagrams of the contributions of lowest order are shown in fig. 17. All of them are nucleon-nucleon-interaction graphs, where the solid lines represent nucleons, dashed lines are exchange mesons and thick solid lines are nucleon resonances and excitations. One assumes that two nucleons interact via the exchange of mesons (e.g. π, ρ, ω, σ), and thereby can be excited into baryonic resonance states. Now the dilepton contributions originate from the fact that a photon can be radiated before, during or after the interaction (as shown in fig. 17), and subsequently converts into a lepton pair.

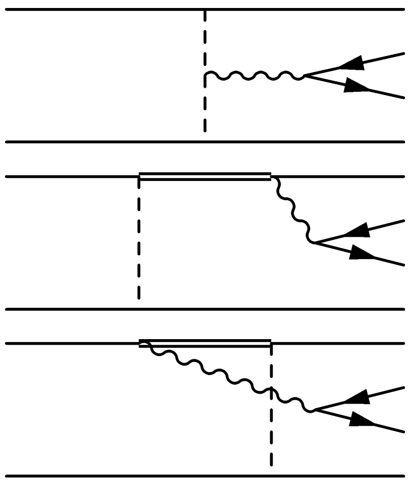

Figure 17: Nucleon-nucleon bremsstrahlung.

The contribution of nucleon-nucleon bremsstrahlung to the dilepton spectrum has not been included in our analysis so far, although it may be significant. It has been subject to quite some discussion lately, since the predictions of Shyam/Mosel and Kaptari/Kämpfer do not match in all cases, although in principle they should. Nevertheless it is important to take into account this component. For a start it could at least be included in the long-wavelength approximation.

11 Results

In this chapter we will present our final results, i.e. dilepton spectra for various reactions. We have chosen a number of processes, roughly corresponding to the setups of the experiments g7, HADES and E325:

- $\gamma + X$@1.5 GeV, with $X = \mathrm{C}, \mathrm{Fe}, \mathrm{Pb}$
- $p +$ Nb@3.5 GeV
- $p +$ Cu@12 GeV

Basically all the plots in this chapter show the mass-differential dilepton cross section $d\sigma/d\mu$ versus the invariant mass μ of the dilepton pair in units of μb/ GeV. We put the data output of our simulation into histograms with a bin size of $\Delta\mu = 10$ MeV, which is roughly in the range of the typical mass resolution of the detectors.
However, we only show the purely theoretical results of our transport model, without dealing with geometric acceptances and resolutions of specific detectors, or additional cuts on the data. The following table gives a quick overview over the properties of the nuclear targets we use:

Nucleus	Z	A	$r = 1.2\ \mathrm{fm} \cdot A^{1/3}$
C	6	12	2.75
Fe	26	56	4.59
Cu	29	63	4.77
Nb	41	93	5.43
Pb	82	208	7.10

Table 4: Properties of nuclear targets.

11.1 Photon-Induced Reactions

In this section we will present dilepton spectra of photon-induced reactions on various nuclei, at a photon energy of 1.5 GeV. We chose this energy because 1) it lies in the energy range of the g7 experiment, 2) it is large enough for a production of all three light vector mesons (ρ, ω and ϕ) and 3) it is not too large, so that the vector mesons have small momenta and therefore a larger probability to decay inside the nucleus.
Fig. 18 shows the dilepton spectra of the $V \to e^+e^-$ channels on three different targets: a light one (^{12}C), an intermediate one (^{56}Fe) and a very heavy one (^{208}Pb). The Dalitz backgrounds have been left out here, since we want to study the influence of in-medium effects on the vector meson channels. For each target and channel, a comparison is shown of two different calculations:

- The dashed lines have been obtained using plain vacuum spectral functions for the vector mesons.

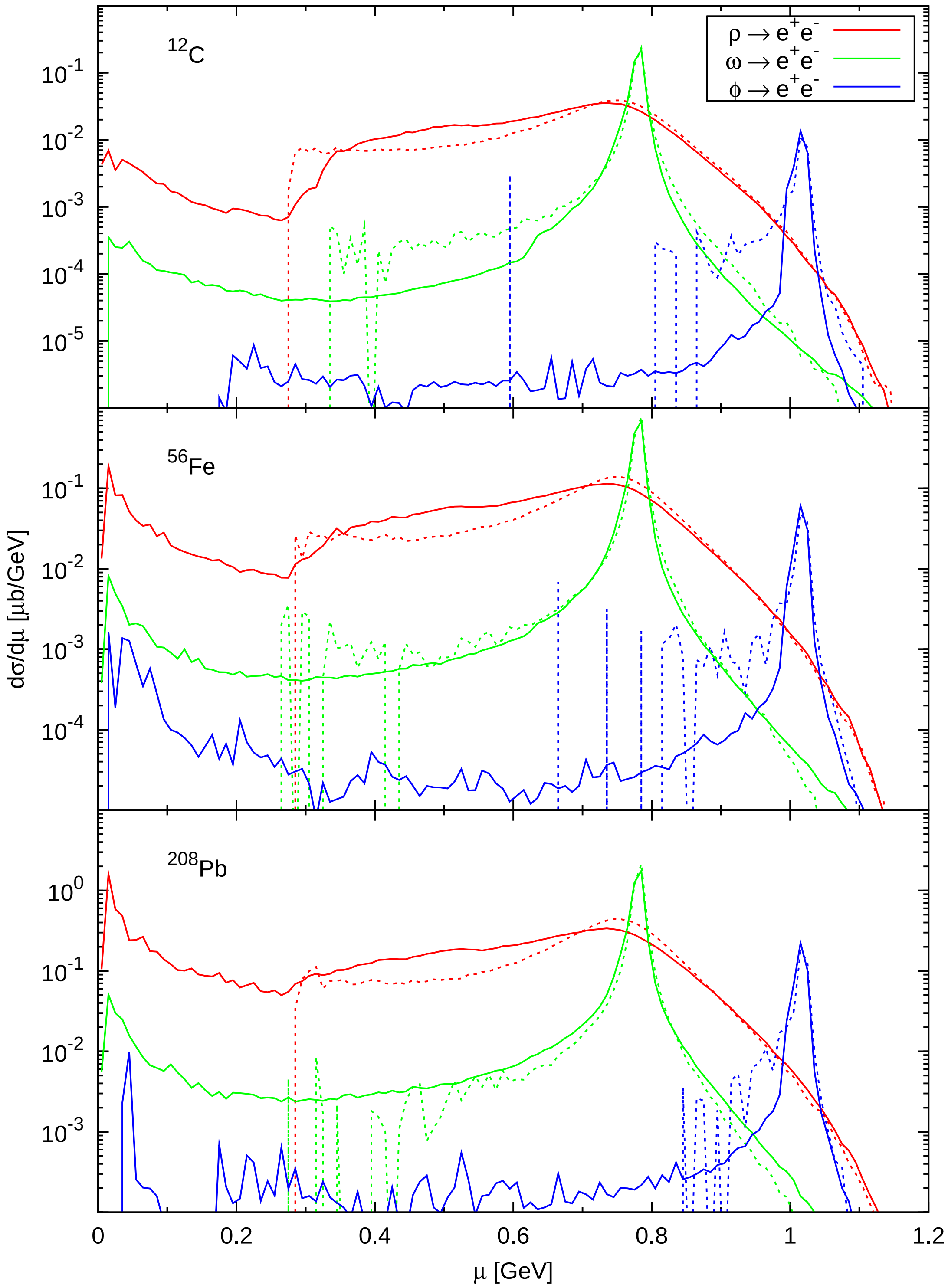

Figure 18: Dilepton spectrum for $\gamma + C$@1.5 GeV, $\gamma + Fe$@1.5 GeV and $\gamma + Pb$@1.5 GeV (from top to bottom), without Dalitz backgrounds. Dashed: vacuum spectral functions, solid: in-medium spectral functions (including collisional broadening) & off-shell potential.

- The solid lines represent a calculation with full in-medium spectral functions, including collisional width, and using an off-shell potential.

Although we will refer to the dashed lines as the "vacuum" calculation here, they do of course include some medium effects, like final-state interactions of the vector mesons (i.e. re-scattering and absorption in the nucleus). However, they use vacuum spectral functions for the production of the vector mesons, where the width (also in the medium) is simply assumed to be the vacuum decay width, and the collisional width in the medium is neglected. Therefore it is not necessary to work with an off-shell potential, since there is no difference between the spectral functions in the vacuum and in the medium (which means the off-shell potential would have no effect at all).
In contrast, the solid lines represent a full in-medium treatment, including both the collisional width in the spectral functions, and the evolution of the particle masses via the off-shell potential. We will refer to this as the "medium" calculation in the following. These calculations do not include any mass-shift (which will be discussed later).

Looking at the $\rho \to e^+e^-$ channel, one can see a clear difference between the vacuum and the medium curve: The peak drops a little, while the region between 300 and 700 MeV is elevated. While this effect is visible on all three targets, it seems to be a bit stronger on the heavier ones. In the region above the peak there is hardly any effect visible. But there is of course another major difference between the vacuum and medium calculation: The spectrum of the vacuum calculation abruptly stops at $\mu_\rho^{min} = 2m_\pi \approx 280MeV$, since our vacuum spectral function vanishes below this threshold (as discussed in chapter 3). The medium calculation however has a contribution below the 2π threshold, since the full in-medium spectral function includes the collisional width, which does not vanish below the threshold. This means that ρ mesons can be created in the medium which are lighter than $2m_\pi$. When these particles propagate into the vacuum, the off-shell potential makes sure that their mass is shifted above the threshold, so that they are able to decay in the vacuum. Following this argument, the sub-threshold contribution in the medium calculation can only come from particles which are in the medium. Therefore this contribution clearly increases for heavier nuclei, since the particles have to travel longer distances through the medium before they reach the vacuum. And so the step, which is still visible for the ^{12}C target at the threshold, is almost gone for ^{208}Pb.
In other works the sub-threshold contributions (below the 2π threshold) have mostly been neglected, justified by the fact that contributions in this region are not important, since they are drowning in the Dalitz backgrounds anyway. In this thesis we explicitly include these contributions, and calculate the in-medium dilepton spectrum down to $\mu = 0$. This may be important since sub-threshold particles can change their mass through the off-shell potential, and thereby also contribute to the spectrum above the threshold.
For the $\omega \to e^+e^-$ channel the story is a little different. Since it has a longer lifetime than the ρ, less in-medium effects are expected, since more particles decay only after they have left the nucleus. And indeed the spectrum around the peak is nearly identical for both calculations. Further away from the peak, one can see some differences. For the light ^{12}C target, one can see that the dilepton yield below the peak (at about 300-600 MeV) is actually lower in the medium calculation. At first glance this is surprising, since one would rather expect this region to come up when turning on collisional broadening, as in the case of the ρ. But one has to keep in mind that ^{12}C is a very light nucleus, so that due

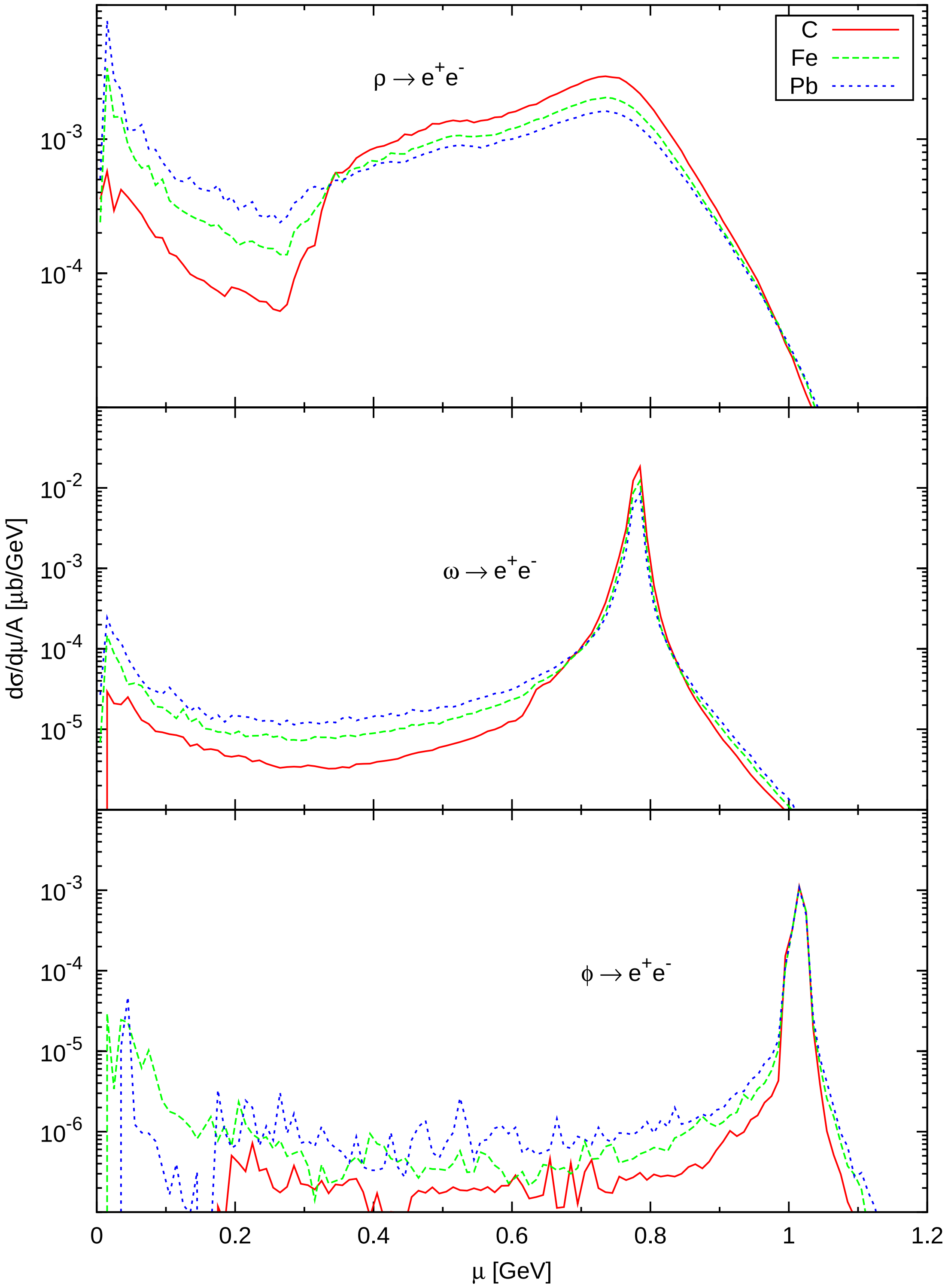

Figure 19: Dilepton spectrum (divided by A) for photon-induced reactions at 1.5 GeV on different targets for ρ (top), ω (center) and ϕ (bottom) channels, including collisional broadening.

to the long lifetime of the ω the effect of collisional broadening is expected to be very weak in the dilepton spectrum. The reason for the "negative" effect one observes is probably a combination of the following facts: In the vacuum calculation, one has a minimal mass of $\mu_\omega^{min} = m_\pi$, below which we have no contributions to the dilepton spectrum. In the plot shown, we do not even get down to this threshold due to low statistics and the fact that the ω is so narrow. In the medium calculation we can easily produce ω mesons below the threshold, due to collisional broadening. This means that a part of the dilepton yield is simply shifted below the threshold in the medium calculation and is missing above, which could account for part of the negative effect observed. In addition one can have problems with particles acquiring negative masses in the medium calculation (see chapter 7), which have to be taken out of the simulation, and are also missing in the spectrum. This could also contribute to the negative effect on light targets. Anyway this effect vanishes for heavier targets. On ^{56}Fe the vacuum and medium contributions are almost the same, while for ^{208}Pb the medium calculation even lies above the vacuum curve, as one would expect. For this heavy target, the effect of the collisional broadening gets larger, since more ω mesons can decay inside the nucleus, and thus outweighs the negative effects discussed before.
For the ϕ channel, one can hardly see any in-medium effect, because the ϕ is even more long-lived than the ω, so that only very few particles decay inside the nucleus. The spectrum at the peak is more or less identical in both calculations, and the only visible difference is the "negative" effect, which has already been observed for the ω. Here it is even stronger, and can not be canceled by effects of the collisional width.
In the whole comparison of the two modes of calculation, which we have performed here, one has to keep in mind that the calculation with vacuum spectral functions in no way gives a good physical result, but is rather an unphysical approximation, to start with for simplicity. Consequently, the differences between both calculations are not all due to real "in-medium" effects, but can also be artifacts of the oversimplified "vacuum" calculation.

To give a clearer display of the pure in-medium effects, fig. 19 shows a direct comparison of the full in-medium calculation on different targets. For better comparability, the mass-differential cross sections have been divided by the number of nucleons A. Without any medium modifications, the cross section would simply scale with A, i.e. $\sigma_A = A \cdot \sigma_N$, so that any deviations in fig. 19 must be due to in-medium effects.
For the ρ one can see that the peak drops with increasing A, due to absorption of ρ mesons in the nucleus. This effect can already be seen in calculations with vacuum spectral functions, where the whole spectrum would drop uniformly. With the full in-medium spectral functions this is not true any more. As noted before, the sub-threshold contribution grows with nuclear mass number, even if A is divided out. And also above the threshold one can observe medium effects.
For the ω, as for the ρ, the region around the peak drops with increasing A. However, the low-mass region rises significantly despite the increasing absorption, which is clearly an effect of collisional broadening.
For the ϕ, the peak drops only slightly, since the cross sections for nuclear absorption are smaller, but one can still see significant broadening effects below the $K\bar{K}$ threshold.

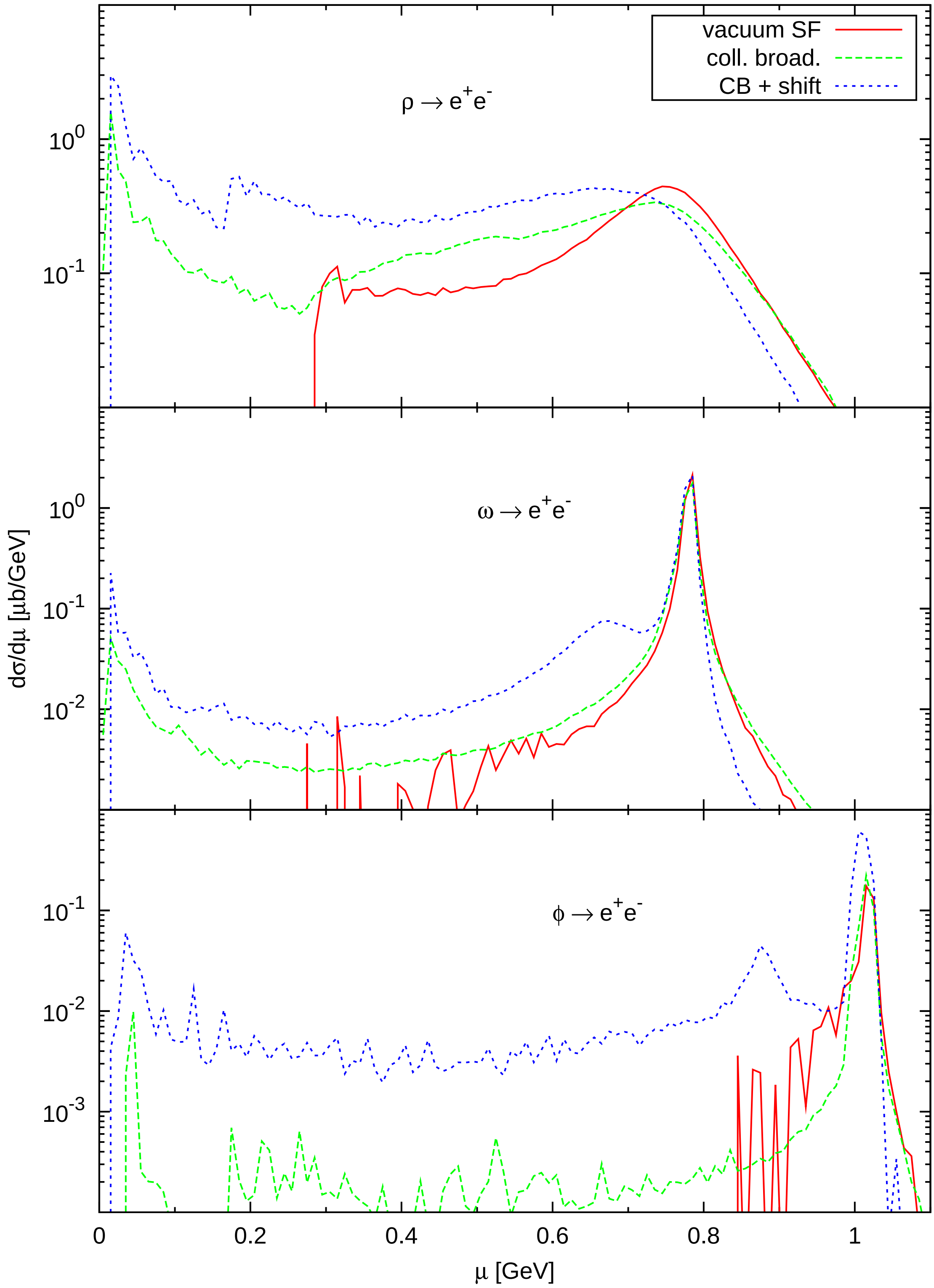

Figure 20: Dilepton spectrum of $\gamma + \mathrm{Pb}@1.5\,\mathrm{GeV}$ for ρ (top), ω (center) and ϕ (bottom) channels, including collisional broadening and mass shift with $\alpha = 0.16$.

After having investigated the effects of collisional broadening on the spectrum, we will now turn to the mass shift. Fig. 20 shows a comparison of three simulations of the reaction $\gamma + \mathrm{Pb}@1.5GeV$: The two discussed before, i.e. vacuum spectral functions and collisional broadening with off-shell potential, plus a new calculation which includes collisional broadening and a 16% mass shift in the medium.
For the ω and ϕ mesons one can see a small additional "in-medium" peak pop up beneath the large "vacuum" peak. The reason for this two-peak structure is of course that some mesons decay in the medium, while most of them decay in the vacuum. The in-medium peaks are also significantly broader, due to collisional broadening in the medium. For the ρ only one peak is observed, which is very broad and a bit shifted. Since the ρ has a large width already in vacuum, and the in-medium peak is even broader, both peaks are in fact too close together to be distinguished. Also the ρ is more short-lived than the ω and ϕ, so that more ρ mesons can decay in medium, and the in-medium peak of the ρ is more dominant than for the other two. For all three mesons one can see that the region below the mass pole is significantly enhanced by introducing a mass shift in addition to the collisional broadening.
For the ϕ meson, even the vacuum peak gets a lot bigger. This seems puzzling at first, but can be explained by the fact that the photon energy of 1.5 GeV is just large enough to produce on-shell ϕ mesons. From eq. 18 one can see that a photon energy of 1.5 GeV is actually too small to produce on-shell ϕ mesons on a nucleon at rest. The threshold energy for this is $E_\gamma = 1.574\,\mathrm{GeV}$ (while the threshold for coherent ϕ production on Pb would be already at $E_\gamma = 1.02\,\mathrm{GeV}$). This means that ϕ mesons on the mass shell can only be produced due to the Fermi momentum of the nucleons, and that this is only possible in certain collisions where the nucleon momentum has the right orientation with respect to the photon beam. Now with the mass shift, on-shell ϕ mesons in the medium have only a mass of $m^*_\phi = (1-0.16)m_\phi \approx 860MeV$. These can be produced in almost all γN collisions, regardless of orientation, so that the total ϕ production rises.
A similar threshold effect also seems be the cause for the ϕ peak not dropping in fig. 19, where a slightly increasing effective cross section may counteract the absorption. To check this, we have performed photon-induced reactions at 2.2 GeV photon energy, where the absorption effects on the ϕ are much more visible.

To close this section, fig. 21 shows the total dilepton spectrum for $\gamma + {}^{208}Pb@1.5\,\mathrm{GeV}$, including all hadronic channels, again comparing three different scenarios (vacuum spectral functions, collisional broadening and collisional broadening + mass shift). The $V \to e^+e^-$ contributions to this have already been shown in fig. 20, and now also the Dalitz backgrounds are included, which (apart from $\omega \to e^+e^-\gamma$) have no medium modifications. One can see that turning on collisional broadening causes an enhancement of the region between 300 and 700 MeV, by a factor of up to 1.5, and a slight drop below the ϕ peak. Apart from this, there are little modifications to the spectrum. If we now in addition include a 16% mass shift of the vector mesons, we observe a further enhancement of the low mass region down to 150 MeV, by an additional factor of 1.5 to 2, while the regions between the ω and ϕ peaks, as well as above the ϕ peak, drop slightly. Between the (vacuum) ω and ϕ peaks one can also see the small in-medium peak of the ϕ. Since our Dalitz backgrounds are slightly underestimated, the enhancements below 500 MeV are probably less significant than shown here. But at least between 500 and 700 MeV this plot should give a rather accurate picture of the expected enhancements for the scenarios we have considered.

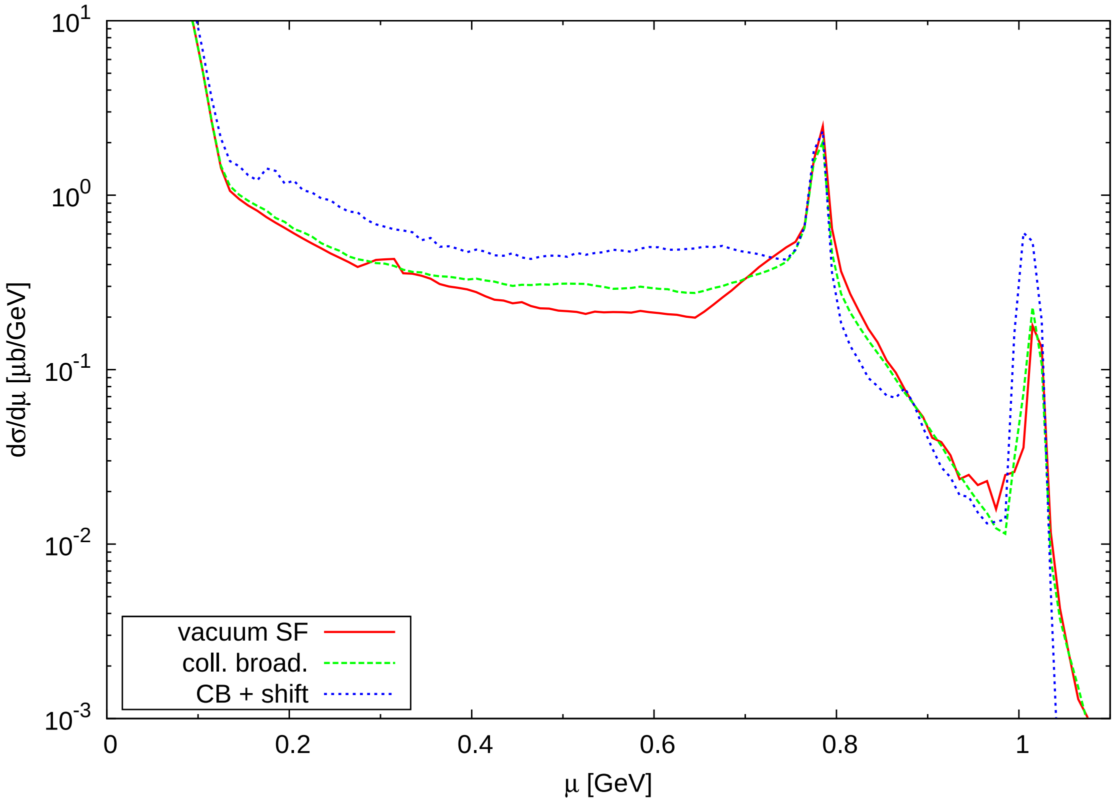

Figure 21: Total dilepton spectrum of $\gamma + \mathrm{Pb}@1.5\,\mathrm{GeV}$ (all hadronic sources), including collisional broadening and mass shift with $\alpha = 0.16$.

11.2 Proton-Induced Reactions

Apart from the photon-induced reactions discussed in the last section, we have also investigated proton-induced reactions. The first setup we simulated is similar to what the HADES detector at GSI will be measuring soon: Protons with a kinetic energy of 3.5 GeV hitting a Nb target. The dilepton spectrum for this case is shown in fig. 22, again comparing the three scenarios we already analyzed for the photon-induced reactions.
The top panel of the figure shows the contribution of the $\rho \to e^+e^-$ channel in the different scenarios, which shows similar effects to what has already been observed for the photon-induced reactions, though slightly less pronounced. The collisional broadening brings down the peak a bit, enhances the region between 350 and 700 MeV, and adds contributions below the 2π threshold. With an additional pole mass shift the region around and above the peak drops, while the whole low-mass region below the peak is further enhanced.
For the $\omega \to e^+e^-$ channel, which is shown in the center panel, the collisional broadening brings some enhancement below the peak plus sub-threshold contributions. On top of that the pole mass shift causes a small in-medium peak to appear, together with a further enhancement of the low-mass region and a drop of the region above the peak.
The $\phi \to e^+e^-$ channel is not shown here explicitly, since the statistics for this simulation was too low to allow for the observation of any effects in the ϕ channel. Instead the bottom panel shows an overview over the total dilepton spectrum for $p + Nb@3.5GeV$, including all hadronic contributions. The ω peak is clearly visible, while the ϕ peak seems to be slightly suppressed here. Between the vacuum curve and the one with collisional broadening one can hardly make out a difference, at most a very small enhancement in the region around 600 MeV. With an additional pole mass shift, however, one does get some modifications, i.e. an enhancement in the region between 500 and 700 MeV (up to a factor 1.5) and a smaller one around 200 MeV, a drop of the whole spectrum above the ω peak, and also a slight drop just below the ω peak. Overall one can see that the enhancement effects are a bit smaller here than for the photon-induced reactions.

In addition to the 3.5 GeV proton projectile, we also analyzed reactions with 12 GeV protons, as measured by the E325 collaboration at KEK. Fig. 23 shows the dilepton spectrum for this setup, using a Pb target. The three panels, as in the previous figure, show the channels $\rho \to e^+e^-$ and $\omega \to e^+e^-$ as well as the total hadronic dilepton spectrum. The collisional broadening for both ρ and ω causes only a weak effect, if any, and consequently in the total spectrum there is hardly any difference visible to the vacuum curve. The pole mass shift brings about the same effects seen earlier, and causes a similar enhancement in the region between 500 and 700 MeV as already seen with the 3.5 GeV protons. The in-medium effects are slightly weaker here than before, due to the high proton energies, causing the vector mesons to have higher momenta, thus spending less time inside the nucleus. Stronger effects may be seen when working with cuts on the lepton momenta, as done in the KEK analysis of the ϕ meson [Mut07].

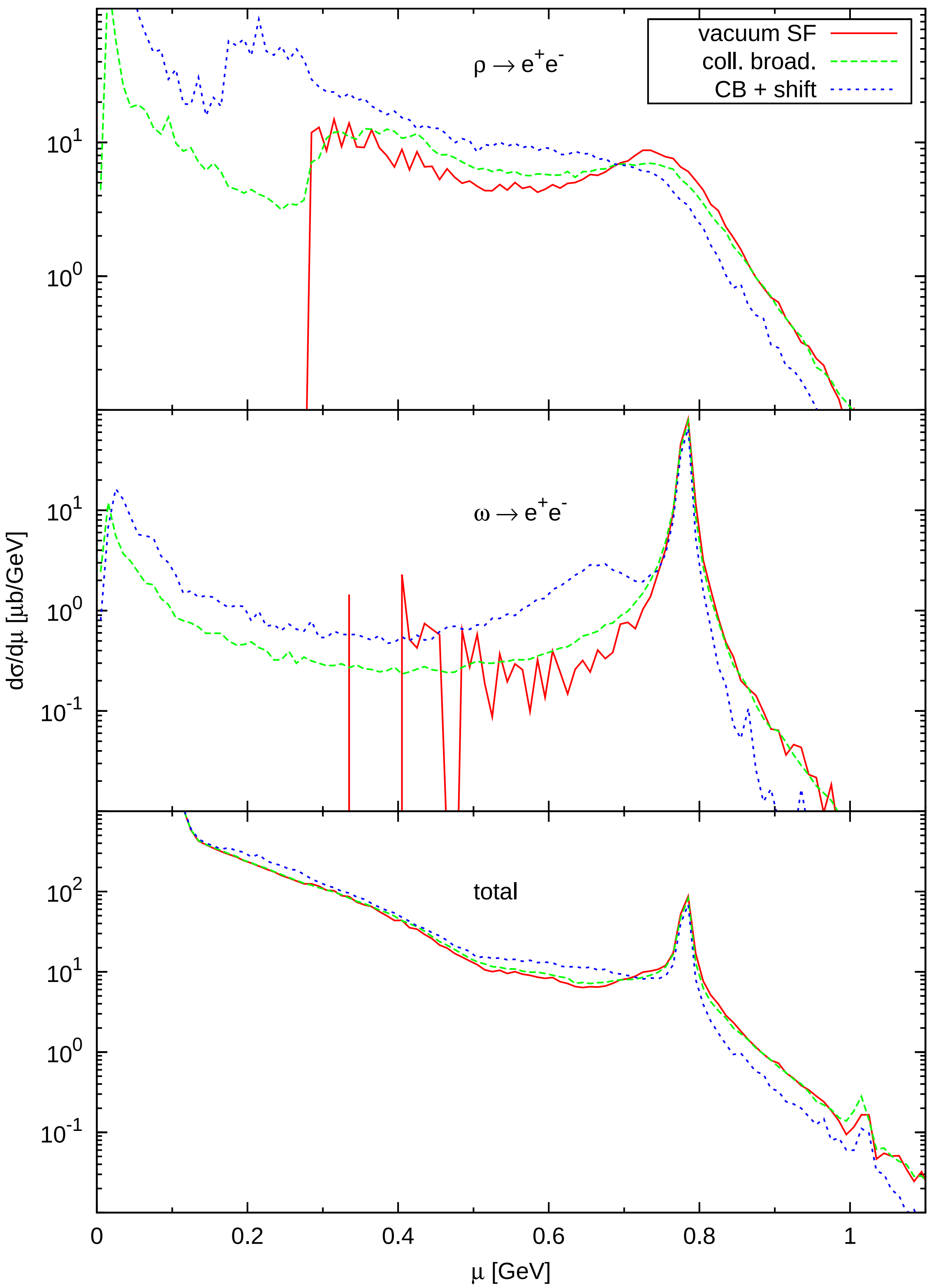

Figure 22: Dilepton spectrum for $p + Nb$@3.5 GeV.

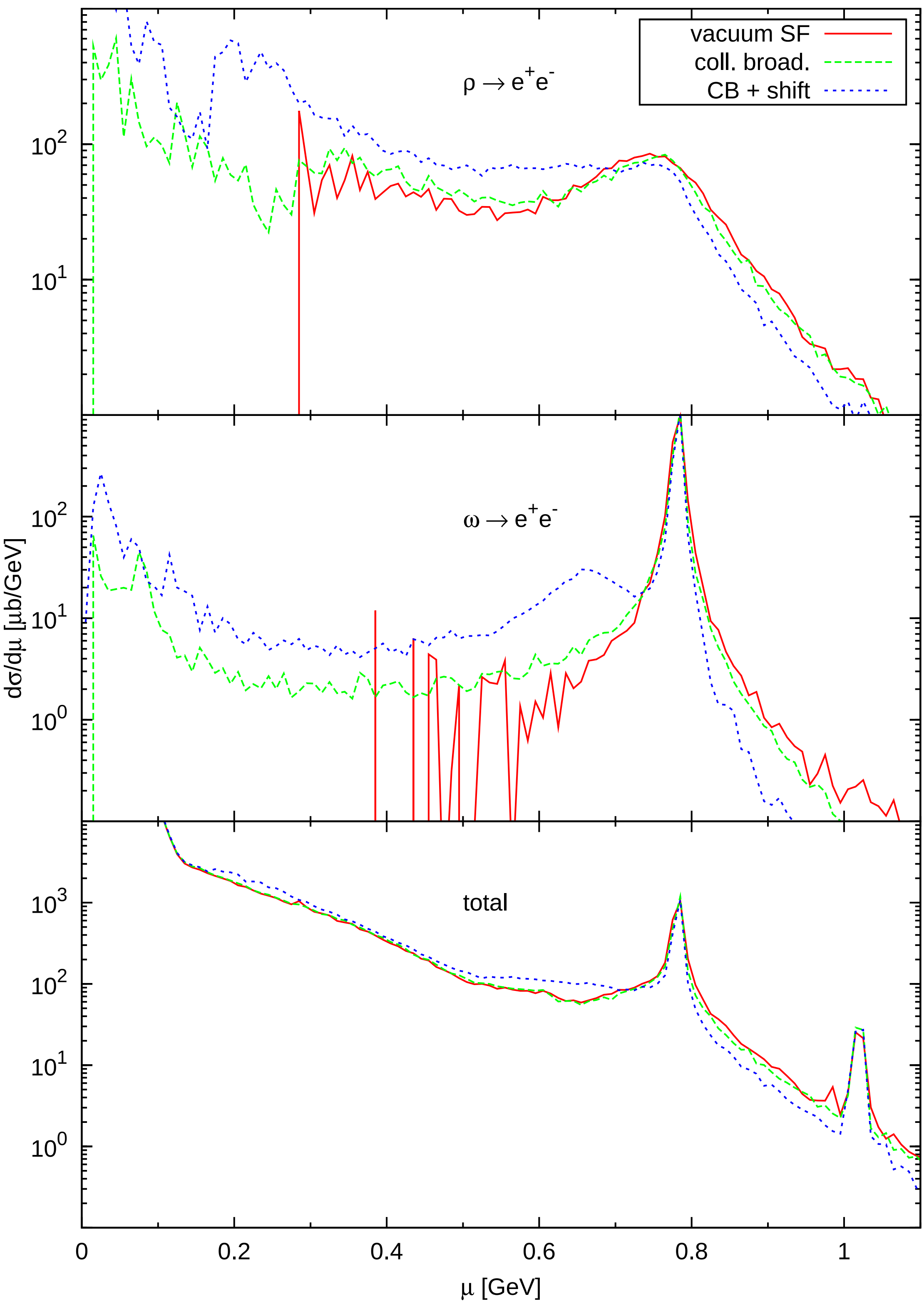

Figure 23: Dilepton spectrum for $p + Pb$@12 GeV.

12 Summary and Outlook

Summing up, this thesis has presented a detailed discussion of dilepton production in elementary nuclear reactions, taking into account all important aspects that may play a role. In particular we have investigated the influence of in-medium modifications of the vector mesons on the dilepton spectrum, including effects like collisional broadening and a possible pole mass shift. The results of these investigations have been shown in the previous chapter for various scenarios.

We have tried to carry out our investigations in as much detail as possible in the scope of a diploma thesis, but of course there is plenty room for improvement. We have already remarked some of the possible extensions as they appeared throughout the work, and will here try to compile a (probably incomplete) list of features which may be subject to future improvements.

One first group of issues we encountered was related to the off-shell transport of the vector mesons. Since vector mesons are quite broad particles with possibly large medium modifications, it is important to have a good description of how they propagate through the nuclear medium. This is not trivial, and our treatment has shown to be not completely perfect. In particular we had to face some problems with particles acquiring unphysically large velocities, which could eventually be overcome. But we had to "pay" the solution by assuming constant cross sections for the VN interaction, which are not fully consistent with our collision term. Surely it would be an improvement to use the fully relativistic equations of motion instead of an off-shell potential. While this would hopefully cure some of the issues we have described, it is not clear if it would completely remove all of them.

A second big area of possible improvements are the backgrounds. In dilepton physics, as in almost any other area of physics, it is absolutely crucial to understand not only the "signal" itself that one is interested in, but also all the possible backgrounds, which contribute to the measured quantity. For dilepton physics this is particularly important, since every measurable dilepton spectrum is always a mixture of several different components. Apart from the direct vector meson channels $V \to e^+e^-$ (which are the signal in this case), it contains many other contributing processes, e.g. several Dalitz decays, which we of course had to include in our analysis. For the proton-induced reactions these should be pretty much under control, while for the photon-induced reactions some of them might be underestimated, due to the fact that our initial γN interaction is missing some channels. These should be implemented as soon as possible to get a correct estimate of the Dalitz backgrounds. For the photon-induced reactions one other important background source is the Bethe-Heitler process, which has been investigated in quite some detail and should be under control (at least from the theoretical point of view). An additional background for proton-induced reactions is nucleon-nucleon-bremsstrahlung, which has not been included in the analysis so far, but should be in the future.

Once all backgrounds are under control, it would of course be nice to compare the "theoretical" spectra, which are the result of our simulations, to real experimental data. Experiments can never measure the full spectra shown here, but always have a limited acceptance given by their geometry and the limited resolution of the detector. Moreover they often use additional cuts and filters to reduce backgrounds and trigger only on “interesting” events. Therefore comparing to experimental data requires applying the same cuts and filters also to the simulation. This issue has not been touched here, but should be rather straightforward, since our simulation gives the complete position/momentum/etc of all particles produced, so one has all the information needed to implement any kind of filter.

Apart from the larger issues and omissions that we have just enumerated, there may be a number of minor aspects which we have not mentioned here, since they are not as important.

Having given an outlook on the possible directions of our future investigations, we want to close this thesis with the statement that the in-medium properties of vector mesons, which have been the main motivation for the analysis presented here, still remain largely unknown from an experimental point of view, hence dilepton physics promises to remain an exciting field in the years to come.

References

[Ada06] D. Adamova et al.: Modification of the rho meson detected by low-mass electron-positron pairs in central Pb-Au collisions at 158 A GeV/c, arXiv:nucl-ex/0611022.

[Ads04] J. Adams et al.: ρ^0 Production and Possible Modification in Au+Au and p+p Collisions at sqrt[sNN]=200GeV, Phys. Rev. Lett. 92 (2004) 092301, arXiv:nucl-ex/0307023.

[Ag95] G. Agakichiev et al.: Enhanced Production of Low-Mass Electron Pairs in 200 GeV/Nucleon S-Au Collisions at the CERN Super Proton Synchrotron, Phys. Rev. Lett. 75 (1995) 1272 - 1275.

[Ag07] G. Agakichiev et al.: Dielectron Production in $^{12}C + {}^{12}C$ Collisions at 2A GeV with the HADES Spectrometer, Phys. Rev. Lett. 98 (2007) 052302.

[Ar05] R. Arnaldi et al.: First Measurement of the ρ Spectral Function in High-Energy Nuclear Collisions, Phys. Rev. Lett. 96 (2006) 162302, arXiv:nucl-ex/0605007.

[BG88] G.F. Bertsch, S.D. Gupta: A guide to microscopic models for intermediate energy heavy ion collisions, Phys. Rep. 160 (1988) 189-233.

[BM88] V. Bernard, U.-G. Meissner: Properties of vector and axial-vector mesons from a generalized Nambu-Jona-Lasinio model, Nucl. Phys. A 489 (1988) 647.

[BR91] G.E. Brown, M. Rho: Scaling effective Lagrangians in a dense medium, Phys. Rev. Lett. 66 (1991) 2720.

[Bu08] O. Buss: Photon- and Pion-Induced Nuclear Reactions in a Transport Approach, Dissertation, Justus-Liebig-Universitaet Giessen, 2008 (in preparation).

[CJ00a] W. Cassing, S. Juchem: Semiclassical transport of particles with dynamical spectral functions, Nucl. Phys. A 665 (2000) 377, arXiv:nucl-th/9903070.

[CJ00b] W. Cassing, S. Juchem: Semiclassical transport of hadrons with dynamical spectral functions in A+A collisions at SIS/AGS energies, Nucl. Phys. A 672 (2000) 417, arXiv:nucl-th/9910052.

[Dev86] L. Devroye: Non-Uniform Random Variate Generation. Springer-Verlag, 1986. `http://cg.scs.carleton.ca/~luc/rnbookindex.html`.

[DL95] A. Donnachie, P.V. Landshoff: Exclusive vector meson production at HERA, Phys. Lett. B 348 (1995) 213-218, arXiv:hep-ph/9411368.

[Eff99] M. Effenberger: Eigenschaften von Hadronen in Kernmaterie in einem vereinheitlichten Transportmodell, Dissertation, Justus-Liebig-Universitaet Giessen, 1999.

[GiB] GiBUU website, `http://gibuu.physik.uni-giessen.de/GiBUU`.

[Gol97] Y.S. Golubeva, L.A. Kondratyuk, W. Cassing: Medium effects in the production and decay of vector mesons in pion nucleus reactions, Nucl. Phys. A 625 (1997) 832, arXiv:nucl-th/9710071.

[HAD] HADES website, `http://www-hades.gsi.de/`.

[HL92] T. Hatsuda, S.H. Lee: QCD sum rules for vector mesons in the nuclear medium, Phys. Rev. C 46 (1992) R34.

[Hu03] G.M. Huber et al.: In-medium ρ^0 spectral function study via the $^2H, ^3He, ^{12}C(\gamma, \pi^+\pi^-)$ reaction, Phys. Rev. C 68 (2003) 065202, arXiv:nucl-ex/0310011.

[Ish05] T. Ishikawa et al.: ϕ photo-production from Li, C, Al, and Cu nuclei at $E_\gamma = 1.5 - 2.4\,\mathrm{GeV}$, Phys. Lett. B 608 (2005) 215, arXiv:nucl-ex/0411016.

[KB94] L. Kadanoff, G. Baym: Quantum Statistical Mechanics. Addison Wesley, 1994.

[KK05] L.P. Kaptari, B. Kämpfer: Di-Electron Bremsstrahlung in Intermediate-Energy pn and Dp Collisions, Nucl. Phys. A 764 (2006) 338-370, arXiv:nucl-th/0504072.

[KKW96] F. Klingl, N. Kaiser, W. Weise: Effective Lagrangian approach to vector mesons, their structure and decays, Z. Phys. A 356 (1996) 193, arXiv:hep-ph/9607431.

[Kot08] M. Kotulla et al.: Modification of the ω-Meson Lifetime in Nuclear Matter, Phys. Rev. Lett. 100 (2008) 192302, arXiv:0802.0989.

[Lar07] A. Larionov et al.: Three-body collisions in Boltzmann-Uehling-Uhlenbeck theory, Phys. Rev. C 76 (2007) 044909, arXiv:0704.1785.

[Leh03] J. Lehr: In-Medium Eigenschaften von Nukleonen und Nukleonresonanzen in einem semiklassischen Transportmodell, Dissertation, Justus-Liebig-Universitaet Giessen, 2003.

[Leu00] S. Leupold: Towards a test particle description of transport processes for states with continuous mass spectra, Nucl. Phys. A 672 (2000) 475, arXiv:nucl-th/9909080.

[LPM98] S. Leupold, W. Peters, U. Mosel: What QCD sum rules tell about the rho meson, Nucl. Phys. A 628 (1998) 311, arXiv:nucl-th/9708016.

[Lyk99] G.I. Lykasov, W. Cassing, A. Sibirtsev, M.V. Rzyanin: ωN final state interactions and ω-meson production from heavy-ion collisions, Eur. Phys. J. A 6 (1999) 71, arXiv:nucl-th/9811019.

[MS92] D.M. Manley, E.M. Saleski: Multichannel resonance parametrization of πN scattering amplitudes, Phys. Rev. D 45 (1992) 4002.

[Müh07] P. Mühlich: Mesons in Nuclei and Nuclear Reactions with Elementary Probes, Dissertation, Justus-Liebig-Universitaet Giessen, 2007.

[Mut07] R. Muto: Evidence for In-Medium Modification of the ϕ Meson at Normal Nuclear Density, Phys. Rev. Lett. 98 (2007) 042501, arXiv:nucl-ex/0511019.

[Nar99] Y. Nara et al.: Relativistic nuclear collisions at 10A GeV energies from p+Be to Au+Au with the hadronic cascade model, Phys. Rev. C 61 (1999) 024901, arXiv:nucl-th/9904059.

[Nrk06] M. Naruki et al.: Experimental Signature of Medium Modifications for ρ and ω Mesons in the 12 GeV p+A Reactions, Phys. Rev. Lett. 96 (2006) 092301, arXiv:nucl-ex/0504016.

[Nas07] R. Nasseripour et al.: Search for Medium Modifications of the ρ Meson, Phys. Rev. Lett. 99 (2007) 262302, arXiv:0707.2324.

[OC97] H.B. O'Connell et al.: Rho-omega mixing, vector meson dominance and the pion form-factor, Prog. Part. Nucl. Phys. 39 (1997) 201, arXiv:hep-ph/9501251.

[PDG] Particle Data Group: Review of Particle Physics, `http://pdg.lbl.gov`.

[Pis95] R.D. Pisarski: Where does the ρ go? Chirally symmetric vector mesons in the quark-gluon plasma, Phys. Rev. D 52 (1995) R3773, arXiv:hep-ph/9503328.

[PS95] M.E. Peskin, D.V. Schroeder: An Introduction to Quantum Field Theory. Westview Press, 1995.

[Py] PYTHIA website, `http://home.thep.lu.se/~torbjorn/Pythia.html`.

[SM03] R. Shyam, U. Mosel: Role of baryonic resonances in the dilepton emission in nucleon-nucleon collisions, Phys. Rev. C 67 (2003) 065202, arXiv:hep-ph/0303035.

[Tr05] D. Trnka et al.: First observation of in-medium modifications of the omega meson, Phys. Rev. Lett. 94 (2005) 192303, arXiv:nucl-ex/0504010.

List of Figures

List of Tables

Deutsche Zusammenfassung

Die vorliegende Arbeit beschäftigt sich mit der Produktion von Elektron-Positron-Paaren, sogenannten Dileptonen, in elementaren Kernreaktionen (Photon- sowie Proton-induziert). Dileptonen spielen in der modernen Hadronenphysik vor allem eine herausragende Rolle als Sonde zur Erforschung von Vorgängen, die sich innerhalb von hadronischer Materie abspielen. Als "elektromagnetische Sonde" sind sie dazu besonders gut geeignet, da sie wie alle Leptonen lediglich an der elektroschwachen Wechselwirkung teilnehmen, nicht jedoch an der starken Wechselwirkung der Quarks und Gluonen. Letztere ist unter anderem verantwortlich für den Einschluss (das sogenannte "Confinement") der Quarks in Hadronen, sowie für die Wechselwirkung jeglicher Form von hadronischer (d.h. aus Quarks aufgebauter) Materie (wie etwa Mesonen, Hadronen oder Kernen). Durch die Immunität der Leptonen gegenüber dieser starken Wechselwirkung können Dileptonenpaare, die im Inneren eines hadronischen Mediums (wie etwa eines Atomkernes) produziert werden, dieses nahezu ungehindert durchdringen und so ohne größere Störungen Informationen aus dem Inneren des Mediums nach außen zum Detektor transportieren.
Insbesondere ist diese Eigenschaft sehr hilfreich für die Untersuchung der In-Medium-Eigenschaften von Hadronen. Seit annähernd zwei Jahrzehnten wird nun bereits mit großem Interesse der Frage nachgegangen, wie Hadronen, also zusammengesetzte Systeme aus Quarks und Gluonen, ihre Eigenschaften ändern, wenn sie sich in hadronischer Materie aufhalten, wie also ihre Charakteristika (wie Masse und Breite) durch den Einfluss eines umgebenden hadronischen Mediums modifiziert werden. Das Interesse an dieser Fragestellung wurde vor allem durch diverse theoretische Vorhersagen bezüglich dieser In-Medium-Eigenschaften angefacht. Insbesondere für die leichten Vektormesonen (ρ, ω und ϕ) wurden Anfang der Neunziger Jahre verschiedene Hypothesen aufgestellt, wie etwa eine Verbreiterung der Spektralfunktion oder eine Verschiebung der Pol-Masse im Medium. Während vor allem eine Massenabsenkung im Medium zu den populärsten Szenarien gehörte, wurde etwa auch der entgegengesetzte Effekt einer Massenerhöhung diskutiert. In den darauffolgenden Jahren mussten sich all diese Hypothesen einer experimentellen Überprüfung unterziehen, jedoch hat sich bis zum heutigen Tage trotz einer intensiven experimentellen Untersuchung der Fragestellung noch kein einheitliches Bild der In-Medium-Eigenschaften von Hadronen herauskristallisieren können, auch wenn schon des öfteren die experimentelle Bestätigung oder Widerlegung der einen oder anderen Theorie proklamiert wurde.
Dabei bietet sich vor allem für die Vektormesonen die Untersuchung der In-Medium-Eigenschaften mittels Dileptonen an, da alle leichten Vektormesonen einen direkten Zerfallskanal in e^+e^- besitzen. Erschwert wird diese Analyse lediglich durch die große Zahl an Hintergrundprozessen, die zum Dileptonenspektrum beitragen, sowie durch die kleinen Partialbreiten der Dileptonenzerfälle.
Wir versuchen durch die vorliegende Arbeit zur Aufklärung der beschriebenen Fragestellungen beizutragen, indem wir die Dileptonenproduktion in elementaren Kernreaktionen mit Hilfe eines semiklassischen Transportmodells numerisch simulieren. Dabei berücksichtigen wir verschiedene Szenarien von In-Medium-Modifikationen und produzieren Dileptonenspektren für diverse Reaktionen, die anschließend mit experimentellen Daten verglichen werden können, um letztendlich zu entscheiden, welche der hypothetischen Szenarien tatsächlich in der Natur realisiert sind.

Erklärung

Ich erkläre hiermit, dass ich die vorliegende Arbeit selbständig verfasst und keine anderen als die angegebenen Quellen und Hilfsmittel verwendet habe.

Giessen, den 11.08.2008 ______________________________